Title
EFFECTS OF PHASE TRANSFORMATION OF STEAM-WATER RELATIVE PERMEABILITIES

Author
Verma, A.K.

Publication Date
1986-03-01

Lawrence Berkeley Laboratory
UNIVERSITY OF CALIFORNIA

EARTH SCIENCES DIVISION

EFFECTS OF PHASE TRANSFORMATION OF STEAM-WATER RELATIVE PERMEABILITIES

A.K. Verma
(Ph.D. Thesis)

March 1986

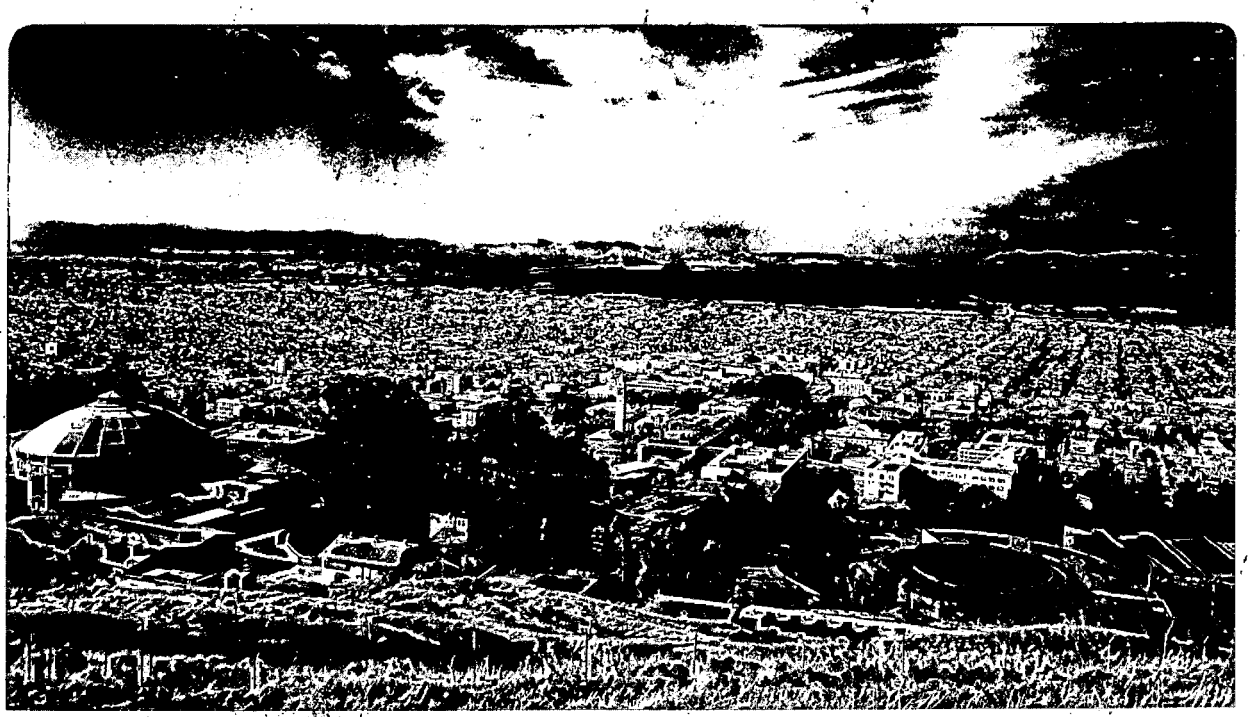

Prepared for the U.S. Department of Energy under Contract DE-AC03-76SF00098

DISCLAIMER

LBL-20594

EFFECTS OF PHASE TRANSFORMATION OF STEAM-WATER RELATIVE PERMEABILITIES

Ashok K. Verma

Earth Sciences Division
Lawrence Berkeley Laboratory
University of California
Berkeley, California 94720

This work was done with support from the U.S. Department of Energy
under Contract No. DE-AC03-76SF00098

TABLE OF CONTENTS

EFFECTS OF PHASE TRANSFORMATION OF STEAM-WATER RELATIVE PERMEABILITIES

Ashok K. Verma

Earth Sciences Division
Lawrence Berkeley Laboratory
University of California
Berkeley, California 94720

ABSTRACT

A combined theoretical and experimental study of steam-water relative permeabilities (RPs) was carried out. First, an experimental study of two-phase concurrent flow of steam and water was conducted and a set of RP curves was obtained. These curves were compared with semi-imperical and experimental results obtained by other investigators for two-phase, two-component flow (oil/gas; gas/water; gas/oil). It was found that while the wetting phase RPs were in good agreement, RPs for the steam phase were considerably higher than the non-wetting phase RPs in two-component systems. This enhancement of steam RP is attributed to phase transformation effects at the pore level in flow channels.

The effects of phase transformation was studied theoretically. This study indicates that there are two separate mechanisms by which phase transformation affects RP curves: (1) Phase transformation in converging-diverging flow channels can cause an enhancement of steam phase RP. In a channel dominated by steam a fraction of the flowing steam condenses upstream from the constriction, depositing its latent heat of condensation. This heat is conducted through the solid grains around the pore throat, and evaporation takes place downstream from it.

solid grains around the pore throat, and evaporation takes place downstream from it. Therefore, for a given bulk flow quality, a smaller fraction of steam actually flows through the throat segments. Since steam has much higher kinematic viscosity than liquid water, and since the throat segments are the primary contributors to the overall flow resistance in the flow channels, the phase transformation effects reduce the overall resistance to steam flow along channels with varying cross sections. This pore-level effect manifests itself as relative permeability enhancement on a macroscopic level; and (2) phase transformation along the interface of a stagnant phase and the phase flowing around it controls the irreducible phase saturation. Therefore, the irreducible phase saturation in steam-water flow will depend, among other factors, on the boundary conditions of the flow.

This study also presents a new solution technique for two-phase steam-water flow through a channel of arbitrary cross section by combined first and second laws of thermodynamics.

LIST OF FIGURES

LIST OF TABLES

NOMENCLATURE

Symbol	Description	Unit	Chapter
A	cross-sectional area	m^2	2–6
C	specific heat	J/kg °K	4
D_{va}	diffusion coefficient of vapor-air mixture	m^2/sec	4
D	coefficient of self diffusion	m^2/sec	7
En	enhancement factor		5
F	mass flux	kg/m^2sec	4
f	flow quality		5
g	acceleration of gravity	m/sec^2	4
ΔG	free energy of formation	ergs	3
k_{lv}	latent heat of evaporation	J/kg	3–7
h	film thickness		3
H	mean curvature	m^{-1}	3
I	intensity of γ-ray	$\frac{\text{photons}}{\text{sec}}$	6
K	thermal conductivity	W/m °k	4
K	hydraulic conductivity	m/sec	2
k	intrinsic permeability	m^2	2–7
k_r	relative permeability		2–7
L	length of flow channel	m	5–7
m	mass flow rate	kg/sec	4,5
M	mass accumulation	kg/sec	4
n	number of moles	mole	3
n	unit normal vector		4
N	number of photons		6
p	partial pressure	N/m^2	3
P	absolute pressure	N/m^2	3–8
P_N	normal component of pressure	N/m^2	3
P_T	tangential component of pressure	N/m^2	3
q	volumetric flux	m/sec	2
q	conductive heat flow rate	W/sec	5

q	mass source	kg/sec	4
Q	volumetric flow rate	m^3/sec	2
Q	energy flow rate	J/sec	5
r	radius	m	2–7
$\tilde{r}$	critical radius	m	3
r*	critical bubble radius	m	3
R	grain diameter	m	5
s	specific entropy of fluid	J/kg °K	5
s_f	specific entropy of flow channel	J/m °K	5
S	saturation		3–7
S	strength of γ-ray source	$\frac{\text{protons}}{\text{sec}}$	6
S_{gen}	entropy generated per unit length of the flow channel	$\frac{\text{J}}{\text{m °K sec}}$	5
t	time	sec	3–7
T	absolute temperature	°K	3–7
T_c	critical temperature	°K	3
T_r	normalized temperature (T/T_c)		3
ΔT_{sh}	degree of superheat ($= T_b - T_s$)	°K	3
U	specific internal energy	J/kg	4
v	specific volume	m^3/kg	3–8
V	volume	m^3	3
X	mass fraction		4
x	linear distance	m	3–7
z	linear distance	m	6

Greek Symbols

α	saturation		6
α	tortuality factor		7
α	constriction factor	r_t/R	5
β	variational parameter		5
γ	surface tension	N/m	3–5
Γ	surface area of an element	m^2	4
ϵ	variational parameter		5
ς	constant defined in Appendix 5.C		5
η	dimensionless distance		5

θ	dimensionless temperature		5
θ	contact angle		3
λ	thermal transmissivity	$\frac{\text{Wm}}{^\circ\text{K}}$	5
μ	absolute viscosity	$\frac{\text{N·sec}}{\text{m}^2}$	3–7
μ	chemical potential	J/kg	3
μ	absorption coefficient for γ-ray	m^{-1}	6
ν	kinematic viscosity	m^2/sec	5
ν	liquid island enhancement factor		7
π	disjoining pressure	N/m^2	3–5
π_m	molecular component of disjoining pressure	N/m^2	3
π_e	electrostatic component of disjoining pressure	N/m^2	3
π_s	structural component of disjoining pressure	N/m^2	3
ρ	density	kg/m^3	3–7
τ	hydraulic transmissivity	m^4	5
τ	resolving time	sec	6
Υ	factor defined in Chapter 5		5
ϕ	porosity		3–7
Φ	piezometric head	m	2
ψ	included angle of cavity		3
Ω	included angle of flow channel		5

Subscripts

a	air		3
av	average		5
b	boiling		3
b	bubble		3
c	critical		3
d	dry		6
f	flow channel		5
i	phase index		2
i	interface		3

i	material index	6
l	liquid	2–7
o	initial condition	5
o	unattenuated	6
s	saturated	3,6
sh	superheat	3
t	throat	5
∞	far away from interface	3
∞	flat interface	3

ACKNOWLEDGMENTS

I take this opportunity to thank my teacher and advisor, Professor Paul A. Witherspoon, for his guidance and encouragement during my graduate studies and many aspects of this research. I am indebted to my colleague, Dr. Karsten Pruess, for providing guidance, scrutiny, and encouragement throughout the course of this work. I wish to thank Dr. Chin-Fu Tsang for his support and encouragement.

I am highly indebted to Professor Kent Udell for some very valuable suggestions during the course of this work.

I am grateful to all the staff of the Lawrence Berkeley Laboratory who helped in fabrication and assembly of the experimental set up. I wish to thank Ms. Jean Wolslegel for her patience during the preparation of this manuscript.

This work was done with support from the U.S. Department of Energy under Contract No. DE-AC03-76SF00098.

CHAPTER 1
INTRODUCTION

Two-phase flow of steam and water in porous media is encountered in many energy-related problems involving, for example, geothermal reservoirs, heat pipes, chemical distillation, and nuclear waste disposal. Simulation studies of these problems require knowledge of the relative permeability and capillary pressure functions for the porous matrix. Much information is available on relative permeabilities for water-oil and oil-gas systems, but steam-water relative permeabilities are poorly known, in spite of considerable theoretical and experimental efforts during the last decade. Since no conclusive results exist, many investigators have used ad hoc parameterizations, or have adopted results obtained from flow of gas and oil (Corey, 1954). Such practices can lead to serious deficiencies (Reda and Eaton, 1980). For example, the results of sensitivity studies on the effects of the relative permeability curves on mass flow rate and flowing enthalpy into geothermal wells indicate that two-phase flow behavior of steam and water depends greatly on the relative permeability curves used (e.g., Bodvarsson et al., 1980, Reda and Eaton, 1980, Sun and Ershaghi, 1979). Hence, there exists a need for obtaining reliable relative permeability functions.

Most of the past efforts towards determining the relative permeability functions have been directed towards flow of two-component, two-phase fluids, such as oil-water or immiscible gas-fluid in porous media. It was found that the relative permeabilities depend primarily on phase saturations, but also on many other

other factors, such as: (i) viscosity ratio of the fluids (e.g., Downie and Crane, 1961; Odeh, 1959; Schneider and Owens, 1980; and LeFebvre du Prey, 1973); (ii) wetting characteristics of the two phases (e.g., Coley et al., 1956; Donaldson et al., 1966; Owens and Archer, 1978;; McCaffery and Bennion, 1974; Heiba et al., 1983); (iii) interfacial tension, or more generally, the capillary number (e.g., Bordon and Longeron, 1980; Fulcher et al., 1983; Laverett, 1939; and Taber, 1969); (iv) saturation history (e.g., Johnson et al., 1959; and Naar et al., 1962).

While rationales have been advanced for some of these factors, a satisfactory theory of relative permeability has not yet been developed (Heiba et al., 1982). However, extensive experimental investigations have produced some reliable relative permeability curves for two-phase, two-component fluid flow through some typical porous media (e.g., Corey, 1954; Brooks and Corey, 1964; Osoba et al., 1951; Hauzenberg and Zaslavsky, 1963). Applicability of these curves to a single-component two-phase flow, such as steam-water, is questionable because of the possibility of phase transformation in the flow channels. Phase change provides an additional degree of freedom in a single-component, two-phase system, which may have a significant effect on the nature of the relative permeability curves.

There are two separate mechanisms by which phase transformation affects relative permeability curves: (1) Phase transformation in converging-diverging flow channels with hydrophilic walls causes an enhancement of the steam phase relative permeability; and (2) Phase transformation along the interface of a stagnant phase and the phase flowing around it controls the irreducible saturation of

the stagnant phase. The first mechanism is directly related to the morphology of the void space in a porous media. The flow channels in porous media are not of uniform cross section at the pore level. The cross-sectional area, and hence the transmissivity, of the flow channel varies considerably from point to point. If the hydraulic radius r_t of the narrow segments, referred to as "pore throats," are very small compared to the hydraulic radius r_b of the wider segment, referred to as "pore bodies," then a very large fraction of the overall flow resistance is due to the resistances of the pore throats. If a fraction of steam condenses upstream from a throat, gets transported and flashes down stream then for a given bulk flow quality, a smaller fraction of steam actually flows through the throat segments. Since steam has much higher kinematic viscosity than liquid water, and since the throat segments are the primary contributors to the overall flow resistance in the flow channels, the phase transformation effects reduce the overall resistance to steam flow along channels with varying cross sections. This pore-level effect manifests itself as relative permeability enhancement on a macroscopic level. However, our studies indicate that for typical pores found in sandstone this effect is negligible.

The second mechanism mentioned above deals with thermodynamic control of irreducible phase saturations in simultaneous flow of steam and water in porous media. Irreducible phase saturation is a result of "phase trapping." Phase trapping takes place when some of the phase gets isolated and is rendered immobile under combined interaction of viscous and capillary forces. In the case of two component, immiscible fluids, the trapped phase remains immobile until,

(i) viscous forces cause the trapped phase to move in the general direction of flow, or (ii) flow lines change such that the trapped phase becomes part of a flow channel in which there is a continuous path for this phase across the flow domain. There is always some molecular diffusion from the trapped phase into the phase flowing around it, but for most practical problems it may be considered to be negligible.

However, in the case of single-component, two-phase flow, part of the trapped phase can disappear when it is not in thermodynamic equilibrium with its surroundings. Depending on the local thermodynamic conditions, a cluster of trapped phase can either grow until it finds a continuous path across the flow domain or it can disappear altogether due to phase transformation. Therefore, irreducible phase saturation in single-component, two-phase steady flow also depends on the thermodynamic conditions in the flow domain.

This work presents a comprehensive study of the effects of phase transformation on two-phase flow of steam and water in porous media. In Chapter 2 we review many experimental studies of two-phase, two-component relative permeabilities to show that the results of the studies have been inconsistent and sometimes inconclusive. We point out some experimental pitfalls that may have plagued past experiments resulting in conflicting results.

Chapter 3 is devoted to the development of some key physical concepts and relationships pertaining to pore level equilibrium and transport of steam and water. We visualize a porous medium as an interpenetrating network of solid matrix and void space in which only one fluid phase is present in any part of the

pore space at any time, apart from thin films and the pendular structure of the wetting phase. We also consider the thermodynamics of curved interfaces and thin films.

Chapter 4 presents the description of the numerical technique which has been used in this study. Numerical simulation was used to (i) design the experiment and obtain optimum operating conditions, (ii) verify the results of the experiment, and (iii) verify the results of the theoretical study.

Chapter 5 presents a new solution technique for two-phase steam and water flow in a flow channel of arbitrary cross section. The first and the second laws of thermodynamics are combined to obtain the temperature distribution in a steady state one dimensional, concurrent flow of steam and water in a flow channel of varying cross section. We use these results to determine the effects of phase transformation on effective permeability of a torroidal flow channel. The conditions for phase trapping are also presented.

The experimental investigation carried out in this work is described in Chapter 6. A numerical study was initially made using the three-dimensional, two-phase steam-water flow code, MULKOM, to arrive at the best experimental design and parameters. The numerical results indicated that the capillary discontinuities at the ends of the flow column could cause very large saturation gradients near the ends. This indicated it would be difficult to interpret data in this regime for the purpose of obtaining relative permeability and capillary pressure functions. End effects were minimized in the experiment by using a rather long (100 cm) insulated column packed with beads of 100 micron grain size. Double-

deionized, degassed water was pumped into the column at a controlled rate. Upon entering the column, a fraction of the water was flashed into steam by means of electrical resistance heaters causing two-phase concurrent flow in the column. Temperature, vapor pressure, and liquid pressure were measured at regular intervals along the column. Saturation readings were obtained with the aid of a γ-ray densitometer. From the experimental data we obtained relative permeability and capillary pressure as a function of saturation for the porous medium. These functions were subsequently used in the numerical model to simulate temperature, pressure, and saturation along the entire column. Good agreement with the experimental results was found, thus confirming the relative permeability functions and capillary pressure curves obtained.

The discussion of the theoretical and experimental results of this work is given in Chapter 7. The combination of these two approaches makes it possible to present a complete picture of how phase transformation effects make steam-water relative permeabilities different from those for two-component, two-phase fluids.

CHAPTER 2

RELATIVE PERMEABILITY: THE CONCEPT AND PREVIOUS INVESTIGATIONS

2.1 INTRODUCTION

The scientific investigation of fluid flow through porous media started with Darcy's experimental observation in 1856 that in creeping flow of water through a column packed with sand the applied mechanical potential between the two ends of the sample brings about a proportional change in the flow rate of water. He enunciated his observation as a difference equation commonly known as Darcy's law. What is useful in the description of practical flow problems is not the difference form Darcy proposed but a differential form correlating the local mechanical potential gradient to the local fluid velocity in porous media. It is understood that both these quantities represent values averaged over a volume element, known as a Representative Elementary Volume or REV, surrounding the point under consideration and large compared to the individual pores but small compared to the total domain of interest. When the porous medium is sufficiently homogeneous at the REV scale, volume averaging of the differential form (or Navier-Stokes equation) leads to the difference form (Slattery, 1967; Philip, 1969; Whitaker, 1969).

The proportionality constant (K) in Darcy's equation:

$$q = -K \nabla \Phi \tag{2.1}$$

is known as hydraulic conductivity and it depends on the absolute viscosity of the fluid and the intrinsic permeability of the porous medium. The intrinsic

permeability (k) is a property of the porous medium alone. It is a scalar constant for an isotropic medium and a symmetrical second-order tensor with constant coefficients for an anisotropic porous medium (Scheidegger, 1960). For creeping flow of a single, incompressible, Newtonian fluid through a rigid porous medium completely filled with that fluid, the intrinsic permeability remains constant because the stream lines are independent of the flow rate as long as the pore Reynold's number is smaller than unity. This phenomenon does not hold when two or more fluids simultaneously flow through porous media.

When two or more fluids flow simultaneously through a porous medium, the pore-level distribution of fluids is governed by well defined laws of physics. The fluids are distributed in the pore space through interaction of the viscous and the capillary forces such that: (i) there exists a local chemical potential and mechanical force equilibrium at each point of the fluid-fluid and fluid-solid interfaces, and (ii) generation of entropy for a given flow rate is minimized. Therefore, the fraction of the void volume occupied by each phase (or, phase saturation) changes with the flow rates of the phases that are simultaneously flowing through (or occupying) the porous medium to satisfy the two conditions stated above. A change in saturation of a phase implies that, in general, the fraction of pore-space that is available to the said flowing phase, changes, causing the stream lines to change with the flow rates. This implies that a change in saturation of a phase will generally not bring about a proportional change in the effective permeability of that phase.

The simultaneous creeping flow of two or more fluid phases in porous media was first described macroscopically by extending Darcy's law to apply to each phase by Buckingham (1907). The permeability to each phase was modified to account for the presence of other fluid phases by multiplying the intrinsic permeability with a scaling factor termed "relative permeability" (k_r) (Hassler et al., 1936). These factors for two-phase flaws are traditionally represented as a set of curves shown in Fig. 2.1. Here S is the wetting phase saturation and k_r represents relative permeabilities. The saturation limits S_r and $S_r^{(n)}$ are known as residual saturations and they represent, respectively, the saturations at which the wetting phase or the non-wetting phase becomes immobilized (or trapped). Similarly, S_m and $S_m^{(n)}$ represent the saturation limits at which the wetting phase or the non-wetting phase, respectively, became fully mobile. The relative permeability of phase i is given by the familiar formula:

$$k_{ri} \equiv \frac{Q_i}{A} \frac{\mu_i}{k} [\nabla \Phi_i]^{-1} \tag{2.2}$$

This definition seems to account for the fluid viscosity in μ_i and the pore space in k, so that the relative permeability depends solely on the division of the pore volume amongst the fluids, i.e., on their saturations, which sum to unity. Therefore, for the case of two phases, the relative permeabilities should depend on only one variable — the phase saturation of one of the phases. In reality the situation is much more complicated (Heiba et al., 1982).

Theoretical studies of multi-phase flow through porous media have been conducted by many investigators who used the volume averaging technique to

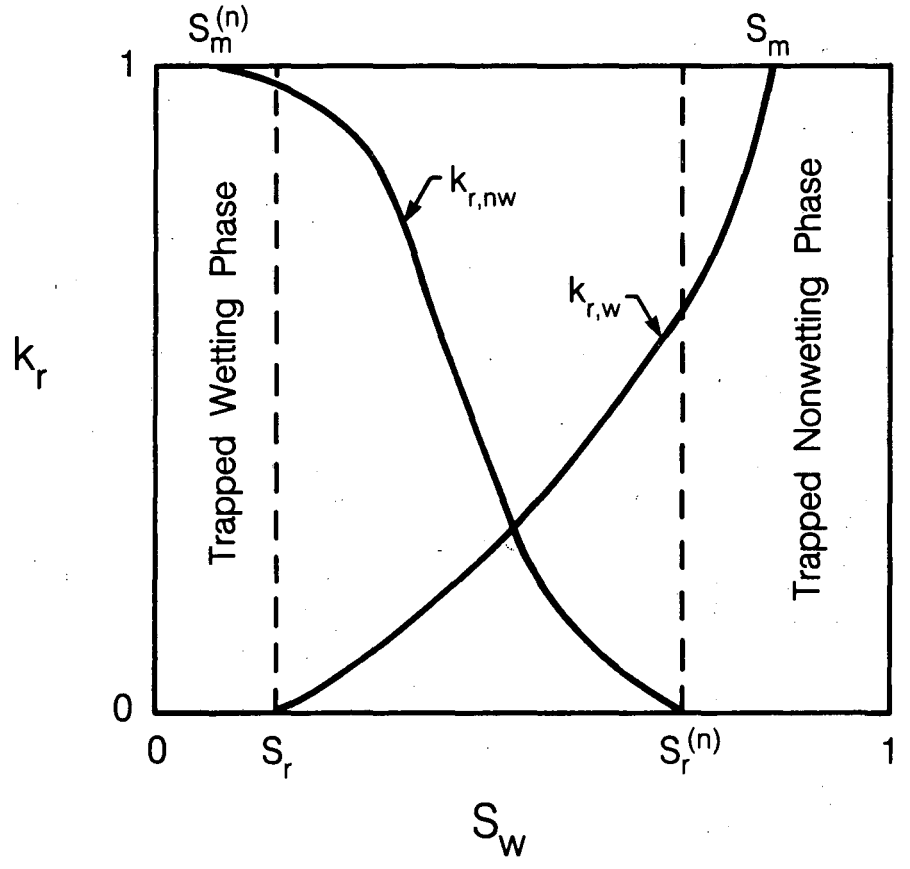

XBL 8511-12657

Fig. 2.1. A typical set of relative permeability curves for two-phase flow.

propose macroscopic descriptions of this phenomenon (e.g., Gray, 1975; Slattery, 1968, 1970; Solbrig and Hughes, 1976). However, direct application of their results to practical problems is far from trivial because one needs to determine parameters which depend on the nature of the porous medium (Cheng, 1978) and, therefore, they are sample specific. The complex nature of pore-space geometry makes it practically impossible to obtain these parameters theoretically even with the aid of modern digital computers. Moreover, all these investigators have presented their formulation for isotropic porous medium only, though Slattery (1967) has proposed a way to extend his analysis to anisotropic cases.

Another group of investigators has based their theoretical study of this phenomenon on either "effective medium approximation" (Bruggeman, 1935; Blackman, 1976; Ahmed and Blackman, 1979) or on "percolation theory" (Broadbent and Hammersley, 1957; Shante and Kirpatrick, 1971; Heiba et al., 1982). The underlying philosophy behind these approximations is that while an exact description of the whole pore-space is hopelessly complex, a statistical description of the pore-space can adequately represent the porous medium for purposes of modeling the essential physics of the two-phase flow through it. While these studies have shed some light on the underlying physical processes behind the phenomenon of relative permeability, they have failed to provide a comprehensive theory of it. The responsibility of presenting a quantitative description of multiphase flow through porous media rests on experiments alone (Heiba et al., 1982). The experimental works also may provide further insight into the physical

processes and, therefore, may lead to more rigorous theoretical treatment of this subject.

In a pioneering work, Leverett (1939) conducted a series of experiments on high permeability (6.8 to 3.6 Darcies), unconsolidated sand samples. He used mixtures of water and oil of different viscosities (viscosity ratio, $\mu_o/\mu_w = 0.057$ to 90.0) and concluded that relative permeabilities depend on phase saturations. A similar claim was made by Gaffen et al., (1951), who concluded that the relative permeabilities for a given set of fluids and a porous medium depend *only* on the fluid saturation within the porous sample. This assumption is often made to this date for two reasons: (i) no conclusive, quantitative representations of dependence of relative permeabilities on other variables exist and (ii) relative permeabilities as functions of saturation alone make the computational effort less tedious. However, in light of ever increasing complexity of problems requiring mathematical description of multi-phase flow in porous media, the validity of the above mentioned assumption becomes questionable in some cases. For example, when steam is injected in a petroleum reservoir, there may be an extended non-isothermal region of multi-phase flow. It is not hard to visualize that the relative permeabilities in this region may vary substantially for identical phase saturations. There are many other practical examples where some property or parameter variation within the domain of interest may cause the relative permeability functions to become non-unique functions of phase saturation. Moreover, there has always been a need to understand how different properties and parameters affect the relative permeability functions in order to develop a theory of this

phenomenon. Many investigators, therefore, have studied the effects of different factors, such as: (1) viscosity ratio of the fluids; (ii) wetting characteristics of the fluids; (iii) interfacial tension, or more generally, the capillary number; and (iv) saturation history, on relative permeability of two-phase two-component fluids. There results, however, are not always in agreement with one another and doubts about quantitative representation of relative permeabilities on these factors persist. Knowledge about steam-water relative premeabilities is even more sketchy and to the best of my knowledge, there is not even one experimental curve presented in existing literature.

2.2 FACTORS AFFECTING RELATIVE PERMEABILITY

Among all the factors affecting relative permeabilities, the effects of temperature have probably been studied the most (Edmondson, 1965, Davidson, 1969, Poston et al., 1970, Weinbrandt et al., 1975, Lo and Mungan, 1973, Sufi et al., 1982, Maini and Batycky, 1983, Miller, 1983, etc.). It is my contention that a change in temperature causes changes in temperature-dependent properties and phenomena such as: surface tension of the fluids, viscosity ratios, capillarity, wettability and absolute permeability of the porous matrix. Hence, the observed change in the relative permeabilities, due to a change in temperature, is the cumulative effect of all these factors. Since all these factors, in general, will affect the relative permeability functions in different ways, their cumulative effect, in general, will be different for different sets of fluids and core samples. Therefore, it is not surprising that the observations of the above mentioned investigators are

not in agreement. For example, Edmondson (1965) and Weinbrandt et al. (1975) report that relative permeabilities change with temperature. Edmondson reports that relative permeability ratios decrease with temperature at higher water saturation, but increase with temperature at lower water saturations. According to Weinbrandt et al., relative permeability for oil shifted towards higher water saturation with increasing temperature, while the relative permeability for water showed no dependence on temperature. On the other hand, Poston et al. (1970) and Sufi et al. (1982) conclude that the relative permeabilities of oil and water do not depend on temperature. Sufi et al. go even further and comment that the temperature effects may be more a result of measurement difficulties and laboratory scale phenomena rather than the actual flow behavior.

The fact that relative permeability of a given phase, at a specific saturation, depends on saturation history has been shown by many investigators (e.g., experimental works of Johnson et al., 1959 and Naar et al., 1962; and theoretical work by Heiba et al., 1983). This seems to indicate that relative permeability of a given phase not only depends on the fraction of void volume occupied by that phase, but also on how the phase is distributed within the pore space.

Effect of viscosity ratio on relative permeabilities is controversial. It is believed that viscosity ratio will affect the relative permeabilities if both fluids coexist in flow channels made of interconnected pores and they exert appreciable shear stress on each other (Yuster, 1951). Experimental evidence (Chatenever and Calhoun, 1952) shows that when oil and water flow simultaneously through porous media, each fluid occupies its own set of channels. If we assume this

phenomenon to be universally true then viscosity ratio will not affect the relative permeability functions. However, based on experimental observations, some investigators (Downie and Crane, 1961, Odeh, 1959, Schneider and Owens, 1980, etc.) claim that relative permeabilities do depend on viscosity ratio while others (Laverett, 1939, Richardson, 1957, etc.) claim just the opposite.

Effects of wettability on the relative permeability have been a subject of many investigations. It is postulated that wettability affects the distribution of fluids within a porous medium, which in turn has a strong influence on relative permeability characteristics (Coley et al., 1956, Donaldson et al., 1966, Owens and Archer, 1971, McCaffery and Bennion, 1974, Heiba et al. 1983, etc.). All these investigators, with the exception of Heiba et al., have experimentally studied the effect of wettability on the relative permeabilities. Heiba et al. have used percolation theory to model the effects of wettability and with aid of this model, they have matched the experimental results of other investigators such as: Treiber et al. (1972), Owens et al. (1971), and Reed and Healy (1977). In spite of the general agreement that the relative permeability functions do indeed depend on rock wettability, a quantitative description of the phenomenon has not emerged because of two major difficulties: (i) inability to measure wettability by using a core sample and a pair of fluids, and (ii) inability to isolate the wettability as a single variable (Hjelmeland and Larrondo, 1983).

The effects of interfacial tension, or more generally, the capillary numbers, (a dimensionless group describing the ratio of viscous to capillary forces) have been studied by many investigators. In an experimental study of oil and gas, Bordon

and Longeron (1980) observed that a decrease in interfacial tension (i.e., increase in capillary number) causes relative permeabilities to increase and become more or less linear at very low interfacial tension. Fulcher et al. (1983), in their experimental study of oil/water flow, observed that while the non-wetting phase (oil) relative permeability showed little correlation with the capillary number, the wetting phase (water) relative permeability increases with an increase in capillary number. In an experiment on artificial cores, Lefebvre du Prey (1973) also observed that relative permeabilities increase with increasing capillary number. Most observations indicate that when the interfacial tension decreases, the relative permeability curves tend to be linear because the nature of flow tends to be that of miscible fluids; this happens due to decrease in interfacial tension.

While there seems to be some agreement about the effects of capillary number and interfacial tension, contradictory results have been reported about the effects of flow velocity, one of the components of capillary number, on relative permeability. For example, while Osoba et al. (1951), Richardson (1957), Sandberg (1958) and Fulcher et al. (1983) report little or no changes due to flow velocity, Heaviside (1983) reports that flow velocity changes the relative permeability of water in oil/water flow.

Thus, it can be concluded that the experimental observations of the effects of various properties and parameters on the relative permeabilities have been inconsistent and inconclusive. These inconsistencies could be due in large part to: (i) failure to isolate the effects of the variables under study, and (ii) the inherent shortcomings of the experimental setups used by the investigators.

Two main sources of errors in the experimental studies are due to: (i) capillary pressure gradient and the end effects resulting from it (Gaffen et al., 1959, Rapoport and Leas, 1953, Perkins, 1957, Kyle and Rapoport, 1958, Batycky et al., 1981, etc.), and (ii) averaging of saturation over the whole core length when there is a substantial saturation gradient in the core and assigning the measured relative permeabilities to the averaged phase saturations.

The experimental procedures used by most of the investigators mentioned previously, are versions of one of the standard methods such as: Penn-State method, Hassler Method, Single Core Dynamic Method, etc. (Described in Osoba et al., 1951). In these experiments, the pressure gradient in the core sample is assumed to be linear and it is evaluated by measuring pressures at either end of the core sample (with the exception of Richardson, 1957 and Arihara et al., 1976). Since the end effects will cause, in general, the pressure distribution to deviate significantly from a linear profile due to capillary pressure, the pressure gradient thus evaluated will, in general, be incorrect. This causes the use of a wrong pressure gradient in interpretation of the experimental data to evaluate the relative permeability of at least one of the phases.

Saturations of the two phases are evaluated by interpreting the volumes of each of the phases in the core sample and dividing them by the total pore volume. The saturation thus obtained is the average saturation over the whole core sample. In actuality, the capillary forces at the ends cause a saturation gradient within the core sample (Osoba et al., 1951, Batycky et al., 1981) and hence, the observed relative permeabilities are the averaged values of the relative

permeabilities at different saturations in the core sample. Since the nature of this averaging process over a range of saturations is unknown, it is incorrect to assign the observed relative permeability to the averaged saturation when the saturation gradients are large.

Although it is argued that the above mentioned experimental techniques alleviate the end effects (see Osoba et al., 1959) the validity of this claim remains questionable because both the Hassler and the Penn-State approaches suffer from significant experimental and interpretive problems (Batycky et al., 1981 and Rose, 1979). Moreover, most of the previously mentioned investigators studying oil/water relative permeabilities, have not mentioned any effort to reduce the end effects. Therefore, it is impossible to identify error-free experimental observations amongst all the works mentioned above. Furthermore, we stress again that an experimental procedure must be free of the two errors mentioned above, for meaningful results.

2.3 PREVIOUS WORK ON STEAM-WATER RELATIVE PERMEABILITY

Direct application of the above mentioned works to steam-water (or any single-component two-phase) relative permeability is questionable because of an additional degree of freedom: phase transformation. Phase transformation phenomenon is expected to have a significant effect on the nature of relative permeability curves (Verma et al., 1985). The effects of other factors mentioned previously on the relative permeabilities of steam and water are not known because there have been very few studies in this field. For example laboratory scale

experiments have been reported by Chen et al. (1978) and Counsil and Ramey (1979). Both these experiments were conducted using the same experimental setup, has been described elsewhere in a paper by Arihara et al. (1976). They performed their studies on synthetic, consolidated cores mounted in a Hassler-type sleeve and obtained their readings within a very narrow zone of saturation. Data points reported by them are so few that it is hard to draw any conclusions about the relative permeability functions. Moreover, Counsil and Ramey (1979) observed some undesired anisotropy caused by the capacitance probe guide and suggest that either γ-ray or some other external saturation measuring device be used in place of capacitance probes.

A completely theoretical model was proposed by Menzies (1982) and Gudmundsson et al. (1983). They have modified and used a streamtube model (Wallis and Richter, 1978) to obtain a unique set of relative permeability functions for steam/water flow. This model was originally developed to study the effect of phase transformation on vapor-liquid flow in high speed jets. The modified version of the model fails to acknowledge the existence of porous media except as a heat source. Hence, this model completely ignores the effects of viscous and capillary phenomena on relative permeability functions. The validity of ignoring these effects has not been justified. Therefore, there is a lingering doubt about validity of their results.

Grant (1977), Horn and Ramey (1978), and Shinohara (1978) have used flow rate and enthalpy data from geothermal wells to obtain information about in-situ relative permeability functions. The analysis technique in all of these works is

essentially the same as that of Grant (1977). Grant's technique involves a set of assumptions, which have not been established either theoretically or experimentally, thus casting doubt on the reliability of the conclusions drawn from such an analysis. Furthermore, the results obtained by Grant's technique present relative permeabilities as functions of flowing enthalpy. Since such functions can not be used in simulation studies of geothermal reservoirs, different representations need to be developed.

CHAPTER 3
PORE-LEVEL DISTRIBUTION OF STEAM AND WATER IN POROUS MEDIA

3.1 INTRODUCTION

The relative permeability factor in fluid flow is an empirical representation of a well defined pore-level transport process in a highly chaotic pore space. Pore-level distribution and transport of multiphase fluids is governed by continuum-level laws of physics such as the Navier-Stokes equation, continuity equation, diffusion equation and the boundary conditions at fluid-fluid, solid-fluid interfaces and at solid-fluid-fluid contact lines (Mohanty and Salter, 1982). Direct implementation of these laws to flow in porous media to predict macroscopic transport properties is virtually impossible, even with the aid of large, modern digital computers, because of the highly complex morphology of naturally occurring porous media. However, an understanding of these pore-level phenomena is essential in defining, at least qualitatively, how different physical mechanisms affect relative permeability. The present chapter discusses some of the key physical concepts which are essential to understand relative permeabilities of a porous medium to steam and water. A geometric description of pore space is presented in Section 3.2. Details of the pore space network and its statistical representation have been omitted because no theoretical attempt was made to predict the relative permeability functions.

The phenomenon of boiling is discussed in some detail in Section 3.3. Knowledge of this phenomenon is essential for determining the location of phase

transformations in the concurrent flow of steam and water. The relationships obtained in this sections are subsequently used in Section 3.4 to determine the thermodynamic stability of steam-water interfaces. All these concepts are integrated in Section 3.5 to present a qualitative picture of the distribution of steam and water in the pore space of porous media.

3.2 STRUCTURE OF POROUS MEDIA

A porous medium is an assemblage of void space and solid matrix in which both the void spaces and the solids form interpenetrating networks. The morphology of naturally occurring porous media, especially in porous sedimentary rocks, appears to be highly chaotic, so much so that the possible configurations can only be statistically known. The cross-sections of pore segments are also highly chaotic and vary considerably from point to point. Pore walls are often rough and highly non-uniform in curvature (Wilson and Pittman, 1977; Wardlaw and Cassan, 1978; Almon, 1977; Brown et al., 1980). Sometimes the minerals on these surfaces vary considerably in chemical composition. An exact description of the whole space is very (and needlessly) complex. The minimum description needed for modeling the essential physics of a given process in such a medium depends on the process itself.

The simplest model that can be used to describe the flow of a single fluid in the pore spaces is the "bundle-of-capillary" model. An excellent review of this approach is given by Van Brakel (1975). The fact that these models are too simplistic to adequately represent the essential capillary phenomena in multi-

phase flow at pore level has long been recognized (Fatt, 1956; Rose and Witherspoon, 1956). Fatt (1956) proposed network models for flow of fluid through porous media in which a multitude of capillaries is arranged in the form of a rectangular network. Rose and Witherspoon (1956) used a "doublet" or a branching capillary flow path to study entrapment of oil in waterflooding. In spite of the inherent simplifying assumptions that the pore spaces are circular capillaries of uniform cross-section, these models served their purpose well.

Later, when more detailed physics of multi-phase flow through porous media was considered, the demands made on such models of pore-spaces also grew. For example, it was recognized that the dynamic displacement of oil by water is controlled by pore level phenomena of chock-off: spontaneous rupture of an oil-neck due to instability of a neck meniscus, and hygron: spontaneous withdrawal of head menisci out of a pore body (Melrose and Brander, 1974). The geometric details of a pore space in models capable of representing the above mentioned phenomena must include the diverging-converging characteristics of real pore spaces. Such models have been used recently by many investigators (e.g., Koplik and Lassetor, 1982; Heiba et al., 1983; Mohanty et al., 1982; Roof, 1970; Arriola et al., 1980.)

Another important feature of the void space considered in recent studies is their high "genus" internal surface; i.e., the pore space is highly interconnected. The connectedness of a network is measured by the average number of distinct continuous pathways which exist between any pair of sites (Graham, 1973). For a given pore space, the connectedness of a network of branches describing the

pore space is roughly equivalent to the genus of the internal surface separating solid matrix from void. Since this representation of connectedness does not lend itself to straightforward mathematical description of practical problems, most investigators (e.g., Mohanty and Salter, 1982; Larson et al., 1981; Heiba et al., 1983) have used "branchiness" of the pore network instead. Branchiness of a network is characterized by co-ordination number, z—number of flow paths connecting a pore to its nearest neighbors.

Two key features of porous media considered in this study are: (1) converging-diverging cross-sections of pore segments, and (2) roughness and irregularity of pore walls. Figure 3.1 shows a schematic cross section of pore spaces in porous medium. The larger of the void segments shall be referred to as "pore body" and the narrower segments connecting the pore bodies shall be referred to as "pore throats." The size of the pore bodies will be represented by the largest of the locally maximum radii of inscribed spheres, r_b, and the size of the pore throat will be represented by the smallest radius of inscribed sphere, r_t. The method of determining these dimensions is rather involved and beyond the scope of this study. The details of the technique are discussed by Pathak (1980). For the present purpose we shall define the "pore throat radius," r_t, as a measure of the smallest mean curvature that a static convex fluid-fluid meniscus can take at any location between the adjacent pore bodies, and the "pore body radius," r_b, as a measure of the largest mean curvature that a static fluid-fluid meniscus can take within a pore body. Moreover, for the purpose of analysis we shall assume

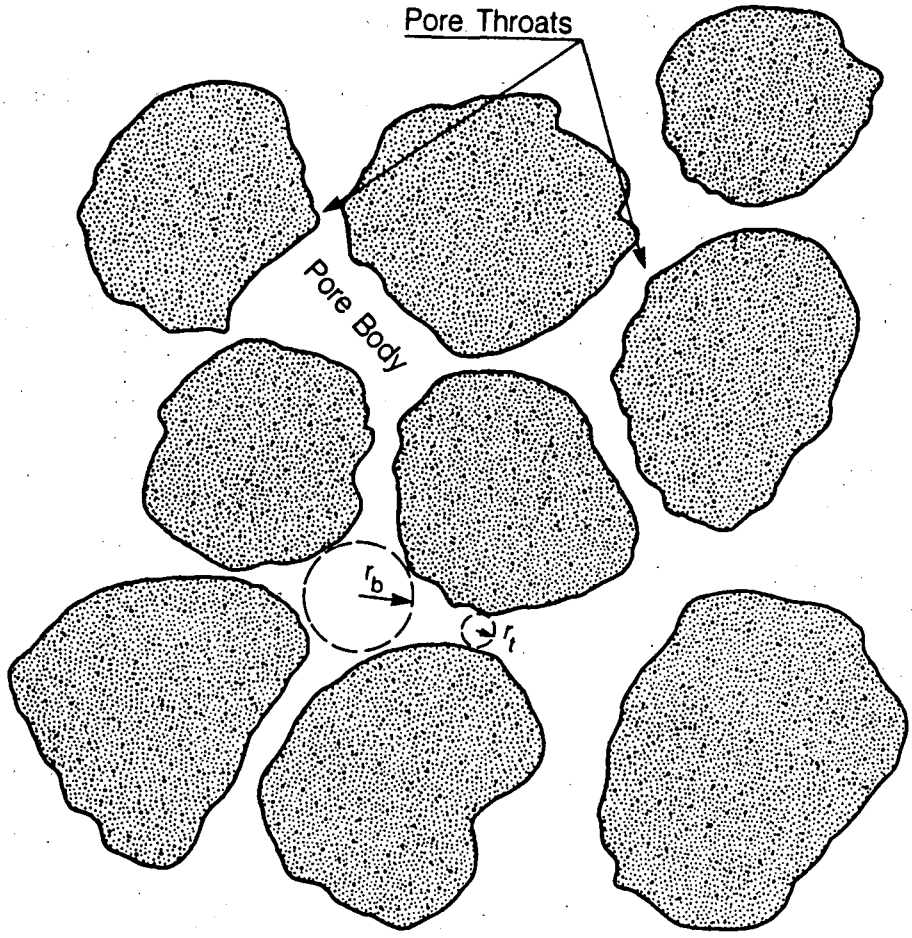

Fig. 3.1. Schematic of pore space in porous media.

that the pore throats are torroidal (Fig. 3.2).

The pore space is considered to be a three-dimensional network of flow channels, consisting of randomly distributed pore bodies connected by pore throats. Depending on its connectivity, a pore, or a cluster of pores, is considered to be (a) sample spanning—when the pores form several flow channels that provide continuous pathways from the inlet face of the sample to the outlet, (b) isolated—when the pore is not connected to any sample spanning flow channel, inlet surface, or outlet surface, and (c) denderatic—when there is only one pathway between the pore (or a cluster of pores) and the sample spanning flow path. Therefore, although these pores are connected to a sample spanning flow path, no flow takes place across denderatic pores.

3.3 PHENOMENON OF BOILING

3.3.1 Overview

The term "boiling" is generally associated, often incorrectly, with the phenomenon of phase transformation from water to steam at a temperature of 100 ° C and 1 atm pressure. This representation is correct only when the water molecules escape from liquid phase into vapor phase across a planar liquid-vapor interface maintained at a temperature 100 ° C and 1 atm pressure. This pressure and temperature are known as saturation pressure (P_s) and saturation temperature (T_s). The locii of these two thermodynamic properties, for a pure substance, are known as the saturation surface (Fig. 3.3). Along this surface the liquid

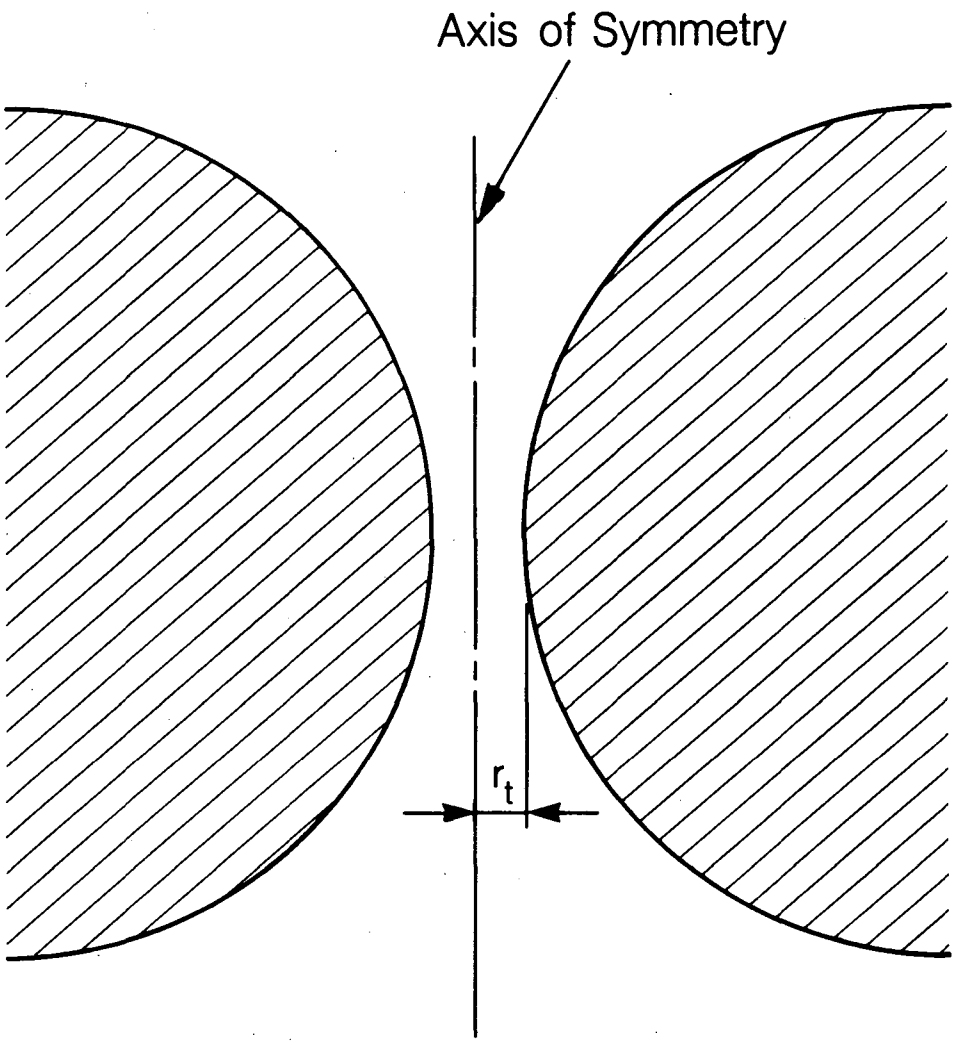

XBL 8511-12645

Fig. 3.2. Schematic of idealized torroidal pore throat.

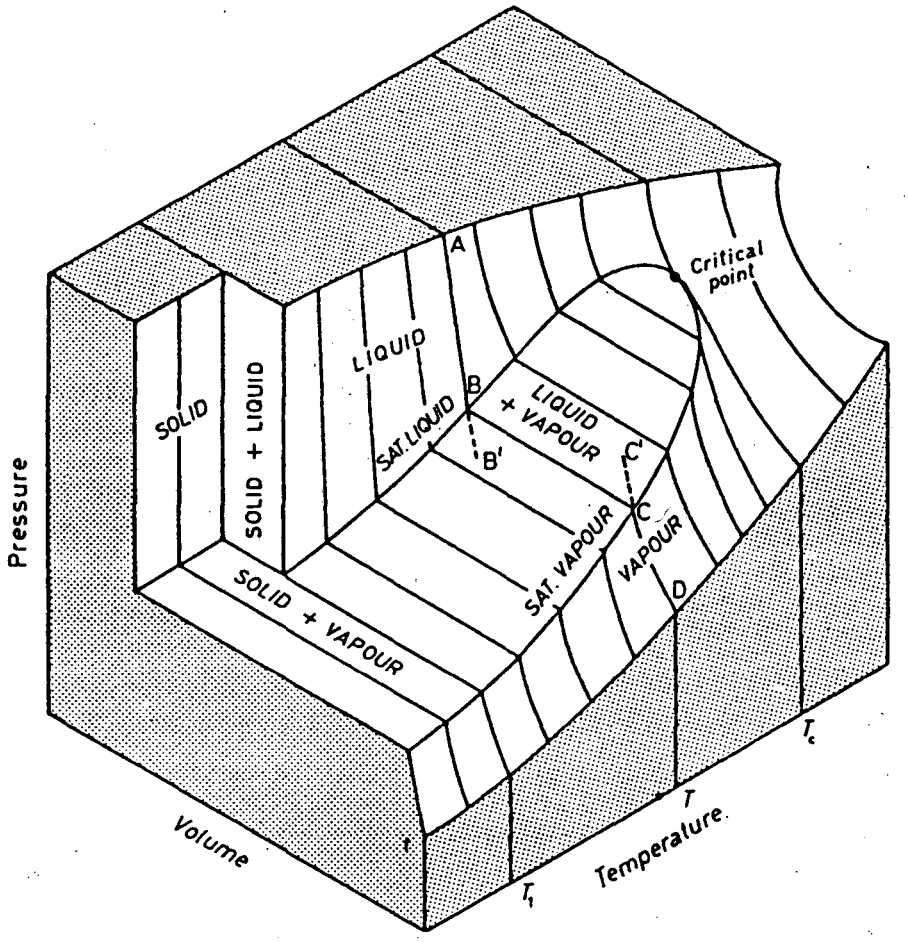

Fig. 3.3. Pressure-volume-temperature (PVT) diagram for a pure substance.

phase and the steam phase are at equal pressure and temperature (P_s and T_s) and they are considered to be in an equilibrium thermodynamic state. These conditions are not met when boiling (or creation of bulk steam phase) is caused by heating of liquid water in the absence of a pre-existing liquid-vapor interface. (NOTE: From here on the term "boiling" will refer to creation of bulk steam phase at places other than pre-existing water-steam interface. "Evaporation" will be used to describe the process that takes place at a pre-existing water-steam interface.)

It is well known that boiling in a pure substance free of dust particles takes place at a temperature (T_b) significantly higher than the saturation temperature (T_s) at the co-existing pressure (Leppert and Pitts, 1964; Knapp, 1958; Kast, 1964; Bankoff, 1957, etc.). The reason for the required superheating ΔT_{sh} ($T_b - T_s$) is explained in terms of the phenomenon of "nucleation" discussed below.

3.3.2 Nucleation Theory

When the temperature of pure water, in the absence of any pre-existing liquid-vapor interface, is raised to (or slightly above) T_s, no spontaneous formation of vapor phase takes place because of the high activation energy required to start creation of a new phase (Chapter 6, Hiemenz, 1977). Instead, vapor molecules came together and break apart forming clusters of different sizes due to flocculation. The free energy of formation of a cluster of radius r is given by (Adamson, 1982)

$$\Delta G = 4\pi r\gamma - \frac{4}{3}\pi r^3 \rho_v RT \ln \frac{P_v}{P_l} \tag{3.1}$$

Since the two terms on the right hand side are of opposite sign when $P_v > P_l$ and depend differently on r, a plot of ΔG versus r goes through a maximum (shown qualitatively in Figure 3.4). It can be seen from Figure 3.4 that on the left of the maxima an increase in the size of the cluster (or nucleus) is associated with an increase in ΔG until the size reaches a critical radius (r_c), after which the trend is reversed. Therefore, if the activation energy is increased slightly above a level where clusters can grow to a size of r_c, the clusters will grow spontaneously to form the bulk vapor phase and boiling will commence. This phenomenon is the basis for the theory of nucleation. The phenomena of nucleus formation within pure liquid, in the absence of any foreign activation sites, is known as homogeneous nucleation. The cases where nucleation takes place around a foreign body, such as a cluster of molecules of dissolved gases or trapped gas molecules in pits and cavities of a solid surface, are referred to as heterogeneous nucleation and solid nucleation, respectively. In the subsequent discussion of these processes, we will start from the stage where some molecules of vapor have come together to form a nucleus (or vapor bubble). A complete discussion of how a nucleus is first formed is beyond the scope of this work and the interested reader is referred to Chapter XIII of Defay and Prigogine (1966).

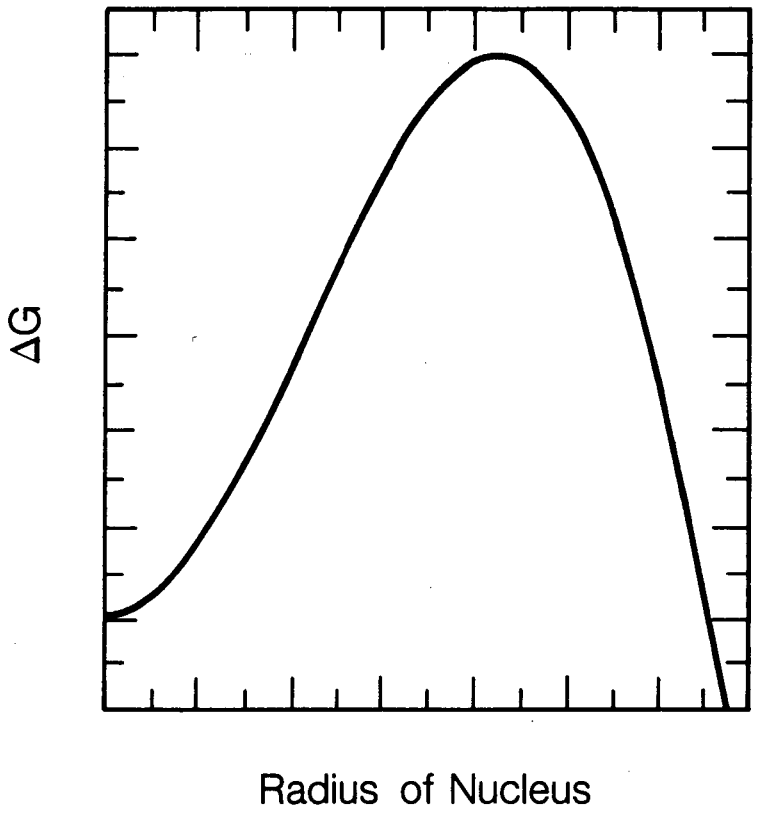

Figure 3.4. Variation of free energy of formation (ΔG) of a nucleus.

3.3.3 Superheat Required for Bubble Formation

At onset of nucleation, first a few molecules of vapor come together forming a "bubble" of vapor separated from bulk liquid by a curved interface. In such a configuration vapor located on the concave side of the interface is at a higher pressure than in the liquid phase. Because of the increased vapor pressure the number of molecules striking and being absorbed by the interface from the vapor phase is greater than when the interface was planar at the same temperature. To maintain equilibrium the number of molecules emitted through the interface from the liquid phase must increase correspondingly and be equal to the molecules being absorbed from the vapor phase. This increase can only be accomplished by increasing the temperature of the system (liquid + bubble) above that necessary for equilibrium with a planar interface, i.e., the saturation temperature (T_s) corresponding to liquid pressure (P_s). This bubble is said to be in a state of metastable equilibrium with the liquid. We consider the metastable equilibrium of a spherical vapor bubble of radius r in a liquid at temperature T_l and pressure P_l. The pressure in the vapor phase (P_v) is given by familier Young-Laplace equation

$$P_v = P_l + \frac{2\gamma}{r} \tag{3.2}$$

where γ is the surface tension of vapor-liquid interface. The relation between P_v and P_∞ — the saturation pressure corresponding to temperature T_l, is given by Kelvin's equation (Defay and Prigogine, 1966)

$$P_v = P_\infty \exp(-2\gamma v_l / rRT) \tag{3.3}$$

The correlation between temperature and saturation pressure is given by the Clasius-Clapeyron equation

$$\frac{dP}{dT} = \frac{h_{lv}}{T(v_v - v_l)} \tag{3.4}$$

Assuming ideal gas law for vapor ($P_v v_v = RT$) and solving Eqs. (3.2), (3.3), and (3.4) simultaneously, we obtain the degree of superheat needed to maintain a bubble of radius r in metastable equilibrium with bulk liquid at pressure P_l and temperature T_l. It is given by equation (see Appendix 3.A)

$$T_l - T_s \equiv \Delta T_{sh} = \frac{RT_s^2}{h_{lv}} \frac{2\gamma}{P_l r} \tag{3.5}$$

Equation (3.5) shows that the degree of superheat is inversely proportional to the size of the bubble and also that at a given superheat (ΔT_{sh}) only the bubbles with radius

$$\tilde{r} = \frac{RT_s^2}{h_{lv}} \frac{2\gamma}{P_l \Delta T_{sh}} \tag{3.6}$$

will remain in metastable equilibrium with the liquid around it. Bubbles smaller than $\tilde{r}$ will collapse and bubbles larger than $\tilde{r}$ will grow spontaneously.

3.3.4 Superheat for Homogeneous Nucleation

Homogeneous nucleation is not exactly a thermodynamic phenomenon (chapter XVII, Defay and Prigogine, 1966). In this process the nuclei are formed by "flocculation" — defined as a process whereby small particles clump together and move as a single unit but retain their identity: only their kinetic indepen-

dence is lost. The onset of boiling is associated with the rate of formation of critical nuclei, which depends on the degree of superheat. This approach, however, does not lead to a straightforward way of evaluating the degree of superheat required to start boiling. A simpler empirical equation for the required super heat was suggested by Lienhard (1976)

$$T_{rv} - T_{rs} = 0.905 - T_{rs} + 0.095\ T_{rs}^{8} \tag{3.7}$$

where T_r represents absolute temperature divided by the critical temperature ($T_r = T/T_c$). This relationship gives a superheat (ΔT_{sh}) of 220.7 °C for liquid water at atmospheric pressure.

3.3.5 Superheat for Heterogeneous Nucleation

Heterogeneous nucleation refers to the phenomenon in which the nuclei form around foreign bodies such as non-condensible gas bubbles held in suspension or gas filled cracks or cavities in the container surface. The superheat required to maintain an air-vapor bubble of radius r in metastable equilibrium is given by (see appendix 3.B)

$$\Delta T_{sh} = \frac{RT_sT}{h_{lv}} \ln \left\{ 1 + \frac{2\gamma}{rP_l}\left(1 + \frac{v_l}{v_v}\right) - \frac{p_a}{P_l}\left(1 + \frac{v_l}{v_v}\right)\right\} \tag{3.8}$$

where p_a is the partial pressure of non-condensible gas such as air in the vapor phase and other symbols have their usual meaning. Comparing this equation to Eq. (3.A.10) of Appendix 3.A, we conclude that the presence of non-condensible gas reduces the superheat requirement compared to the homogeneous case for a given bubble radius in the same thermodynamic environment.

When a bubble of radius r and partial pressure of air p_a starts to grow due to phase transformation, it can be assumed that the rate of increase in mass of the vapor is much larger than the rate of increase in air, because air enters the bubble by diffusion—a slower process. Therefore, the mole fraction of vapor (x_v) increases and the mole fraction of air (x_a) decreases when the bubble grows. An increase in bubble radius also results in lower gas phase pressure ($p_v + p_a$) if the liquid pressure remains unchanged (Eq. (3.B.1)). Since the partial pressure of air in the bubble is proportional to the mole fraction of air in the bubble, an increase in bubble size is accompanied by a reduction in p_a over and above a proportional change due to reduction in gas phase pressure. Therefore, the last two terms on the right hand side of Eq. (3.8) decrease when the bubble grows in size due to vapor formation while P_l remains unchanged. These two terms have the opposite effect on ΔT_{sh}. Therefore, a bubble can grow only if the combined effect of the last two terms on the right hand side do not contribute to an increase in ΔT_{sh} when the bubble grows.

In order to identify appropriate conditions for heterogeneous nucleation let us consider a bubble of radius r containing n_a moles of air, in liquid at pressure P_l and temperature T. The partial pressure (p_a) of air in the bubble is correlated to n_a and volume (V) of the bubble by

$$p_a = \frac{n_a R\, T}{V} \tag{3.9}$$

where $V = \frac{4}{3}\pi r^3$. Boiling due to heterogeneous nucleation in the liquid at

steady pressure (P_l) and temperature (T) can proceed if

$$\frac{d(\Delta T_{sh})}{dv} \leq 0 \tag{3.10}$$

Substituting for ΔT_{sh} from Eq. (3.8), assuming $v_v >> v_l$ and n_a = constant, and representing r as a function of V, Eq. (3.10) can be shown to become

$$p_a \leq \frac{2\gamma}{r} \tag{3.11}$$

Substituting for $\frac{2\gamma}{r}$ from Eq. (3.B.1), Eq. (3.11) reduces simply to

$$p_v - p_l \geq 0 \tag{3.12}$$

This condition is always met when vapor resides on the concave side of the curved gas-liquid interface. The liquid phase is superheated in this configuration. Therefore, a bubble of critical size in a superheated liquid will grow for any given mole fraction of air when the temperature is raised infinitesimally above the equilibrium temperature ($T_s + \Delta T_{sh}$).

3.3.6 Superheat for Surface Nucleation

The pits and cavities in the surface of a solid provide the active sites for initiation of vapor formation. Once vapor is formed in these cavities, the shape of the vapor-liquid interface depends on the contact angle (θ) and the included angle of the cavity (ψ). There are three possible configurations, depending on θ and ψ, a vapor-liquid interface can take. These are shown schematically in Figure 3.5. Figure 3.5(a) represents a case where vapor is at a higher pressure than liquid and, therefore, equilibrium conditions can only be met by superheated liquid. Case (b) is representative of the case where vapor and liquid are at equal pressure

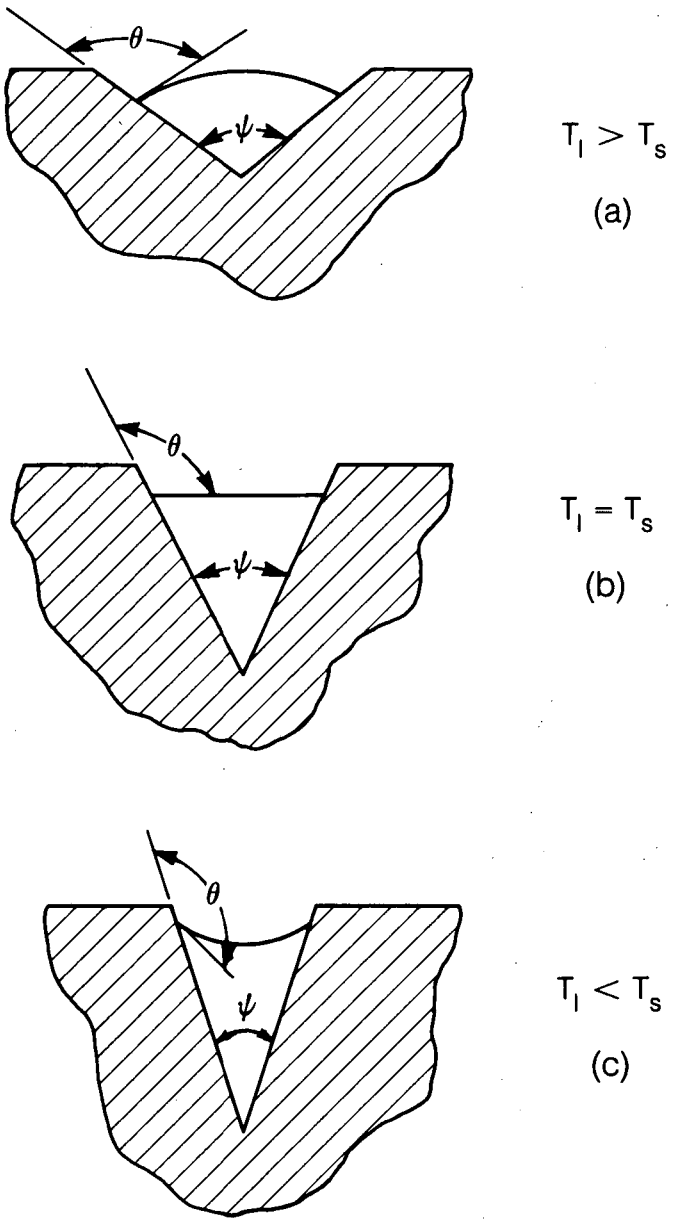

Fig. 3.5. Schematic of three possible liquid-vapor interfaces with bubbles of vapor forming in cavity.

and no superheat is required for equilibrium. The third case (c) represents the case in which vapor is at a lower pressure than liquid and, therefore, vapor formation can proceed in subcooled ($T_l < T_s$) liquid.

It is not hard to imagine that the walls of a natural porous medium will contain at least some cavities of type c. Therefore, one may conclude, erroneously, that in such cases boiling could begin at temperatures below the saturation temperature. This paradox is resolved upon examination of the growth of the bubbles in the cavities. Figure 3.6 shows, qualitatively, the liquid temperature needed to maintain vapor-liquid equilibrium in the three cases for different volumes of vapor residing in the cavities. When phase transformation takes place, the volume of vapor in the cavity increases and the interface moves upwards. Upon hitting the lip of the cavity, the interface becomes convex into the liquid phase (interface-1) irrespective of its previous shape. This configuration is in equilibrium only with superheated liquid. As the vapor volume increases, the radius of curvature of the interface decreases until the interface occupies position-3. Therefore, superheat requirement also increases until it hits a maxima at position 3. Further increase in volume is accompanied by a decrease in curvature and superheat requirement. Therefore, the superheat required for onset of boiling corresponds to the required superheat for interface-3. The above discussion is valid only in the case of uniform surface wettability. The effects of a heterogeneous surface could easily be included (Lorentz, Mikic, and Rohsenow, 1974).

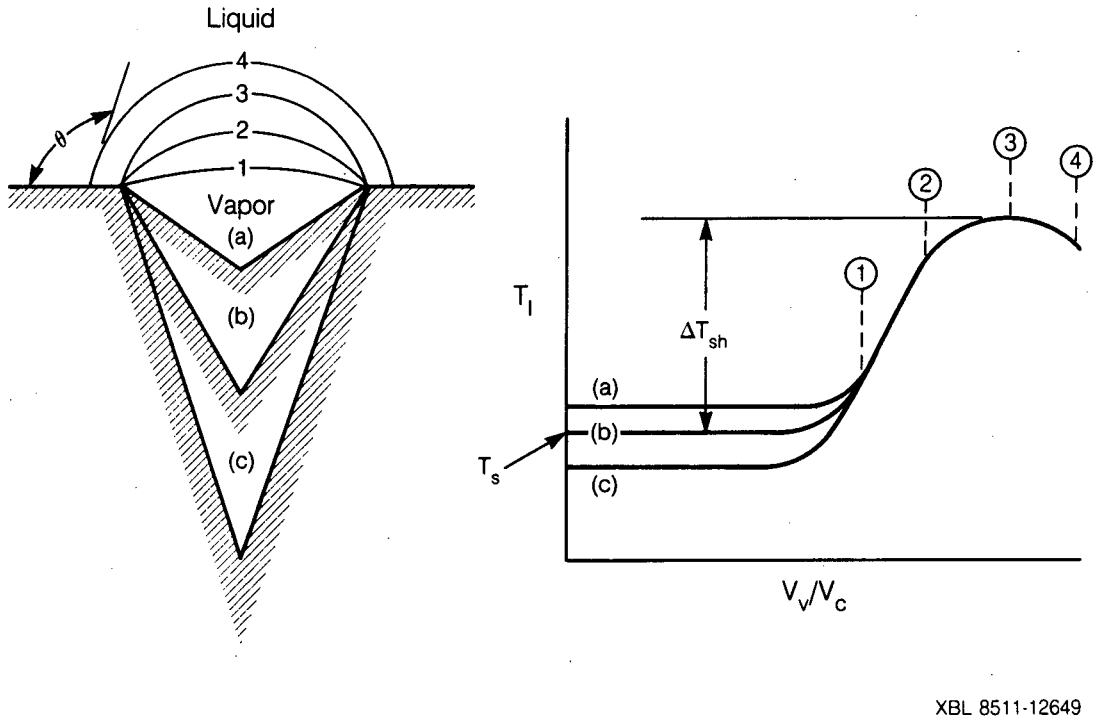

Fig. 3.6. Superheat requirements for bubble growth in cavity.

3.4 THERMODYNAMICS OF STEAM-WATER INTERFACE IN POROUS MEDIA

3.4.1 Overview

When two fluid phases such as steam and water simultaneously occupy a porous medium, their distribution in the void spaces is governed by well defined laws of physics. For example the shape and the mechanical equilibrium of the interfaces between the bulk fluid phases (Fig. 3.7) is given by the classic Young-Laplace equation and the energy minimization principle that is equivalent to it (Huh, 1969). The thermodynamic equilibrium of these interfaces are given by a combination of Clausius-Clapeyron and Kelvin's equations. These two criteria can be combined to obtain a relationship between the local thermodynamic conditions which must be satisfied for an interface to exist in steady-state (Udell, 1985). But, when one of the fluid phases is submicroscopically thin, which is invariably the case when an interface comes near the contact zone on a solid wall, the effect of long-range dispersion interactions between the film phase and the solid wall come into effect. The classical thermodynamic analysis would not apply in this region if the film of the wetting liquid is in an absorbed state — i.e., only a few molecules thick (Davis and Scriven, 1981). However, when the film is at least as thick as the thickness of Gibb's interface, the thermodynamic criteria for its existence can be obtained by augmenting the Young-Laplace equation with "disjoining pressure," an entity defined by Deryaguin (1937). Therefore, two separate studies — one for the bulk fluid menisci and the other for thin films, are

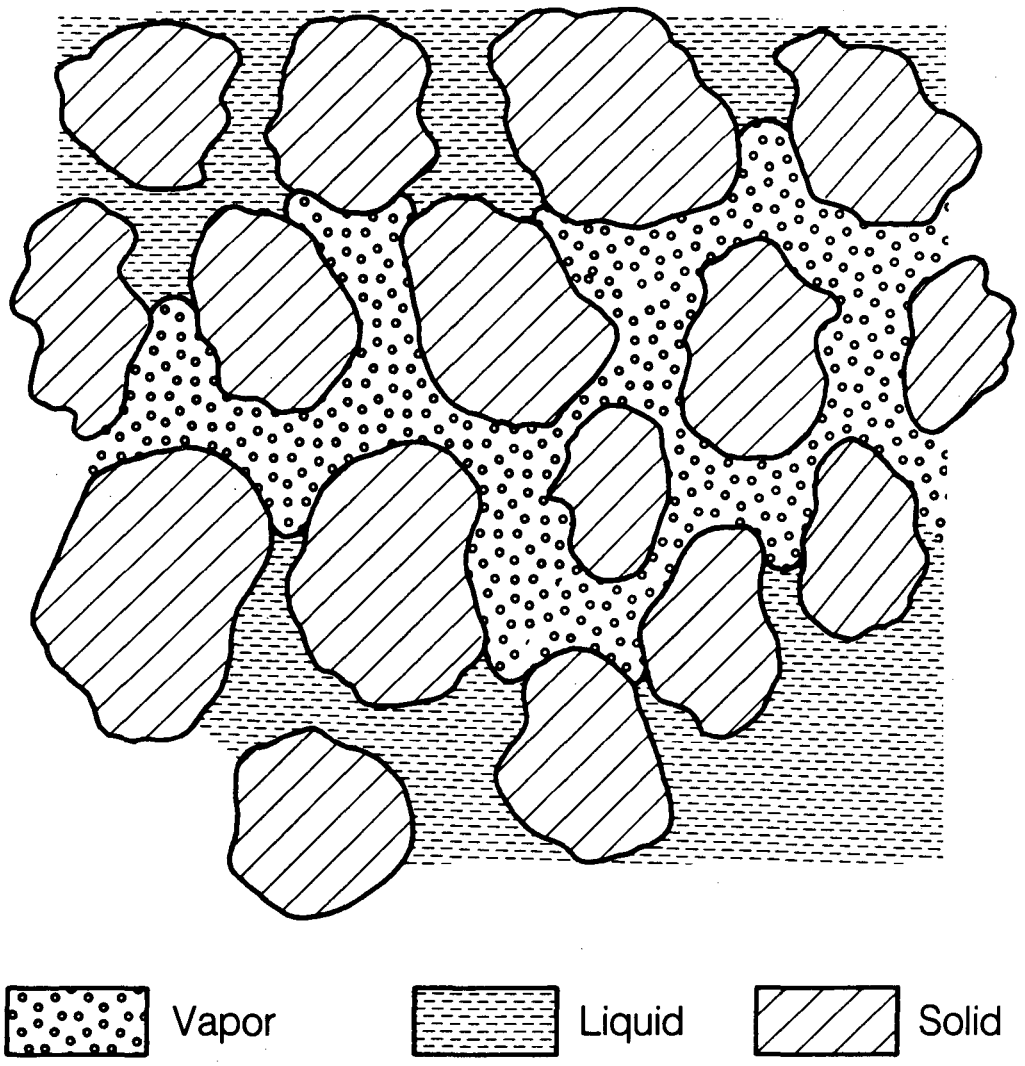

Fig. 3.7. Schematic of two-phase fluid distribution in porous media.

XBL 8511-12656

made to define the thermodynamic properties of vapor-liquid interfaces in porous media.

3.4.2 Thermodynamics of Vapor-Liquid Meniscus

The liquid-vapor meniscus in porous media is a curved interface, the mechanical equilibrium of which is given by Young-Laplace equation (Eq. (3.2)). In the presence of water-wet solids, the type we are concerned with in this study, the liquid phase resides on the convex side and the vapor on the concave side of the meniscus. In the network of voids in porous media, there will, in general, be many menisci separating a continuous liquid phase from a continuous vapor phase. The interaction between these menisci takes place through connecting bulk fluids and/or the layers of wetting fluid on the solid surface. Not all interfacial configurations are stable; only the stable ones persist under static equilibrium. Under a slow change of external conditions, the interfacial configuration may loose its stability, the consequence being either a rapid withdrawal out of a pore — a jump — or a rapid rupture in a pore throat — a choke-off. Only a set of these menisci which give the minimum interfacial energy and conserve volume will be hydrodynamically stable. A rigorous analysis of this process for two incompressible fluids has been presented by Mohanty (1981). This analysis could be adopted for vapor-liquid distribution if the pressure gradients are small and vapor can be treated as an incompressible fluid. However, since we are concerned only with the steady-state distributions, we assume that all the vapor-liquid interfaces under consideration are hydrodynamically stable.

The condition of thermodynamic equilibrium of these menisci requires that the chemical potential of an interface and that of the phases separated by it are all equal ($\mu_v = \mu_l = \mu_\sigma$). This condition combined with the Young-Laplace equation was used by Udell (1985) to show that the only stable configurations are those in which the liquid phase resides on the convex side of the menisci and it is at a lower pressure than the vapor phase, which is superheated. He also developed an expression for the local temperature in terms of local thermodynamic properties and capillary pressure for pure liquid-vapor systems. It was further extended by Schuh and Udell (1985) to take into account the effects of a non-condensible gas in the vapor phase. The local superheat for pure vapor-liquid and vapor-gas-liquid systems can be obtained by substituting a local mean curvature (H) for (1/r) in Eqs. (3.5) and (3.8), respectively, of this chapter.

3.4.3 Thin-film on Solids

Whenever a drop of wetting fluid is placed on a smooth, flat solid surface, the fluid seems to rest on the surface in form of a drop within a well defined line of contact, and the free liquid surface seems to meet the solid surface at a characteristic contact angle, θ (see Figure 3.8). In actuality, a thin film of fluid, often thinner than the wave length of light, extends beyond the visible line of contact between the fluid and the solid surface due to long-range dispersion interactions between the fluid molecules and the solid surface (Hardy, 1919). In this case the apparent line of contact is the extrapolation of visible surface of the drop onto the solid surface. The contact angle which is visible to eye is not the true con-

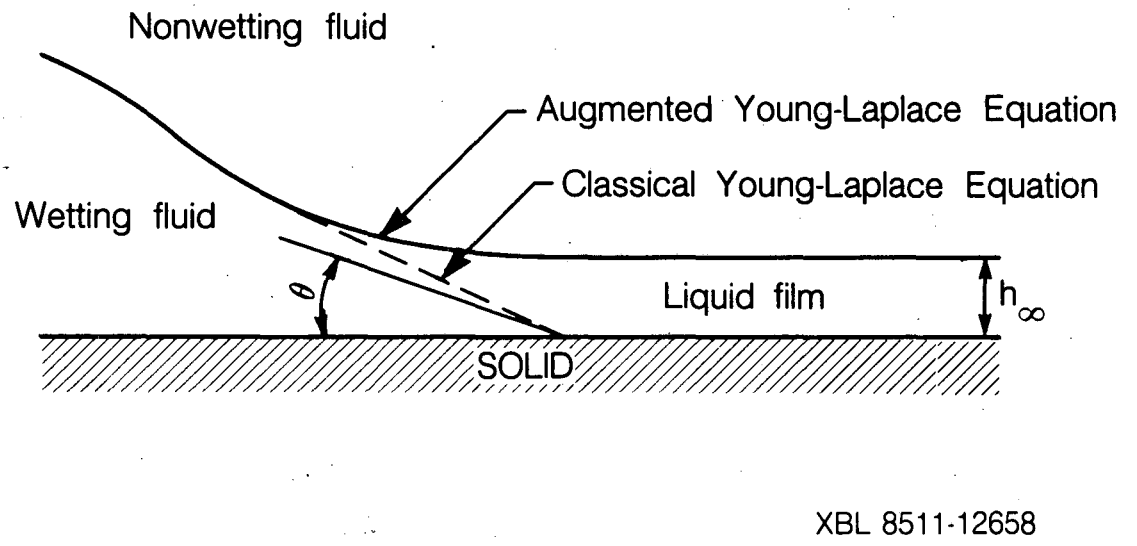

Fig. 3.8. Spreading of thin film on solid surface.

tact angle but an extrapolation of drop curvature onto the solid surface. This angle is commonly known as the apparent contact angle.

Thin films are also formed by the wetting fluid which is left behind after the bulk of it has been displaced by a non-wetting phase (Bretherton, 1962; Ruschak, 1978; and Kesghi and Scriven, 1979), or due to multilayer adsorption from the vapor phase onto the solid (Baugham and Fakhoury, 1931). The stability of these films depends on the complex interplay of the capillary forces of interfacial tension in curved menisci in contact with a film, and "special forces" active in the thin film. Only the stable configurations persist under static conditions and unstable ones break up to form droplets on the surface (Deryaguin and Zorin, 1957).

In order to understand the meaning of "special forces," let us consider the mechanical equilibrium of a stationary, long air bubble in a narrow, horizontal, smooth walled capillary tube shown schematically in Figure 3.9. If we assume that the tube is so narrow that the effect of gravity can be neglected, then pressure at each point in the liquid phase should equal P_l. Similarly the gaseous phase pressure is P_{air} everywhere within the bubble. Applying Young-Laplace equation to the hemispherical and the cylindrical portion of the air-water interface we obtain

$$P_{air} - P_l = \frac{2\gamma}{r} \quad , \tag{3.13}$$

and

$$P_{air} - P_l = \frac{\gamma}{r} \quad , \tag{3.14}$$

respectively. These equations indicate that the pressure difference between the gaseous phase and the liquid phase at the ends are twice as much as the pressure difference along the cylindrical portion of the interface. This is inconsistent with our assumption that the pressures in liquid and the gaseous phases are the same everywhere. The answer to this paradox is revealed upon close examination of the state of the liquid in the thin film of thickness (h_∞) shown schematically in Figure 3.10. The state of stress, $\bar{P}$, inside the thin-film is non-isotropic and different from that in the bulk phase due to molecular interaction with the solid surface, and it is given by

$$\bar{P} = P_N ii + P_T(jj + kk) \tag{3.15}$$

where P_N is the normal component of the liquid phase pressure and P_T is the tangential component. It is the normal component of the liquid pressure which satisfies Eq. (3.14) and not the bulk phase liquid pressure P_l. The difference between P_N and the pressure in connected bulk phase (P_l) is known as the "disjoining pressure" (π).

$$\pi(h) = P_N - P_l \tag{3.16}$$

P_N in the present case is given by $(P_{air} - \frac{\gamma}{r})$, but for a planar interface it would simply equal P_{air}. The disjoining pressure (π) for a given set of fluid and solid depends only on the film thickness (h) when there are no bending or torsional stresses. Disjoining pressures for many different configurations have been studied experimentally and estimated theoretically by Buscall and Ottewill (1975).

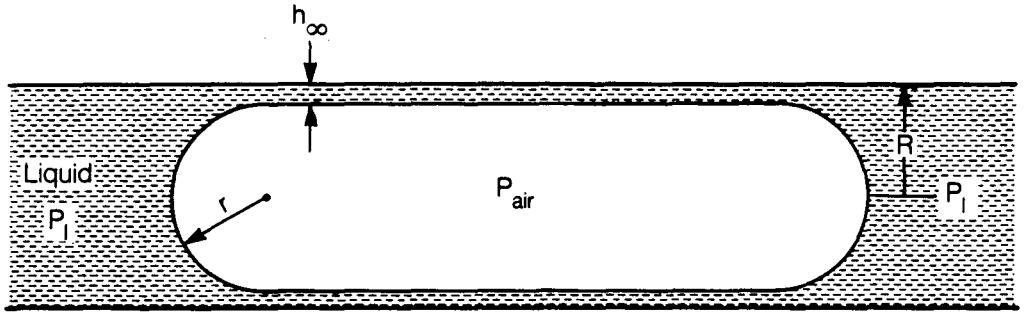

XBL 8511-12648

Fig. 3.9. Schematic of a long air bubble in water filled tube.

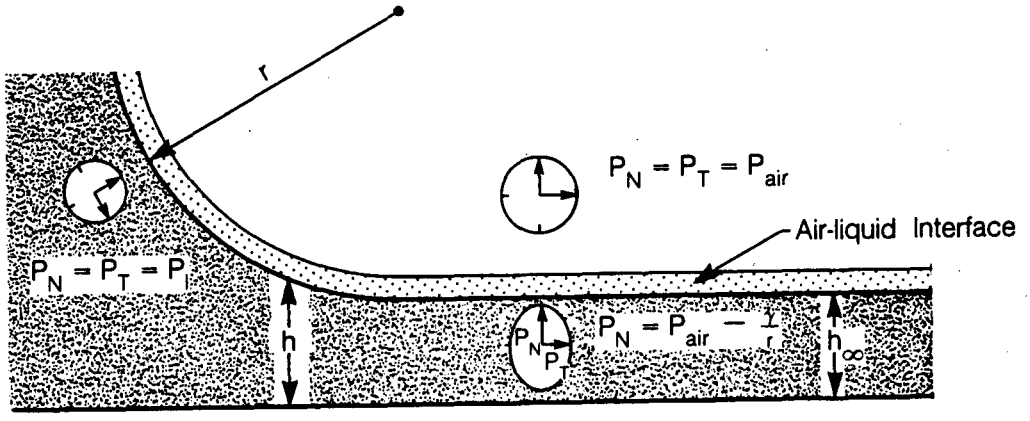

XBL 8511-12654

Fig. 3.10. State of stress in thin film.

The mechanical potential balance between liquid and air could be represented by one equation for every point along the air-liquid interface (also see Fig. 3.8), known as the Augmented Young-Laplace equation

$$P_{air} - P_l = 2H\gamma + \pi(h) \tag{3.17}$$

where H is the mean curvature and γ is the interfacial tension. This equation shows that in the above mentioned problem the mean curvature of the end caps near the wall will be less than 1/r because of the disjoining pressure effects. Therefore, the end caps of the bubble will not be exactly hemispherical. The apparent contact angle, θ (see Fig. 3.8) is given by

$$\cos\theta = 1 + \frac{1}{\gamma}\left\{ h_\infty\, \pi(h_\infty) + \int_{h_\infty}^{\infty} \pi(h)\, dh \right\} \tag{3.18}$$

The disjoining pressure (π) may be regarded as the net effect of several components. These include the molecular component π_m — due to long-range forces between neutral molecules, the ionic-electrostatic component π_e — due to the compression of electrostatic double layers, and a structural component π_s — due to alteration of the adsorbent structure in the boundary layer region and/or the overlapping of adsorbed layers of neutral molecules on to the solid surface. When the film thickness (h) is much smaller than the characteristic wave length of molecular interaction, π_m given by

$$\pi_m = A/h^3 \tag{3.19}$$

and for thicker films it is given by

$$\pi_m = B/h^4 \tag{3.20}$$

where A and B are constants. These representations by no means cover all possible cases (Hirschfelder, et al. 1954, Lifshitz, 1956). Similarly there are many expressions for π_e. However, for β-films of water on glass, quartz or mica, π_e could be given by (Deryaguin and Chauraev, 1974).

$$\pi_e = C/h^2 \tag{3.21}$$

where C is a constant dependent on physical properties of the film.

The structural component π_s is significantly larger than other components for a thin water film on clean quartz with a film thickness $h < 800$ and it is proportional to the inverse of h, i.e., $\pi_s \approx h^{-1}$. But on contaminated dehydroxylated quartz it is smaller and changes sign at a film thickness $h \sim 100$. (Pashley and Kitchener, 1979, Pashley, 1980).

The total disjoining pressure could be taken as the sum of all the above-mentioned components, and it may change sign depending on how individual components vary with h. Many such possibilities are catalogued by Dzyaloshinkii et. al. (1860) and presented here in Figure 3.11. It can be seen from Figure 3.11 that disjoining pressure can vary differently with increasing film thickness depending on the contributions of the individual components of π. A detailed discussion of this phenomena is beyond the scope of this study but it is presented in other studies by Deryaguin (1957), Deryaguin et al. (1957, 1961, 1965, 1968 and 1978).

Stability of a thin film of a given configuration depends primarily on the π-h relationship. A detailed discussion of the exact nature of the stability criteria is

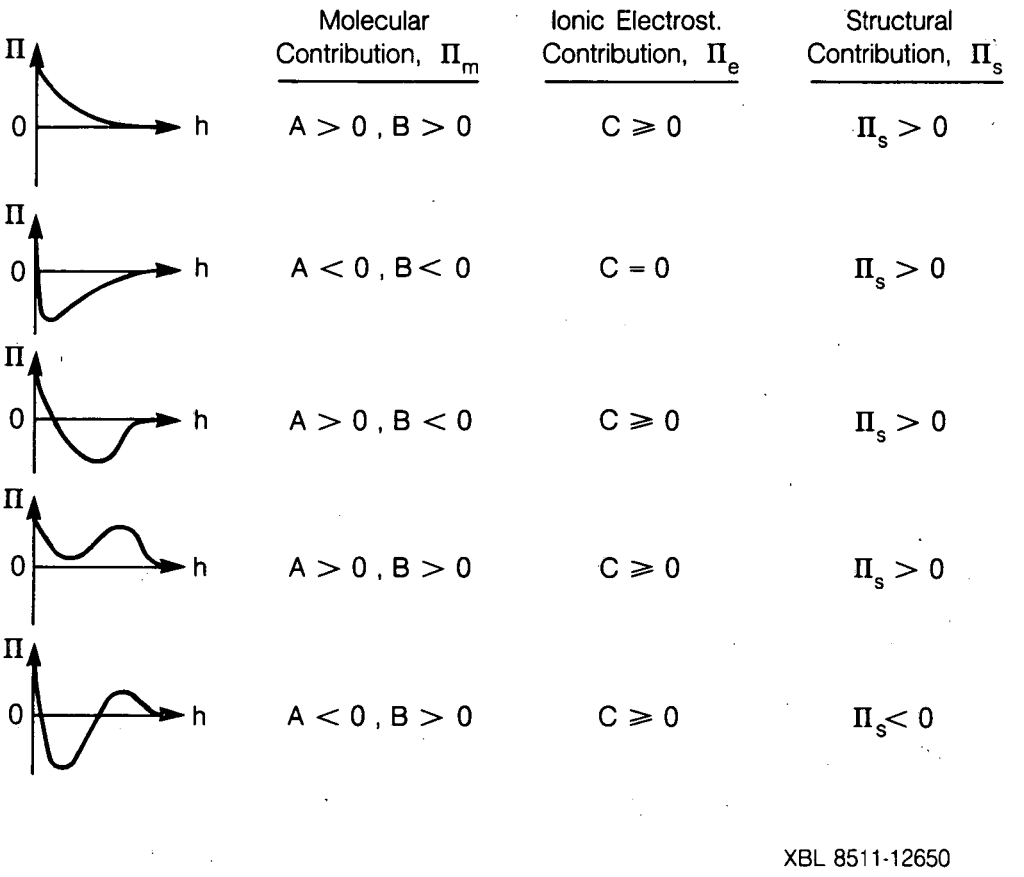

Fig. 3.11. Variation of disjoining pressure (π) with film thickness (h).

also beyond the scope of this study and unnecessary in the present context. Since we are concerned only with steady-state distribution of steam and water in pore spaces, it can be safely assumed that all existing thin films are stable.

3.4.4 Thermodynamics of Thin-Film

The disjoining pressure, π, is the normal principle stress a film of thickness h has over and above the isotropic pressure of the bulk phase with which it can be in equilibrium. Hence, for liquid water

$$\pi = P_N(T,\mu,h) - P(T,\mu,h = \infty) \tag{3.22}$$

where μ is the chemical potential of liquid water. Th disjoining potential, $\Delta\mu$, is given by

$$\Delta\mu(h) = \mu(P_N,T,h) - \mu(P = P_N,T,h = \infty) \quad . \tag{3.23}$$

where the first term on the right hand side represents the chemical potential of liquid water in a film of thickness h and normal principle stress P_N. The second term represents the chemical potential of liquid water in the bulk phase at isotropic pressure P ($= P_N$).

Chemical Potential of Liquid in Film

Now let us consider the chemical potentials of bulk liquid phases at pressures P and P + π. They are correlated according to

$$\mu(P + \pi,T,h = \infty) = \mu(P,T,h = \infty) + \int_P^{P+\pi} v_l^{(m)}\, dp \tag{3.24}$$

where $v_l^{(m)}$ represents the molar volume of liquid water. Combining Eqs. (3.23)

and (3.24) we obtain

$$\mu(P + \pi,T,h) = \mu(P,T,h = \infty) + \int_{P}^{P+\pi} v_l^{(m)}\ dp + \Delta\mu(h) \tag{3.25}$$

Since the liquid phase at $(P + \pi,T,h)$ is in chemical equilibrium with liquid at $(P,T,h = \infty)$, Eq. (3.25) reduces to

$$\Delta\mu(h) = -\int_{P}^{P+\pi} v_l^{(m)}\ dp \tag{3.26}$$

Equation (3.26) is integrated for incompressible liquid to yield

$$\Delta\mu(h) = -v_l^{(m)}\ \pi(h) \tag{3.27}$$

Substituting this expression for $\Delta\mu$ into Eq. (3.23) and rearranging we obtain

$$\mu_l(P_N = P + \pi,T,h) = \mu_l(P = P + \pi,T,h = \infty) - v_l^{(m)}\ \pi(h) \tag{3.28}$$

where the subscript l refers to the liquid phase. This equation gives the chemical potential of liquid in a liquid film at the condition specified.

Vapor Pressure Reduction in Presence of Film

Let us consider the thermodynamic equilibrium of a long bubble such as the one shown in Figure 3.9, filled with pure vapor at pressure P_v and temperature T. Since the vapor phase is in contact with both bulk liquid phase and thin film in this configuration, the mechanical equilibrium of this bubble is given by Augmented Young-Laplace equation

$$P_v - P_l = \frac{2\gamma}{r} + \pi(h) \tag{3.29}$$

and the physicochemical equilibrium of the curved segment of the interface is given by the classic Kelvin's equation. Since we know that chemical equilibrium

exists in the liquid phase around the bubble, we could infer, without any rigorous proof, that the physicochemical equilibrium conditions are also satisfied at the vapor-film interface. However, doubts arise when one considers the fact that the state of stress within the film is anisotropic. To resolve this doubt we present a rigorous derivation of the physicochemical equilibrium conditions at the vapor-film interface by considerating the equilibrium of a flat film with vapor (Fig. 3.12). The mechanical equilibrium of the interface is given by $P_N = P_v$ and the chemical potential of the liquid phase in the film is given by Eq. (3.28). By taking variations of these equations it can be shown that (for details see Appendix-3.C) the physicochemical equilibrium of the vapor-film interface is given by

$$\ln \frac{P_v}{P_\infty} = \frac{-\pi(h) v_l}{RT} \tag{3.30}$$

A comparison of Eq. (3.30) with Kelvin's equation (Eq. (3.3)) shows that these two equations are identical if one represents the capillary pressure $P_c (= P_v - P_l)$ by the Augmented Young-Laplace equation (Eq. (3.17)). Therefore it can be concluded, by induction, that the generalized form of Kelvin's equation applicable to each and every point of the bubble-liquid interface of Figure 3.9 (or any generalized interface) is given by

$$\ln \frac{P_v}{P_\infty} = \frac{-(2H\gamma + \pi(h))\, v_l}{RT} \tag{3.31}$$

By substituting this equation for the classic Kelvin's equation in Appendix 3.A we obtain an equation for the superheat required to maintain vapor in equilibrium with liquid across a general curvilinear interface composed of a set of menisci and thin film,

$$\Delta T_{sh} = \frac{RT_s^2}{h_{lv} P_l} \{2H\gamma + \pi(h)\} \tag{3.32}$$

This is supported by the experiments conducted and reported by Schuh and Udell (1985), i.e., the fact that an effect P_c, including the adsorption term can be used in Kelvin' s equation.

3.5 DISTRIBUTION OF STEAM AND WATER IN PORE SPACE

Steam and water behave as two distinct, immiscible fluids in the subcritical region and they are separated by a distinct interface which has a characteristic Gibb's free energy corresponding to the local thermodynamic conditions. In the simultaneous flow of steam and water at high velocities in large flow channels, the two phases are known to exist in many configurations within a flow channel as shown in Figure 3.13. In each of these cases, the solid is water wet and there always exists a film of liquid water on the solid surface. There are extrained bubbles of vapor in a flow channel occupied by liquid water (Bubbly flow) at low flow qualities ($m_v/m_v + m_l$). At higher qualities of flow the pattern can change from Bubbly to Slug, Churn, or Annular. When the flow is turbulent, there may be entrained droplets of water within the vapor regions at high flow velocities, This condition is encountered when the viscous drag on liquid water far exceeds the adhesion forces and a chunk of liquid is torn away from the bulk phase and carried by flowing steam. Moreover, thermodynamic equilibrium may not exist between the two phases at all points if the velocity is sufficiently large. As opposed to these flow conditions encountered in boiler tubes and heat exchangers, simultaneous flow of steam and water in geologic media, such as geothermal

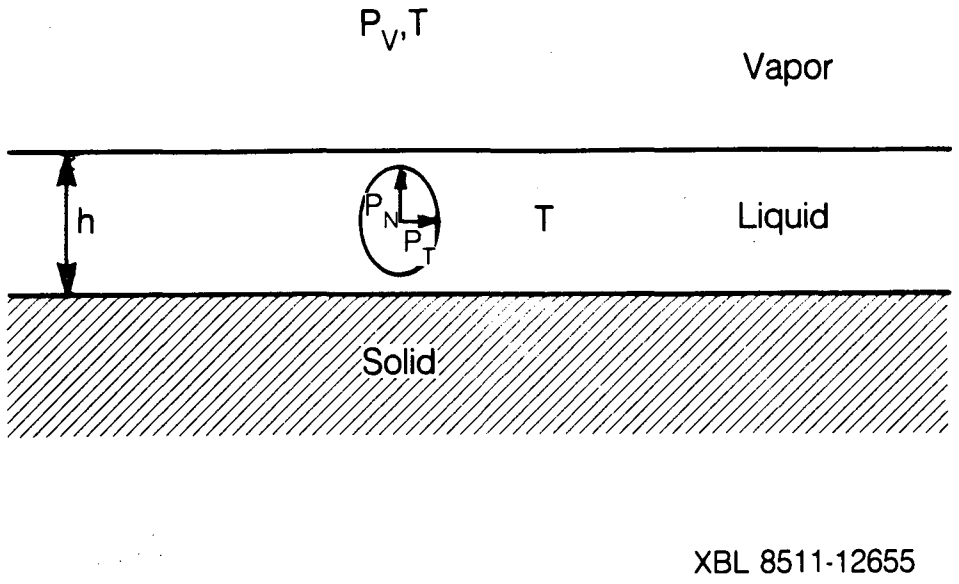

Fig. 3.12. State of stress in thin film on a flat surface.

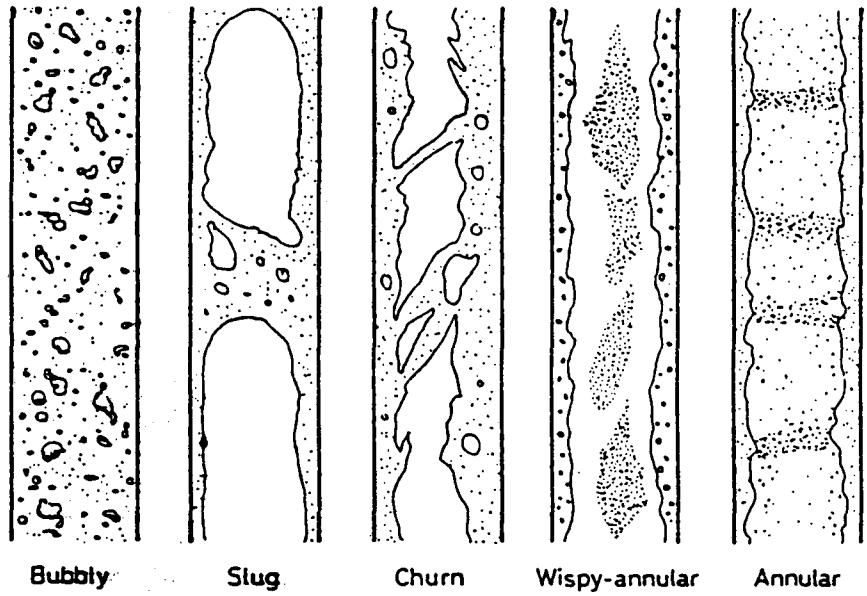

Fig. 3.13. Schematic of flow configurations in two phase flow in a tube.

reservoirs or petroleum reservoirs, takes place at small velocities in very narrow flow channels. Flow velocities are usually so small that entrainment of liquid droplets is not possible and local thermodynamic equilibrium always exists between the two phases. In such cases, distribution of steam and water in the pore space is only controlled by capillary forces and thermodynamic conditions.

The bulk of the two phases is separated by an interface composed of a set of menisci and a number of regions connecting them (Fig. 3.7), with liquid water on the convex wide of the interface and vapor on the concave side. These menisci obey the Young-Laplace equation of capillary hydrostatics. In pores of about 10 μm in size the buoyancy force is negligible compared to the capillary forces when the interfacial tension, γ, is more than 1 dyne/cm (Morrow, 1979). The thermodynamic state of the phases across the menisci is defined by Kelvin's equation. Liquid water in this configuration is superheated with the degree of superheat given by Eq. (3.5) for pure vapor-liquid interfaces and by Eq. (3.8) for a mixture of vapor and non-condensible gas and liquid. Therefore, all the menisci of a static water-vapor interface will have the same mean curvature if the system is isothermal and isobaric. Menisci with mean curvature larger than the curvature which defines the local thermodynamic equilibrium will experience evaporation and menisci with smaller mean curvature will experience condensation until the equilibrium state is achieved.

If the solid matrix is water wetted then the regions connecting the menisci are covered with thin films of wetting fluid which conform in shape to the local pore-wall configuration. Such films, whether left behind after displacement of the

wetting fluid or built up due to surface condensation, will tend to accumulate around regions of high mean curvature such as pore throats, grooves, bits and pockets because of high capillarity in these regions. Inasmuch as pore-walls of most naturally occurring porous media are full of grooves and pits, a draping layer of wetting fluid will cover all of these irregularities. These draping layers provide a path for wetting fluid to transfer between adjacent menisci. Other than this they do not contribute significantly to advection of wetting fluid in porous media. The thermodynamic stability of these thin films is given by Eq. (3.26). In fact the mechanical and thermodynamic equilibrium of all the vapor-liquid interfaces separating liquid water from vapor are expressed by the Augmented Young-Laplace equation (Eq. (3.13)) and the Augmented Kelvin's equation (Eq. (3.27)), respectively.

It is known from experimental observations that when two or more immiscible fluids flow simultaneously through a porous medium, each fluid establishes its own tortuous channels of flow through the medium. These channels are very stable and a unique set of channels appears to occur for every range of saturation (Chatenever and Calhoun, 1952). This phenomenon has been accepted by many investigators in their recent studies of two-phase, two-component fluid flow through porous media (Koplik and Lasseter, 1982; Mohanty and Salter, 1982; Heiba et al., 1983, etc.). It is worth noting at this stage that the original observation by Chatenever and Calhoun (1952) was performed with oil and water, where the fluid molecules maintain their identity and always remain within their parent liquid, except for diffusion of one phase into another, which in the case of

oil and water is negligibly small. The scenario for the flow of steam and water is just the opposite. Almost all simultaneous flows of steam and water in porous media are accompanied by phase transformation due to varying thermodynamic conditions along the flow paths. Therefore, one has to consider the possibility of the formation of one phase in a flow channel in the presence of the other phase. For example, in the simultaneous, concurrent flow of steam and water the specific enthalpies of both fluids decrease down stream and a phase transformation from liquid water to steam takes place to conserve the flowing enthalpy. If the phase transformation takes place within a channel that is fully occupied by liquid water or within the thin film occupying a vapor dominated flow channel (Fig. 3.14) due to boiling, then both phases simultaneously occupy the same flow channel. We shall examine these cases one by one.

First, let us consider the mechanism of boiling within a flow channel initially filled with water. If the two phases are distributed "sufficiently" homogeneously, within the porous medium and the flow rates are "small," then we can assume that the temperature at any point in the liquid equals the temperature of the steam-water interface closest to this point. If the capillary pressure at this interface is given by a characteristic interfacial radius r_i, then bubbles of pure vapor with a radius of curvature r_b less than r_i cannot exist. Bubbles with $r_b = r_i$ will exist in equilibrium and bubbles with $r_b > r_i$ will grow spontaneously. The critical bubble radius r_b^* of bubbles containing a mixture of vapor and noncondensible gas is given by

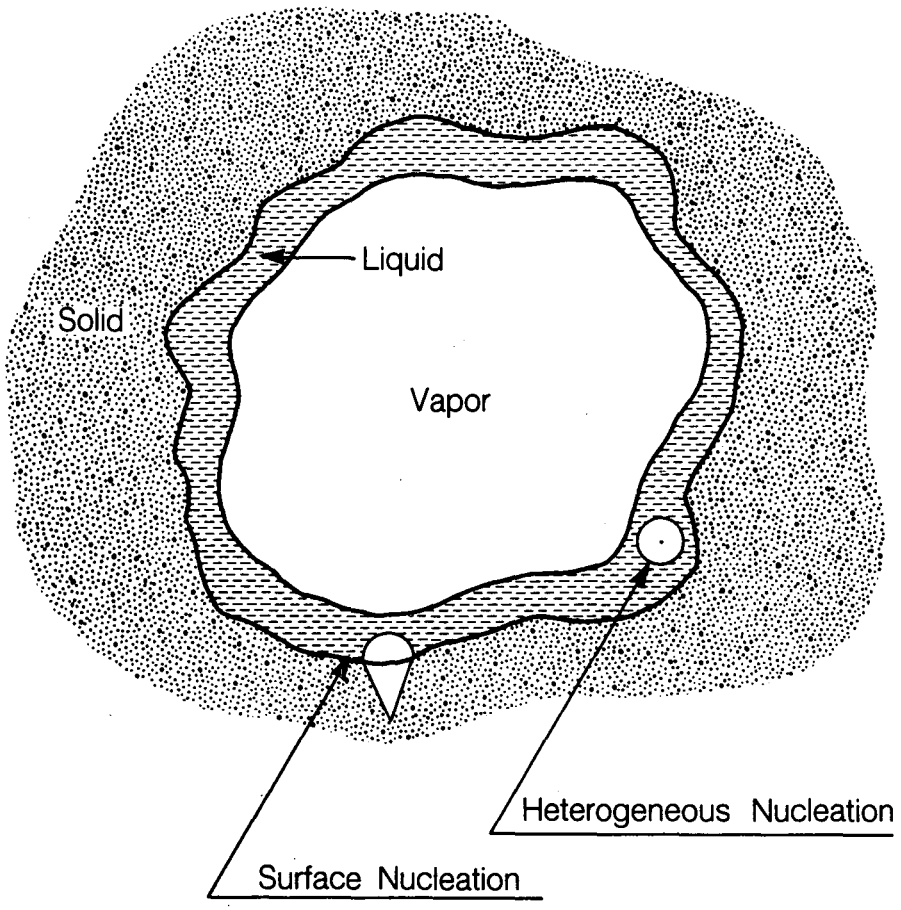

XBL 8511-12647

Fig. 3.14. Schematic of possible nucleation sites in a channel dominated by vapor.

$$\frac{r_b^*}{r_i} = \left\{1 + \frac{p_a r_i}{2\gamma}\right\}^{-1} \quad . \tag{3.33}$$

Critical opening radius of cracks or cavities is correlated to r_b^* by

$$r^* = r_b^* \sin\theta \quad , \tag{3.34}$$

where θ is the contact angle. Substituting Eq. (3.33) into Eq. (3.34), the expression for r* is given by

$$r^* = r_i \sin\theta \left\{1 + \frac{p_a r_i}{2\gamma}\right\}^{-1} \tag{3.35}$$

If the thermodynamic conditions are favorable, a bubble forms within the flow channel and flows with the liquid until it encounters a pore throat so small that the existing pressure gradients are incapable of pushing the bubble through the throat. The bubble then gets trapped in the flow channel and blocks it. the flow channel can remain blocked only if the bubble is stable at the local thermodynamic conditions. Similarly a bubble formed on a solid surface can either stay attached to the surface and block a part of the liquid filled flow channel or it can break away and get trapped at a throat down stream.

Phase transformation in a vapor dominated channel (Fig. 3.14) can occur either at the vapor-liquid interface or within the film. The nucleation sites within the film can be either at a free floating gas bubble or a gas filled crack or cavity. The critical bubble radii in either of these cases is given by Eq. (3.33). The local mean curvature (H) of the film interface is correlated to r_i according to

$$r_i = \left\{H + \frac{\pi}{2\gamma}\right\}^{-1} \tag{3.36}$$

The film thickness, in general, will be very small compared to the pore radius,

therefore, it is unlikely that the film will contain any bubble large enough to nucleate. However, if such a bubble exists, then it will soon grow and penetrate the interface and steam will flow into the pre-existing steam flow channel. Therefore, it is unlikely that phase transformation in a steam dominated channel will result in trapping of the steam phase.

APPENDIX 3.A
SUPERHEAT FOR BUBBLE FORMATION

We consider metastable equilibrium of a vapor bubble of radius (r) in liquid a pressure (P_l) and temperature (T_l). The pressure inside the bubble is given by Young-Laplace equation

$$P_v = P_l + \frac{2\gamma}{r} \tag{3.A.1}$$

Since the liquid phase is superheated, the saturation pressure (P_∞) corresponding to T will be larger than P_l. The relation between P_∞ and P_v is given by Kelvin's equation

$$P_v = P_\infty \exp(-2\gamma v_l/rRT) \tag{3.A.2}$$

Since $2\gamma v_l/rRT_l$ is small, Eq. (3.A.2) may be approximated as

$$P_v = P_\infty \left(1 - \frac{2\gamma v_l}{rRT}\right) \tag{3.A.3}$$

Using the ideal gas law

$$P_\infty v_v = RT_l \tag{3.A.4}$$

and Eq. (3.A.2) can be written as

$$P_v = P_\infty \left(1 - \frac{2\gamma v_l}{rP_\infty v_v}\right) \tag{3.A.5}$$

Combining Eqs. (3.A.1) and (3.A.5) we obtain

$$P_\infty - P_l = \frac{2\gamma}{r}\left(1 + \frac{v_l}{v_v}\right) \tag{3.A.6}$$

The relation between saturation temperature and saturation pressure is given by

Clausius-Clapeyron equation

$$\frac{dP}{dT} = \frac{h_{lv}}{T(v_v - v_l)} \tag{3.A.7}$$

Assuming $v_l << v_v$ and substituting $v_v = RT/P$ into Eq. (3.A.7) we obtain

$$\frac{dP}{P} = \frac{h_{lv}}{R\,T^2}\,dT \tag{3.A.8}$$

Integrating Eq. (3.A.8) from (P_l, T_s) to (P_∞, T) we obtain

$$\ln\left(\frac{P_\infty}{P_l}\right) = \frac{h_{lv}}{R\,T\,T_s}\,(T - T_s) \tag{3.A.9}$$

Substituting for P_∞ from Eq. (3.A.6) and rearranging we obtain

$$T - T_s = \frac{RT_sT}{h_{lv}} \ln\left\{1 + \frac{2\,\gamma}{P_l\,r}\left[1 + \frac{v_l}{v_v}\right]\right\} \tag{3.A.10}$$

Assuming $v_v >> v_l$, $\frac{2\gamma}{rP_l} << 1$, and $T_s \sim T$, the expression for superheat is given by

$$T - T_s \equiv \Delta T_{sh} = \frac{R\,T_s^2}{h_{lv}}\,\frac{2\gamma}{P_l\,r} \tag{3.A.11}$$

APPENDIX 3.B.
SUPERHEAT FOR HETEROGENEOUS NUCLEATION

Consider the metastable equilibrium of an air bubble, saturated with water vapor, in liquid water. The mechanical equilibrium of bubble is given by Young-Laplace equation

$$p_a + p_v - P_l = \frac{2\gamma}{r} \tag{3.B.1}$$

where p represents partial pressures and subscripts a, v and l refer to air (or non-condensible gas), vapor and liquid, respectively. The effect of curvature on vapor pressure reduction in presence of nonreacting, noncondensible gas is given by Kelvin's equation (Section XVI-3, Defay and Prigogine, 1966)

$$p_v = p_{v,\infty} \exp\left(-\frac{2\gamma}{r}\frac{v_l}{RT}\right) \tag{3.B.2}$$

where $p_{v,\infty}$ represents the partial pressure of vapor, for a given molecular fraction of air, at temperature T when the interface between the gas phase and the liquid phase is planar.

The effect of non-condensible gas on saturation pressure is given by (Sec. 7.15, Lee and Sears, 1955)

$$p_{v,\infty} = P_\infty \exp\left\{\frac{v_l}{RT}(p_v + p_a - p_{v,\infty})\right\} \tag{3.B.3}$$

For small exponents, Eq. (3.B.2) and (3.B.3) can respectively be represented as

$$p_v = p_{v,\infty}\left(1 - \frac{2\gamma}{r}\frac{v_l}{RT}\right) \tag{3.B.4}$$

and

$$p_{v,\infty} = P_\infty \left\{ 1 + \frac{v_l}{RT} (p_v + p_a - p_{v,\infty}) \right\} \tag{3.B.5}$$

where P_∞ represents the vapor phase pressure, in absence of air, in equilibrium with liquid at temperature T across a planar interface. Since we are considering high molecular fraction of air in the bubble, $p_a >> p_v - p_{v,\infty}$. Therefore, Eq. (3.B.5) reduces to

$$p_{v,\infty} = P_\infty \left(1 + \frac{v_l}{RT} p_a \right) \tag{3.B.6}$$

Combining Eqs. (3.B.2) and (3.B.6) and invoking ideal gas law we obtain

$$p_v = P_\infty - \frac{2\gamma}{r} \frac{v_l}{v_v} + \frac{v_l}{v_v} p_a \left(1 - \frac{2\gamma}{r} \frac{v_l}{P_l v_v} \right) \tag{3.B.7}$$

Combining Eq. (3.B.1) and (3.B.7) and assuming $\frac{2\gamma}{r} \frac{v_l}{P_\infty v_v} << 1$, we obtain

$$\begin{aligned} p_v - P_l &= \frac{2\gamma}{r} - p_a \\ &= P_\infty - \frac{2\gamma}{r} \frac{v_l}{v_v} + p_a \frac{v_l}{v_v} - P_l \end{aligned} \tag{3.B.8}$$

Dividing the right hand sides of Eq. (3.B.8), and rearranging, we obtain

$$\frac{P_\infty}{P_l} = 1 + \frac{2\gamma}{rP_l} \left(1 + \frac{v_l}{v_v} \right) - \frac{p_a}{P_l} \left(1 + \frac{v_l}{v_v} \right) \tag{3.B.9}$$

Substituting this into integrated Clausius-Clapeyron relation (eqn. 3.A.9) and rearranging, we obtain

$$T - T_s = \frac{RT_sT}{h_{lv}} \ln \left\{ 1 + \frac{2\gamma}{rP_l} \left(1 + \frac{v_l}{v_v} \right) - \frac{p_a}{P_l} \left(1 + \frac{v_l}{v_v} \right) \right\} \tag{3.B.10}$$

APPENDIX 3.C.
VAPOR PRESSURE REDUCTION IN PRESENCE OF A THIN FILM

We consider the physicochemical equilibrium of a thin film with bulk vapor phase. The mechanical balance is given by

$$P_N = P_v \tag{3.C.1}$$

and chemical potential of the liquid phase in the film is given by (Eq. (3.24))

$$\mu_l(P_N,h) = \mu_l(P_l = P_N,h = \infty) - \pi(h)\, v_l \tag{3.C.2}$$

If we pass from one equilibrium state to another neighboring equilibrium state, then

$$\delta P_N - \delta P_v = 0 \tag{3.C.3}$$

and

$$\delta\mu_v = \delta\mu_l(P_N,h) \tag{3.C.4}$$

Applying Gibbs-Duhem equation and taking variation of chemical potentials at constant temperature

$$\delta\mu_v = v_v\, \delta P_v \tag{3.C.5}$$

$$\delta\mu_l(P_l = P_N,h = \infty) = v_l\, \delta P_l \tag{3.C.6}$$

Therefore, variation of Eq. (3.C.2) yields

$$\delta\mu_l(P_N,h) = v_l \delta P_N - v_l\, \delta\pi(h) \tag{3.C.7}$$

Substituting Eqs. (3.C.5) and (3.C.7) into Eq. (3.C.4) and using Eq. (3.C.3)

$$\delta\pi(h) = \frac{v_l - v_v}{v_l}\, \delta p_v \tag{3.C.8}$$

Using the assumption of ideal gas law for the vapor phase and $v_v >> v_l$, Eq. (3.C.8) reduces to

$$\delta\pi(h) = \frac{-RT}{v_l} \frac{\delta p_v}{p_v} \tag{3.C.9}$$

If we integrate this equation from $\pi = 0$ (i.e., $h \to \infty$) and $P_v = P_\infty$ to some other state $(\pi(h), P_v)$ and assume that v_l is constant along the path, we obtain

$$\ln \frac{P_v}{P_\infty} = \frac{-\pi(h)\, v_l}{RT} \tag{3.C.10}$$

CHAPTER 4
NUMERICAL STUDIES

4.1. INTRODUCTION

Numerical studies were carried out to (i) design the experimental setup and select optimum experimental conditions, (ii) verify the results of the experiment, and (iii) verify the results of theoretical studies. These studies were carried out with a compositional simulator for thermal processes, called TOUGH (Pruess, 1985) — a member of the MULKOM family of multi-phase, multi-component codes (Pruess, 1983). This simulator was developed and validated by Karsten Pruess and his co-workers at Lawrence Berkeley Laboratory. A brief description of the numerical technique used in TOUGH is included in this chapter for completeness.

This chapter also includes a study of two-phase steam-water flow through a torroidal flow channel. The effects of phase transformation on the effective permeability of the flow channel have also been examined in this chapter.

4.2. NUMERICAL TECHNIQUE

4.2.1. Overview

The numerical method implemented in this study is known as the "Integrated Finite Difference," or IFD, method (Narasimham and Witherspoon, 1976; Narasimhan, 1982). In this method, all thermophysical and thermodynamic properties are represented by averages over explicitly defined finite subdomains,

while fluxes of mass or energy across surface segments are evaluated through finite difference approximations. An important aspect of this method is that the geometric quantities required to evaluate the conductance between two communicating volume elements are provided directly as input data rather than having them generated from data on nodal arrangements and nodal coordinates. Thus, a remarkable flexibility is attained by which one can allow a volume element in any one continuum to communicate with another element in its own or any other continuum. This allows us to obtain solutions for an anisotropic, non-homogenous domain of arbitrary shape. The code seeks simultaneous solution of heat and mass conservation equations in multi-phase flow through porous media. Liquid and gas phases flow in response to pressure gradients and gravity according to Darcy's Law. Capillary pressure is considered to depend on saturation and temperature, but not on the flow history of the system. The interaction between flowing liquid and gaseous phases is represented by nonhysteretic relative permeability functions. Capillary pressures and relative permeabilities can be specified differently for different flow regions, which is considered an important capability for fractured rocks with spatially variable pore size distribution. Apart from Darcy flow, the code also includes a term for vapor transport via binary diffusion. Phase change effects are included both in the mass flux terms and in the heat transport. We have assumed local thermodynamic equilibrium; i.e., solid and fluid are always at the same temperature and pressure locally, and the vapor partial pressure is always equal to the saturation pressure at the given local temperature. No allowance is made for vapor pressure lowering due to capillary and

adsorptive effects. Temperature differences between connected fluid-filled pores and large chunks of solid rock can be handled through appropriate space discretization. Heat transport is by means of conduction or convection.

The thermophysical properties of water substance, such as density, viscosity, and enthalpy, are represented within experimental accuracy by the steam table equations given by the International Formulation Committee (1967). Air is approximated as an ideal gas, the additivity of partial pressures is assumed for air and vapor. The (small) solubility of air in water is represented by Henry's Law.

4.2.2. Governing Equations

The formulation used in TOUGH is analogous to the multi-phase treatment customarily employed in geothermal reservoir simulators. The basic mass- and energy-balance equations are written in integral form for an arbitrary flow domain V_n as follows (Pruess and Narasimhan, 1985):

$$\frac{d}{dt}\int_{V_n} M^{(\kappa)} dv = \int_{\Gamma_n} \mathbf{F}^{(\kappa)} \cdot \mathbf{n}\, d\Gamma + \int_{V_n} q^{(\kappa)}\, dv \tag{4.1}$$

($\kappa = 1$: water; $\kappa = 2$: air; $\kappa = 3$: heat)

The mass accumulation terms ($\kappa = 1,2$) are

$$M^{(\kappa)} = \phi \sum_{\beta=l,g} S_\beta \rho_\beta X_\beta^{(\kappa)} \tag{4.2}$$

where ϕ is porosity, S_β is saturation of phase β (= liquid, gas), ρ_β is density of phase β , and $X_\beta^{(\kappa)}$ is the mass fraction of component κ present in phase β. The heat accumulation term contains rock and fluid contributions

$$M^{(3)} = (1-\phi)\,\rho_R\,C_R T + \phi \sum_{\beta=l,g} S_\beta\,\rho_\beta\,u_\beta \tag{4.3}$$

where ρ_R is rock grain density, C_R is rock specific heat, T is temperature, and u_β is specific internal energy of phase β.

The mass flux terms contain a sum over phases

$$\mathbf{F}^{(\kappa)} = \sum_{\beta=l,g} \mathbf{F}_\beta^{(\kappa)} \tag{4.4}$$

where the flux in each phase is

$$\mathbf{F}_\beta^{(\kappa)} = -k\,\frac{k_{r\beta}}{\mu_\beta}\,\rho_\beta\,X_\beta^{(\kappa)}\,(\nabla P_\beta - \rho_\beta \mathbf{g}) - \delta_{\beta g}\,D_{va}\,\rho_\beta\,\nabla X_\beta^{(\kappa)} \tag{4.5}$$

Here k is absolute permeability, $k_{r\beta}$ is relative permeability of phase β, μ_β is viscosity of phase β, $P_\beta = P + P_{cap,\beta}$ is the pressure in phase β (sum of a reference phase pressure and capillary pressure), and $\mathbf{g}$ is gravitational acceleration. The last term in Eq. (4.5) contributes only for gas phase flow and represents a binary diffusive flux, with D_{va} the diffusion coefficient for vapor-air mixtures.

Heat flux contains conductive and convective components

$$\mathbf{F}^{(3)} = -K\nabla T + \sum_{\substack{\beta = l,g \\ \kappa = 1,2}} h_\beta^{(\kappa)}\,\mathbf{F}_\beta^{(\kappa)} \tag{4.6}$$

Here K is heat conductivity of the rock-fluid mixture, and $h_\beta^{(\kappa)}$ is specific enthalpy of component κ in phase β.

The transport equations given above need to be complemented with constitutive relationships, which express all parameters as functions of a set of primary thermodynamic variables. The thermophysical properties of water are accurately represented by the steam table equations, as given by the International Formula-

tion Committee (1967). Air is approximated as an ideal gas, and additivity of partial pressures is assumed for air and vapor, $P_g = P_v + P_a$. The viscosity of air-vapor mixtures is computed from a formulation given by Hirschfelder et al., (1954), but using steam table values for vapor viscosity instead of approximations from kinetic gas theory. Henry's Law was assumed for solubility of air in liquid water.

$$P_a = K_H X_l^{(air)} \cdot \frac{M_{H_2O}}{M_{air}} \tag{4.7}$$

where $K_H = 10^{10}$ Pa is Henry's constant, $X_l^{(air)}$ is the mass fraction of air in liquid water, and M_{H_2O}, M_{air} are the respective molecular weights.

Capillary pressures and relative permeabilities will usually depend on phase saturations, but more general relationships are possible (e.g. temperature dependence; however, TOUGH does not allow for hysteresis).

The vapor-air diffusion coefficient is written as (Vargaftik, 1975; Walker et al., 1981)

$$D_{va} = \tau \phi S_g \frac{D_{va}^0}{P} \left(\frac{T + 273.15}{273.15} \right)^{\psi} \tag{4.8}$$

where τ is a tortuosity factor, which is dependent on pore geometry, and D_{va}^0 and ψ are material parameters which for air/vapor mixtures have values of $D_{va}^0 = 2.13 \times 10^{-5}$ m^2/s (at standard conditions of P = 1 bar, T = 0 °C), and $\psi = 1.80$ (Vargaftik, 1975).

Heat conductivity can depend on liquid saturation according to one of the following two relationships (Somerton et al., 1973, 1974)

$$K(S_l) = K(S_l = 0) + \begin{cases} \sqrt{S_l} \cdot (K(S_l = 1) - K(S_l = 0)) \\ S_l \cdot (K(S_l = 1) - K(S_l = 0)) \end{cases} \quad (4.9a)\ (4.9b)$$

4.2.3. Mathematical and Numerical Methods

The continuum Eq. (4.1) are discretized in space using the "integral finite difference" method (Edwards, 1972; Narasimhan and Witherspoon, 1976). Introducing appropriate volume averages, we have

$$\int_{V_n} M dv = V_n M_n \quad (4.10)$$

Here M is a volume-normalized extensive quantity, and M_n is the average value of M over V_n. Surface integrals are approximated as a discrete sum of averages over surface segments A_{nm}:

$$\int_{\Gamma_n} \mathbf{F} \cdot \mathbf{n}\, d\Gamma = \sum_m A_{nm} F_{nm} \quad (4.11)$$

Time is discretized fully implicitly as a first order finite difference, to obtain the numerical stability needed for an efficient calculation of multi-phase flow. Eq. (4.1) reduce to the following set of coupled algebraic equations:

$$R_n^{(\kappa)k+1} \equiv M_n^{(\kappa)k+1} - M_n^{(\kappa)k} - \frac{\Delta t}{V_n} \left\{ \sum_m A_{nm} F_{nm}^{(\kappa)k+1} + V_n\, q_n^{(\kappa)k+1} \right\} = 0 \quad (4.12)$$

Here k labels the time step, $\Delta t = t^{k+1} - t^k$. For a flow system which is discretized into N grid blocks, Eq. (4.12) represent a set of 3N algebraic equations. These are strongly coupled because of interdependence of mass and heat flow. They are highly non-linear, because of order-of-magnitude changes in parameters during phase transitions, and because of non-linear material properties (chiefly

relative permeabilities and capillary pressures). Because of these features of the equation system, TOUGH performs a completely simultaneous solution of the discretized mass- and energy-balance equations, taking all coupling terms into account. To handle the non-linearities we perform Newton/Raphson iteration. The unknowns in Eq. (4.12) are the 3N independent "primary" variables, which completely define the thermodynamic state of the flow system at time level t^{k+1}. For each volume element (grid block) there are three primary variables, the choice of which depends upon the phase composition (see Table 4.1).

Table 4.1. Primary thermodynamic variables.

Phase composition	variable #1	variable #2	variable #3
single phase	P-pressure (Pa)	T-temperature (° C)	X-air mass fraction
two-phase	P-pressure (Pa)	S_g-gas saturation	T-temperature (° C)

Denoting these primary variables collectively as $(x_i;\ i=1, ..., 3N)$, the Newton/Raphson iteration process can be written as follows. Demanding that the residuals $R_n^{(\kappa)k+1}$ in Eq. (4.12) vanish at iteration index p + 1, and expanding to first order in terms of the residuals at iteration index p, we have

$$R_n^{(\kappa)k+1}(x_{i,p+1}) \approx R_n^{(\kappa)k+1}(x_{i,p}) + \sum_i \left.\frac{\partial R_n^{(\kappa)k+1}}{\partial x_i}\right|_p (x_{i,p+1}-x_{i,p}) = 0 \qquad (4.13)$$

Equation (4.13) represent a set of 3N coupled linear equations for the $x_{i,p+1}$,

which are solved with an efficient direct solver, using sparse storage techniques (Duff, 1977). Iteration is continued until the residuals are reduced to a small fraction of the accumulation terms (for all n, κ).

$$\left| \frac{R_{n,p+1}^{(\kappa)k+1}}{M_{n,p+1}^{(\kappa)k+1}} \right| \leq \epsilon \quad . \tag{4.14}$$

All derivatives $\partial R_n/\partial x_i$ needed in the coefficient matrix are obtained by numerical differentiation.

It is appropriate to add some comments about the space discretization technique. As an example let us consider a discretized version of the mass flux term, Eq. (4.5).

$$\begin{aligned} F_{\beta,nm}^{(\kappa)} = & - k_{nm} \left(\frac{k_{r\beta}\, \rho_\beta}{\mu_\beta} \right)_{nm} (X_\beta^{(\kappa)})_{nm} \\ & \times \left[\frac{P_{\beta,n} - P_{P_{\beta,m}}}{D_{nm}} - \rho_{\beta,nm}\, g_{nm} \right] \\ & - \delta_{\beta g} (D_{va})_{nm}\, (\rho_\beta)_{nm}\, \frac{X_{\beta,n}^{(\kappa)} - X_{\beta,m}^{(\kappa)}}{D_{nm}} \end{aligned} \tag{4.15}$$

The subscripts (nm) indicate that the respective quantities are to be evaluated at the interface between volume elements n and m, based on average values within V_n and V_m. As has been discussed elsewhere (e.g. Pruess and Narasimhan, 1985), this requires different weighting procedures for different parameters, such as harmonic weighting, spatial interpolation, and upstream weighting.

The entire geometric information of the space discretization in Eq. (4.12) is provided in the form of a list of grid block volumes V_n, interface areas A_{nm},

nodal distances D_{nm}, and components g_{nm} of gravitational acceleration along nodal lines. There is no reference whatsoever to a global system of coordinates, or to the dimensionality of a particular flow problem. The discretized equations are in fact valid for arbitrary irregular discretizations in one, two or three dimensions, and for porous as well as for fractured media. This flexibility should be used with caution, however, because the accuracy of solutions depends upon the accuracy with which the various interface parameters in equations such as (4.15) can be expressed in terms of average conditions in grid blocks. A necessary condition for this to be possible is that there exists approximate thermodynamic equilibrium in (almost) all grid blocks at (almost) all times (Pruess and Narasimhan, 1985). For systems of regular grid blocks referenced to global coordinates (such as r – z, x – y – z), Eq. (4.12) reduce to the conventional finite difference formulation (e.g., Peaceman, 1977).

4.3. FLOW OF STEAM AND WATER THROUGH A TORROIDAL FLOW CHANNEL

4.3.1. Problem Statement

A segment of torroidal flow channel considered in this study is shown schematically in Figure 4.1. The meridional radius ($R + r_t$) is taken to be 1100 μm and the throat radius (r_t) is 100 μm. Steam and water enter the flow channel at the left face, which is the inlet face. We assume that water resides on the flow channel wall in the form of a thin film and that the presence of this film does not

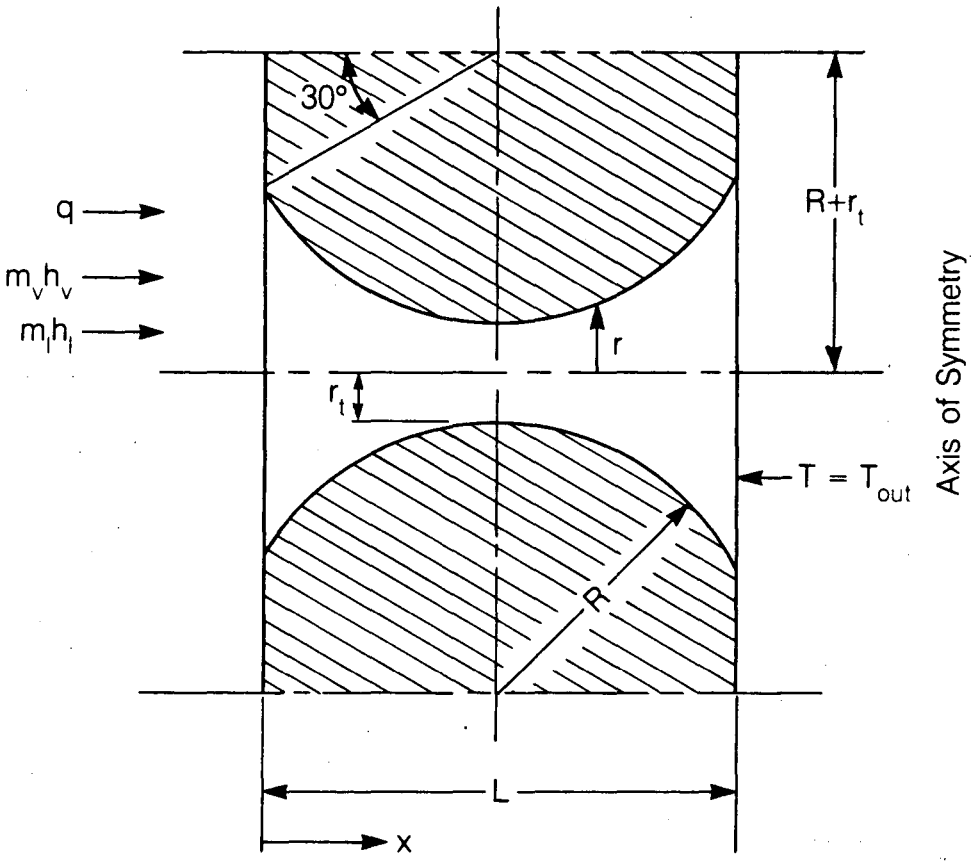

XBL 862-10595

Fig. 4.1. Cross section of a torroidal flow channel used in numerical study.

alter the permeability of the flow channel to the steam phase. This concept has been incorporated into the numerical simulator by appropriate choice of relative permeability functions,

$$k_{rv} = 1 \quad , \quad \text{and} \tag{4.16}$$

$$k_{rl} = S_l^3 \quad , \tag{4.17}$$

where k_{rl} and k_{rv} are the liquid phase and steam phase relative permeabilities, respectively.

The relationship between the local flow rate and the local pressure gradient is assumed to be given by the Hagen-Poiseulle equation

$$m(x) = - \frac{\pi}{8} r^4(x) \frac{P}{\mu} \left. \frac{\partial P}{\partial x} \right|_x \quad . \tag{4.18}$$

Therefore, the intrinsic permeability of the flow channel at any cross section is given by

$$k(x) = \frac{r^2(x)}{8} \quad . \tag{4.19}$$

The outlet face of the flow channel is maintained at $T_{out}(= 101.5\,^\circ C)$ and the corresponding saturation pressure. The solid material forming the wall of the flow channel is impervious to fluids but conducts heat. Capillary pressure within the flow channel is given by

$$P_c = 10^3 \times \frac{1 - S_l}{0.999} \ N/m^2 \tag{4.20}$$

The computational grid used in this study is shown in Figure 4.2. All the elements shown in Figure 4.2 are axisymmetric. Flow in the channel is assumed to be one dimensional — there is no pressure or temperature gradient in the

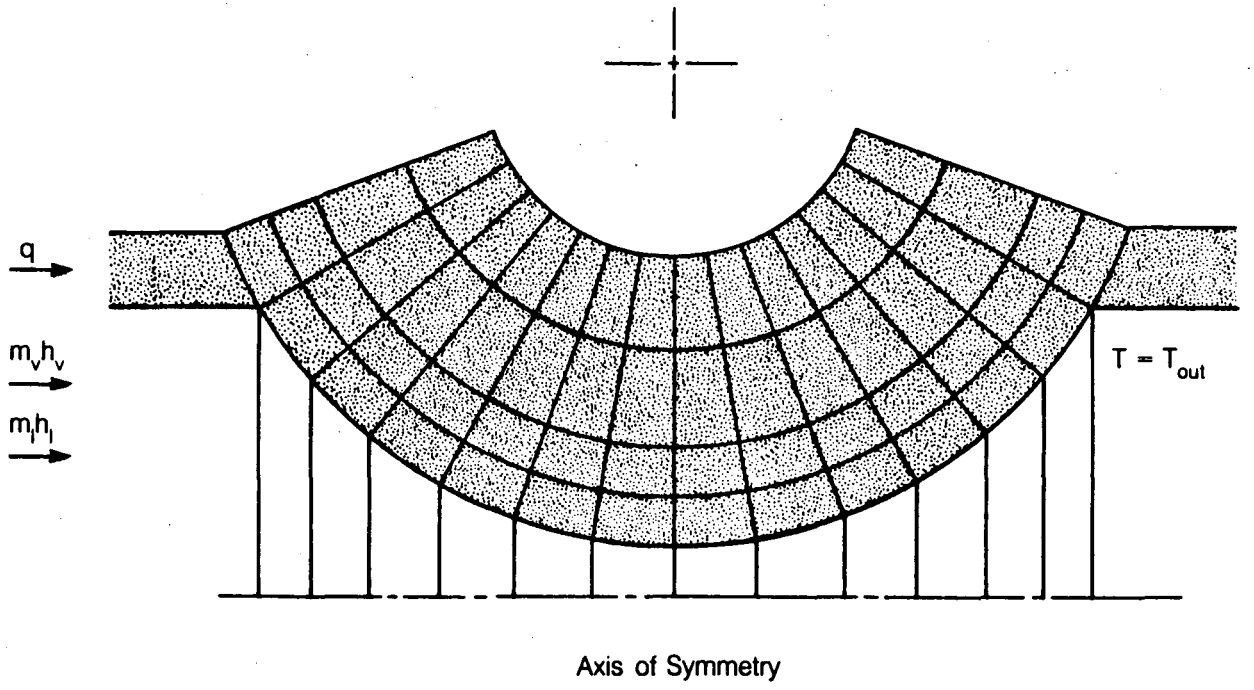

Fig. 4.2. Discretization of the torroidal flow channel in axisymmetric elements.

radial direction in the void space. The wall temperature is assumed to be equal to the local fluid temperature. Mobilities of the fluids are spatially interpolated between adjacent elements.

Five different cases were simulated to study the effect of thermal conductivity and mass flow rate. The parameters used in these studies are listed in Table 4.2.

Table 4.2: Parameters used in numerical study.

Run	$m_{v,o} \times 10^5$ kg/sec	K W/m °C	$\Delta T = T_{in} - T_{out}$ °C
NR-1	7.5634	0.0	3.7
Nr-2	7.5634	2.3	3.7
NR-3	7.5666	2300.0	3.48
NR-4	12.28	2.3	5.67
NR-5	13.108	2.3	5.99

4.3.2. Results

The results of the study are presented in graphical form, showing vapor pressure, temperature, and flow quality distribution in the flow channel. The results for NR-1 are presented in Figure 4.3. The results show that a major fraction of the overall pressure drop across the flow channel takes place in 20% of the flow channel around the throat ($0.4 < x/L < 0.6$). Therefore, the flow characteristics of this segment have a major effect on the overall flow characteristics. It is also indicated in Figure 4.3 that the flow quality, f, increases downstream. This phenomenon is attributed to decreasing specific enthalpies of steam and water in the direction of flow. Since total mass flow rate ($m_l + m_v$) remains

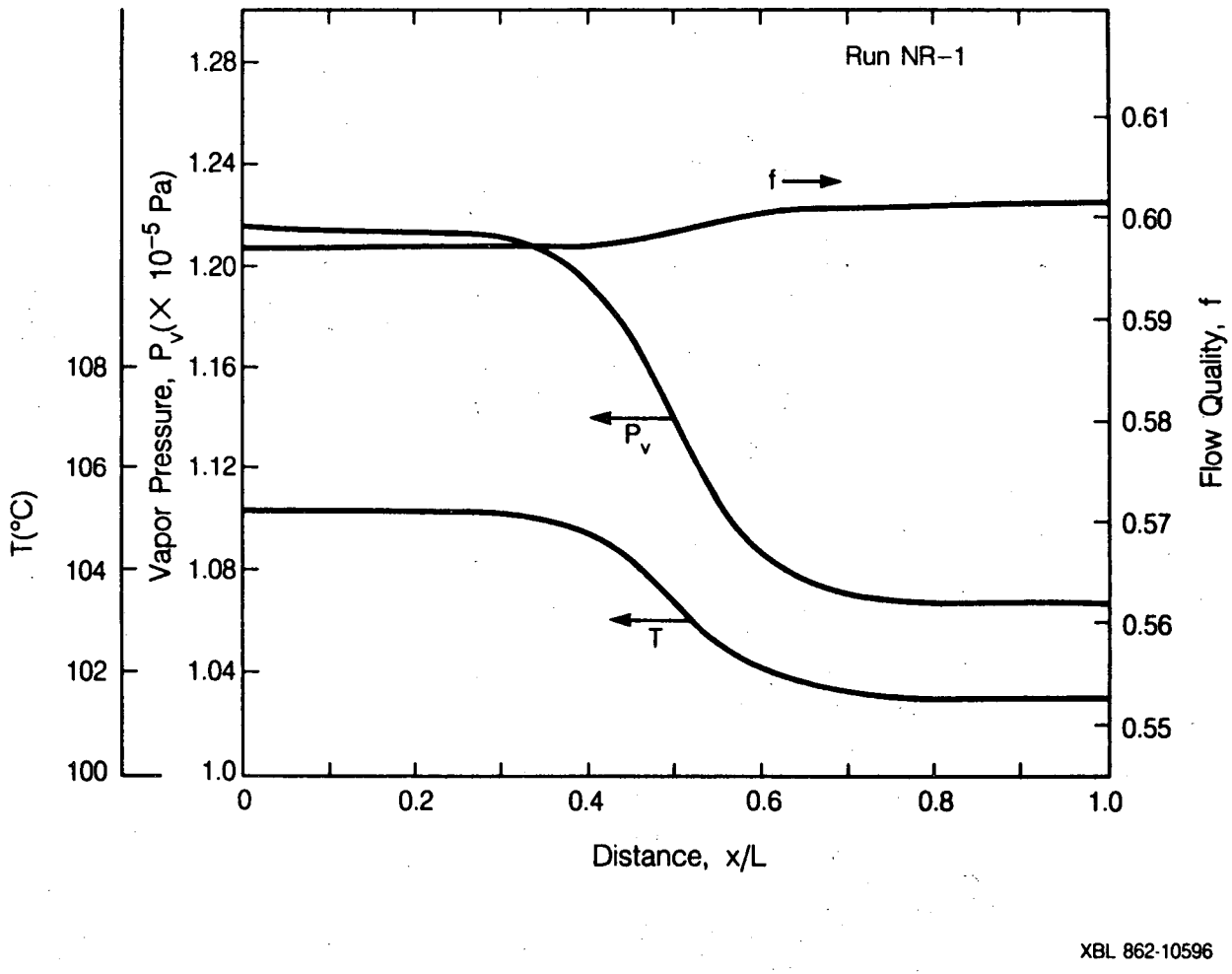

Fig. 4.3. Plot of numerical results for P_v, T, and f in the torroidal flow channel for Run NR-1.

constant and specific enthalpies decrease downstream, total energy flow can only be conserved by phase transformation from liquid to steam.

The results of NR-2 fall within 0.001% of the results of NR-1, indicating that a change in the thermal conductivity of a solid does not have a noticeable effect on the flow characteristics of the flow channel as long as the thermal conductivities are small.

The results of NR-3 are illustrated in Figure 4.4. A major difference between the results of NR-1 and NR-3 is the variation of flow quality within the flow channel. As indicated by the plot, only about 93% of the steam actually goes through the throat in the form of steam. The remaining 7% flows through the throat in liquid form and evaporates downstream. Since the throat segment is the major contributor to the overall flow resistance and because liquid has a much higher mobility than the steam phase, this phase transformation phenomenon results in a lower pressure drop across the flow channel. The results indicate that the pressure drop in NR-3 is 6.3% less than that in NR-2 or NR-1. This indicates that phase transformation effects in high conductivity medium can lead to enhancement of steam phase relative permeability.

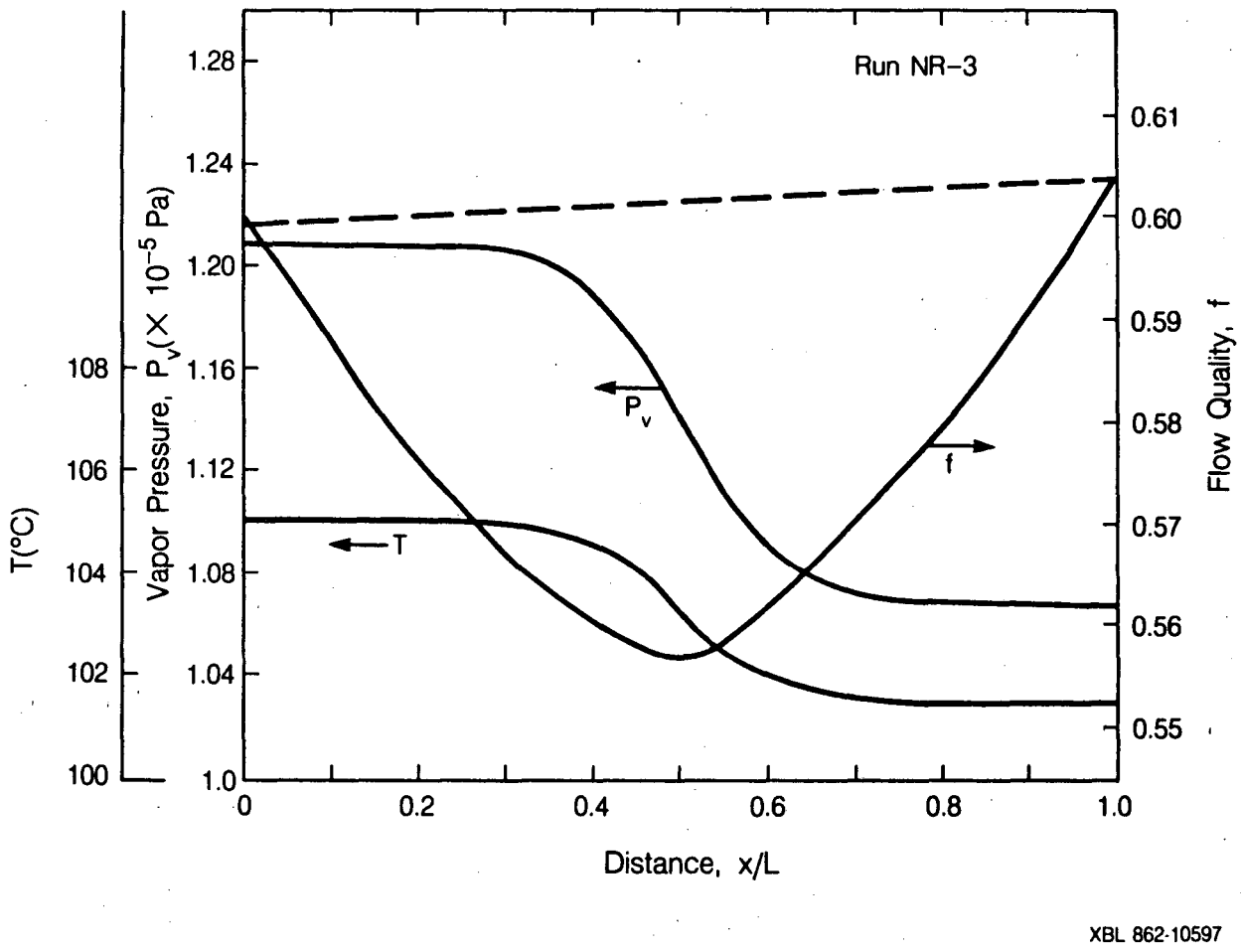

Fig. 4.4. Plot of numerical results for P_v, T, and f in the torroidal flow channel for Run NR-3.

CHAPTER 5
THEORETICAL DEVELOPMENTS

5.1. INTRODUCTION

There are two separate mechanisms by which phase transformation affects relative permeability curves: (1) phase transformation in converging-diverging flow channels with hydrophilic walls can cause an enhancement of steam phase relative permeability; and (2) phase transformation along the interface of a stagnant phase and the phase flowing around it controls the irreducible phase saturation of the stagnant phase. An analytical study of both these phenomena is conducted in the present chapter.

The first mechanism was studied numerically in Chapter 4 of this work where we have obtained results for two-phase steam and water flow through a torroidal pore. However, we have not used the results of the numerical studies to predict permeability enhancement because of two reasons:

(i) We could not disengage the phase transformation mechanism in the numerical code and obtain results without phase transformation to evaluate its effects.

(ii) Our preliminary investigation showed that at low flow rates, such as the ones shown in Table 4.2, and low thermal conductivities, the effects of phase transformation would probably be masked by space discretization errors. Therefore, the impact of this effect is investigated in this chapter using an analytical technique.

An analytical solution to steam-water flow, with phase transformation, through a flow channel of arbitrary cross section has been obtained with the aid of the combined first and second laws of thermodynamics. This solution technique was applied to a torroidal flow channel and the effects of phase transformation were evaluated.

An analysis of the irreducible phase conditions is presented in Chapter 5.3. We have obtained the thermodynamic conditions under which a "cluster" of trapped phase can exist in equilibrium with its surroundings. If such conditions exist then the phase can remain trapped and contribute to irreducible phase saturation of that phase. We have shown, therefore, that irreducible phase saturations in steam-water flow depend, in part on local thermodynamic conditions.

5.2. SOLUTION TO TWO-PHASE STEAM-WATER FLOW THROUGH A FLOW CHANNEL OF ARBITRARY CROSS SECTION BY COMBINED FIRST AND SECOND LAWS OF THERMODYNAMICS

5.2.1. Overview

It is customary in the discipline of heat and mass transfer to seek a solution based only on the conservation equations. However, most problems in two-phase, single component flow are highly nonlinear and not amenable to the analytical solution techniques available. The nonlinearities arising out of variable properties and phase transformation make the problem so complex that simultaneous solution of the conservation equations can be obtained by numerical techniques only. In the present chapter we propose a novel solution technique to these nonlinear

problems, by combining the first and second laws of thermodynamics. We propose that the solution to these problems is given by the functional form of the dependent variable which satisfies the conservation equations and also minimizes the entropy generation in the flow channel.

5.2.2. Theory

Simultaneous flow of steam and water through a channel of arbitrary cross section is irreversible because: (1) there are friction losses in the flow channel; and (2) the flow is associated with transfer of heat energy from a high temperature reservoir to one at a lower temperature. Therefore, this flow, like any other irreversible flow, results in generation of entropy along the flow path (Bejan, 1982).

It is a well known law of nature that the steady state of any physical system, under given constraints, represents the state of minimum potential energy which the system is capable of achieving. By analogy, we can state that for a given mass and energy flow rate of steam and water through a flow channel of given properties, the flow adjusts itself such that the flow tends to be as reversible as possible. In the present context, where all parameters and properties are specified, we can rephrase the above statement to propose that for a given mass flow rate of a mixture of steam and water of given quality into a flow channel, the local, nonlinear parameters adjust themselves such that the overall generation of entropy across the flow channel is minimum.

5.2.3. Problem Statement

We consider two-phase, steady, creeping flow of steam and water through a flow channel of arbitrary cross section, of length L, as shown schematically in Figure 5.1. The hydraulic transmissivity and the thermal conductivity of the flow channel are assumed to depend on the location within the flow channel. As the flow progresses downstream, there will, in general, be transformation of phases depending on the local thermodynamic conditions and flow quality will also vary from point to point.

The governing equations for this problem are:

(i) Continuity equation

$$m_v + m_l = m = \text{constant} \quad ; \tag{5.1}$$

(ii) Momentum equation,

$$m_v = - \frac{k k_{rv} A \rho_v}{\mu_v} \frac{dP_v}{dx} \quad , \tag{5.2}$$

$$m_l = - \frac{k k_{rl} A \rho_l}{\mu_l} \frac{dP_l}{dx} \quad , \tag{5.3}$$

(iii) Energy equation,

$$m_v h_v + m_l h_l + q = Q = \text{constant} \quad ; \tag{5.4}$$

where m_v and m_l are the mass flow rates of steam and water, respectively. Specific enthalpies of steam and water are denoted by h_v and h_l, q is the conductive heat flux, and Q is the total energy transported through the channel. The boundary conditions at the inlet face and the outlet face are:

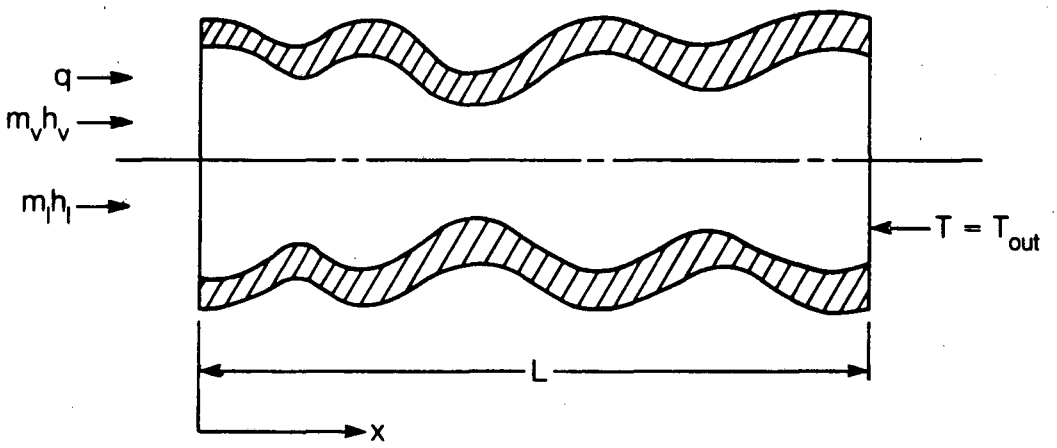

XBL 862-10592

Fig. 5.1. Schematic of a flow channel of arbitrary cross section.

$$m_v \Big|_{x=0} = - \frac{k k_{rv} A \rho_v}{\mu_v} \frac{dP_v}{dx} \Big|_{x=0} \quad ; \tag{5.5}$$

$$m_l \Big|_{x=0} = - \frac{k k_{rl} A \rho_l}{\mu_l} \frac{dP_l}{dx} \Big|_{x=0} \quad ; \tag{5.6}$$

and

$$T \Big|_{x=L} = T_{out} \quad . \tag{5.7}$$

In order to simplify the problem, we can assume without loss of generality that the flow quality (f) at the inlet is close to unity, i.e.,

$$f \equiv \frac{m_v}{m_v + m_l} \sim 1 \quad . \tag{5.8}$$

We also invoke the following assumptions:

(i) The channel wall is hydrophilic so liquid resides on the channel wall in the form of film. The mechanical and the thermodynamic equilibrium of this film is given, respectively, by the Augmented Young-Laplace equation (Eq. (3.17)) and modified Kelvin's equation (Eq. (3.31)).

(ii) Small changes in the flowing quality due to condensation in the flow channel do not affect the transmissivity of the channel to the steam phase. The validity of this assumption can be demonstrated with the aid of the following example. Let us consider steam flowing at a velocity of 1 mm per second in a circular flow channel of 100 μm radius. Assume that 10% of the steam condenses and gets transported in the form of liquid at some location. If the local temperature is 110 ° C and the slip ratio is 5, then the condensed liquid will form a 250 angs (0.025 μm) thick film on the wall. If we assume the relative permeability to steam depends on phase saturation according to

(Yuster, 1951),

$$k_{rv} = 2\,S_v\,\frac{\mu_v}{\mu_l} + S_v^2\left(1 - 2\,\frac{\mu_v}{\mu_l}\right) \quad , \tag{5.9}$$

then the transmissivity of the flow channel to steam due to the presence of the liquid film would decrease by less than 0.09%.

(iii) Conductive heat flux is given by $q = -\lambda\,\frac{dT}{dx}$ where λ is effective heat transmissivity and $\frac{dT}{dx}$ is the temperature gradient in the flow channel. We assume λ to be constant.

(iv) Pressure and temperature in steam phase are correlated according to the modified Clausius-Clapeyron equation (see Appendix 5.A)

$$dp = \left(\frac{h_{lv}}{v_v T}\right)_{av} dT \tag{5.10}$$

where subscript "av" represents an averaged quantity.

(v) Hydrodynamic fluid properties, ρ and μ, are constant.

Upon invoking the above assumption the governing equations can be rewritten as

$$m_v + m_l = m = \text{constant}, \tag{5.11}$$

$$m_v = -\,\frac{\tau(x)\,\rho_v}{\mu_v}\left(\frac{h_{lv}}{v_v T}\right)_{av}\frac{dT}{dx} \quad , \tag{5.12}$$

$$m_l = -\frac{\tau_l(s_l,x)\,\rho_l}{\mu_l}\,\frac{dP_l}{dx} \quad , \text{ and} \tag{5.13}$$

$$m_v h_v + m_l h_l + q = Q = \text{constant} \quad , \tag{5.14}$$

where $\tau(x)$ is the transmissivity of the flow channel (= kA) and $\tau_l(s_l,x)$ is the

transmissivity of the flow channel to the liquid phase. It is worth noting at this stage that the transmissivity to the steam phase is taken to be an intrinsic property of the flow channel but transmissivity to liquid phase, τ_l, depends on the liquid phase saturation.

The boundary conditions can be written as

$$m_v \Big|_{x=0} = - \frac{\tau \rho_v}{\mu_v} \left(\frac{h_{lv}}{v_v T} \right)_{av} \frac{dT}{dx} \Big|_{x=0} , \tag{5.15}$$

and

$$T \Big|_{x=L} = T_{out} . \tag{5.16}$$

We attempt to solve the above problem and obtain a solution for the temperature distribution in the flow channel. Since pressure and temperature are correlated, we can also obtain the pressure distribution from the above mentioned solution.

5.2.4 Solution Technique

The solution technique involves finding that functional for temperature which satisfies the governing Eqs. (5.11)-(5.14) and also minimizes the generation of entropy in the flow channel, subject to the boundary conditions given by Eqs. (5.15) and (5.16).

Entropy generation in an element of length dx, normal to the axis of the flow channel, is given by (Bejan, 1982)

$$S_{gen} dx = \frac{\partial s_f}{\partial t} dx - \left(\frac{q}{T} + m_l s_l + m_v s_v \right)_{in}$$

$$+\left(\frac{q}{T} + m_l s_l + m_v s_v\right)_{out} \tag{5.17}$$

Where s_f is the entropy content of the element, S_{gen} is the entropy generation per unit length of the flow channel, s_i is the specific entropy of phase i, and the other symbols have their usual meaning. We can substitute $\frac{\partial s_f}{\partial t} = 0$, for the steady case and rewrite Eq. (5.17) in the differential form as,

$$S_{gen} = \frac{d(m_v s_v)}{dx} + \frac{d(m_l s_l)}{dx} + \frac{d(q/T)}{dx} \quad . \tag{5.18}$$

The conservation equations (Eqs. (5.11) and (5.14)) can be represented in differential form as

$$\frac{dm_v}{dx} + \frac{dm_l}{dx} = 0 \quad , \tag{5.19}$$

and

$$\frac{d(m_v h_v)}{dx} + \frac{d(m_l h_l)}{dx} + \frac{dq}{dx} = 0 \quad . \tag{5.20}$$

Equations (5.18), (5.19), and (4.20) can be combined together along with thermodynamic relationships

$$s_{lv} = \frac{h_{lv}}{T} \quad , \tag{5.21}$$

and

$$ds = \frac{1}{T}\, dh + \frac{v}{T}\, dP \tag{5.22}$$

to obtain (see Appendix 5.B)

$$S_{gen} = \left\{\frac{\lambda}{T^2} - \frac{\tau}{\mu_v T}\left(\frac{h_{lv}}{v_v T}\right)^2\right\}\left(\frac{dT}{dx}\right)^2 \tag{5.23}$$

where λ is the thermal transmissivity given by

$$\lambda = -q\left(\frac{dT}{dx}\right)^{-1} \quad , \tag{5.24}$$

and other symbols have their usual meaning.

It is worth noting at this stage that the mass and energy conservation equations are already accounted for in Eq. (5.23)

We seek, as our solution, that functional form for temperature, T, which minimizes

$$\bar{S}_{gen} = \int_0^L S_{gen}\, dx \tag{5.25}$$

subject to the boundary conditions given by equations (5.15) and (5.16). In order to obtain our solution we introduce the following dimensionless parameters

$$\hat{\tau}(\eta) = \frac{\tau\, T_{out}}{\lambda\, \mu_v}\left(\frac{h_{lv}}{v_v T}\right)_{av}^2 \quad , \tag{5.26}$$

$$\theta(\eta) = \frac{T}{T_{out}} \quad , \tag{5.27}$$

$$\eta = \frac{x}{L} \quad , \tag{5.28}$$

and

$$\hat{S}_{gen} = \frac{L^2 S_{gen}}{\lambda} \tag{5.29}$$

into equation (4.23) to obtain

$$\hat{S}_{gen} = \left(\frac{1}{\theta^2} - \frac{\hat{\tau}}{\theta}\right)\left(\frac{d\theta}{d\eta}\right)^2 \quad . \tag{5.30}$$

The boundary conditions (Eqs. (5.15) and (5.16)) can be rewritten in terms of these dimensionless parameters as

$$\left.\frac{d\theta}{d\eta}\right|_{\eta=0} = \theta'(0) \quad , \tag{5.31}$$

and

$$\theta(1) = 1 \tag{5.32}$$

where

$$\theta'(0) \equiv \frac{-m_v L}{\lambda \rho_v \hat{\tau}} \left(\frac{h_{lv}}{v_v T}\right)_{av} \Bigg|_{\eta=0} \quad . \tag{5.33}$$

Now the problem reduces to finding that functional form of θ which minimizes

$$\int_0^1 \left\{\frac{1}{\theta^2} - \frac{\hat{\tau}}{\theta}\right\}\left\{\frac{d\theta}{d\eta}\right\}^2 d\eta \tag{5.34}$$

subject to the boundary conditions in equation (5.31) and (5.32). It is a variational problem and we solve this by variational methods (Appendix 5.C) to obtain a differential equation for θ, given by

$$\left(\frac{1}{\theta} - \hat{\tau}\right)\frac{d^2\theta}{d\eta^2} - \left(\frac{1}{\theta^2} - \frac{\hat{\tau}}{2\theta}\right)\left(\frac{d\theta}{d\eta}\right)^2 - \frac{d\hat{\tau}}{d\eta}\frac{d\theta}{d\eta} = 0 \quad . \tag{5.35}$$

Solution of equation (5.35) subject to equations (5.31) and (5.32) gives the solution to the problem specified in the previous section.

5.3 EFFECTS OF PHASE TRANSFORMATION ON EFFECTIVE PERMEABILITY OF A TORROIDAL FLOW CHANNEL

5.3.1. Problem Statement

Let us consider two-phase flow of steam and water through a torroidal flow channel shown schematically in Figure 4.1. We assume that, under suitable approximations, the governing equation for the flow is given by equation (5.35) and that the boundary conditions are given by equations (5.31) and (5.32).

The transmissivity (τ) of the flow channel at any location (x = X) is given by (see Appendix 5.D)

$$\tau = \frac{\pi R^4}{8} (1 - \alpha - \{1 - \cos^2\Omega(1 - 2\eta)^2\}^{1/2})^4 \tag{5.36}$$

where $\eta = x/L$, $\alpha = r_t/R$, and Ω is the excluded angle (see Fig. 5.2). Substituting equation (5.36) into equation (5.26) we obtain an expression for dimensionless transmissivity,

$$\hat{\tau} = \Upsilon (1 - \alpha - \{1 - \cos^2\Omega(1 - 2\eta)^2\}^{1/2})^4 \tag{5.37}$$

where

$$\Upsilon = \frac{\pi R^4}{8} \frac{T_{out}}{\lambda \mu_v} \left(\frac{h_{lv}}{v_v T} \right)_{av}^2 . \tag{5.38}$$

This expression for $\hat{\tau}$ was introduced in equation (5.35) and the resulting equation was solved numerically using a multiple shooting technique using Newton's method (Keller, 1968). Twelve different cases were solved for different parameters shown below in Table 5.1.

Notation En in Table 5.1 denotes enhancement due to phase transformation and is defined as

$$En = \frac{(T_{in} - T_{out})_1 - (T_{in} - T_{out})_2}{(T_{in} - T_{out})_1} \times 100 \quad , \tag{5.39}$$

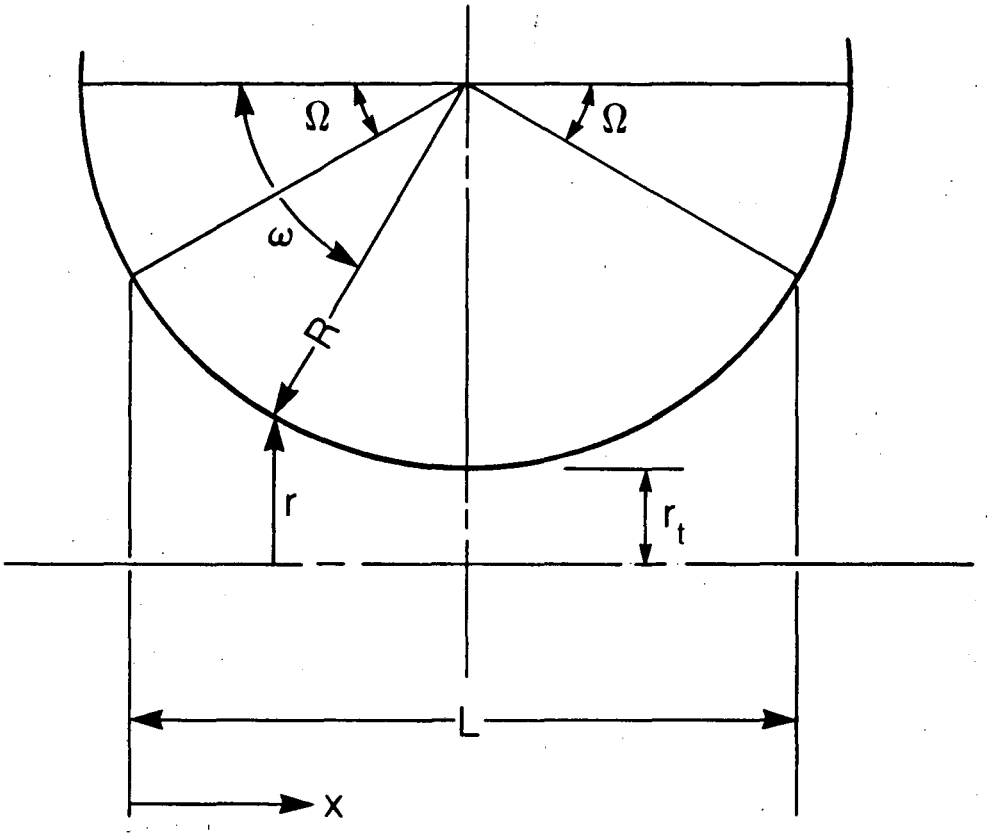

XBL 862-10593

Fig. 5.2. Geometry of torroidal flow channel.

Table 5.1.
Parameters used in semianalytic solution.

Run	$\Upsilon \times 10^{-9}$	$\theta'(0) \times 10^{-2}$	α	En (%)	Single phase run
SA-1	1.8	–1.0	0.1		
SA-2	1.0	–1.0	0.1		
SA-3	100.0	–1.0	0.1		
SA-4	1.8	–0.5	0.1		
SA-5	1.0	–0.5	0.1		
SA-6	100.0	–0.5	0.1		
SA-7	4.11	–1.0	0.1	0.79	SSA-1
SA-8	4.11	–0.5	0.1	0.399	SSA-2
SA-9	4.11	–10.0	0.1	6.614	SSA-3
SA-10	4.11	–1.0	0.05	5.50	SSA-4
SA-11	4.11	–0.5	0.05	2.977	SSA-5
SA-12	4.11	–10.0	0.05	27.16	SSA-6

where T_{in} and T_{out} denote the temperatures at the inlet face and the outlet face of the flow channel, respectively. Subscript 2 denotes the solution of Eq. (5.35) (i.e., with phase transformation), while subscript 1 denotes the solution for temperature in a case where phase transformation has been supressed. Therefore, under present assumptions, subscript 1 represents the temperature drop across the flow channel, for steam flow, corresponding to the intrinsic permeability of the flow channel. The method for obtaining this solution is straight forward and is described below.

If we assume that there is no phase transformation in the flow channel, then the mass of steam crossing any cross section of the flow channel is constant and is given by

$$m_{v,o} = \frac{-\tau \rho_v}{\mu_v} \frac{dP_v}{dx} \quad . \tag{5.40}$$

Substituting for pressure gradient from Eq. (5.40), for τ from Eq. (5.26), and representing T and x in dimensionless form with the aid of Eqs. (5.27) and (5.28), we obtain

$$\frac{d\theta}{d\eta} = \frac{-\hat{m}}{\hat{\tau}} \quad , \tag{5.41}$$

where

$$\hat{m} = \frac{m_{v,o} L}{\lambda P_v} \left(\frac{h_{lv}}{T v_v} \right)_{av} \quad , \tag{5.42}$$

and $\hat{\tau}$ is given by Eq. (5.37). Differentiating Eq. (5.41) with respect to η and rearranging we obtain

$$\frac{d^2\theta}{d\eta^2} = \frac{1}{\hat{\tau}} \frac{d\hat{\tau}}{d\eta} \frac{d\theta}{d\eta} \quad . \tag{5.43}$$

Solution of Eq. (5.43) with the boundary conditions given in Eqs. (5.31) and (5.32) yields the solution represented by subscript 1 in Eq. (5.39).

Six different cases corresponding to SA-7 through SA-12 were solved for single phase steam transport. These cases are referred to as SSA-1 through SSA-6.

5.3.2. Results

The results of analytic study, showing the distribution of θ and θ' in the channel for the 12 different cases listed in Table 5.1, are tabulated in Table 5.2.

Table 5.2 : Semianalytic Solution to Two Phase Flow

RUN SA-1

η	θ	θ'
0.00000000	1.03208814	-0.00010000
0.10000000	1.03205889	-0.00062885
0.20000000	1.03188927	-0.00356166
0.30000000	1.03096179	-0.01884513
0.40000000	1.02676463	-0.07361487
0.50000000	1.01598073	-0.12858454
0.60000000	1.00525377	-0.07283971
0.70000000	1.00110931	-0.01857030
0.80000000	1.00019578	-0.00350654
0.90000000	1.00002879	-0.00061902
1.00000000	1.00000000	-0.00009843

RUN SA-2

0.00000000	1.03208814	-0.00010000
0.10000000	1.03205889	-0.00062885
0.20000000	1.03188927	-0.00356166
0.30000000	1.03096179	-0.01884514
0.40000000	1.02676463	-0.07361487
0.50000000	1.01598073	-0.12858454
0.60000000	1.00525377	-0.07283970
0.70000000	1.00110931	-0.01857030
0.80000000	1.00019578	-0.00350654
0.90000000	1.00002879	-0.00061902
1.00000000	1.00000000	-0.00009843

Table 5.2 (Cont.)

RUN SA-3

0.00000000	1.03208814	-0.00010000
0.10000000	1.03205889	-0.00062885
0.20000000	1.03188927	-0.00356166
0.30000000	1.03096179	-0.01884514
0.40000000	1.02676463	-0.07361487
0.50000000	1.01598073	-0.12858454
0.60000000	1.00525377	-0.07283971
0.70000000	1.00110931	-0.01857030
0.80000000	1.00019578	-0.00350654
0.90000000	1.00002879	-0.00061902
1.00000000	1.00000000	-0.00009843

RUN SA-4

0.00000000	1.01610642	-0.00005000
0.10000000	1.01609179	-0.00031443
0.20000000	1.01600698	-0.00178091
0.30000000	1.01554317	-0.00942510
0.40000000	1.01344297	-0.03685434
0.50000000	1.00803713	-0.06454210
0.60000000	1.00264574	-0.03665750
0.70000000	1.00055892	-0.00935532
0.80000000	1.00009865	-0.00176692
0.90000000	1.00001451	-0.00031193
1.00000000	1.00000000	-0.00004960

Table 5.2 (Cont.)

RUN SA-5

0.00000000	1.01610642	-0.00005000
0.10000000	1.01609179	-0.00031443
0.20000000	1.01600698	-0.00178091
0.30000000	1.01554317	-0.00942510
0.40000000	1.01344297	-0.03685434
0.50000000	1.00803713	-0.06454210
0.60000000	1.00264574	-0.03665750
0.70000000	1.00055892	-0.00935532
0.80000000	1.00009865	-0.00176692
0.90000000	1.00001451	-0.00031193
1.00000000	1.00000000	-0.00004960

RUN SA-6

0.00000000	1.01610642	-0.00005000
0.10000000	1.01609179	-0.00031443
0.20000000	1.01600698	-0.00178091
0.30000000	1.01554316	-0.00942510
0.40000000	1.01344296	-0.03685434
0.50000000	1.00803712	-0.06454210
0.60000000	1.00264574	-0.03665750
0.70000000	1.00055892	-0.00935531
0.80000000	1.00009865	-0.00176692
0.90000000	1.00001451	-0.00031193
1.00000000	1.00000000	-0.00004960

Table 5.2 (Cont.)

RUN SA-7

0.00000000	1.03208814	-0.00010000
0.10000000	1.03205889	-0.00062885
0.20000000	1.03188927	-0.00356166
0.30000000	1.03096179	-0.01884514
0.40000000	1.02676463	-0.07361487
0.50000000	1.01598073	-0.12858454
0.60000000	1.00525377	-0.07283971
0.70000000	1.00110931	-0.01857030
0.80000000	1.00019578	-0.00350654
0.90000000	1.00002879	-0.00061902
1.00000000	1.00000000	-0.00009843

RUN SA-8

0.00000000	1.01610642	-0.00005000
0.10000000	1.01609179	-0.00031443
0.20000000	1.01600698	-0.00178091
0.30000000	1.01554317	-0.00942510
0.40000000	1.01344296	-0.03685433
0.50000000	1.00803712	-0.06454210
0.60000000	1.00264574	-0.03665750
0.70000000	1.00055892	-0.00935531
0.80000000	1.00009865	-0.00176692
0.90000000	1.00001451	-0.00031193
1.00000000	1.00000000	-0.00004960

Table 5.2 (Cont.)

RUN SA-9

0.00000000	1.30335192	-0.00100000
0.10000000	1.30305943	-0.00628789
0.20000000	1.30136383	-0.03559282
0.30000000	1.29210970	-0.18773930
0.40000000	1.25059296	-0.72296231
0.50000000	1.14666020	-1.21560068
0.60000000	1.04723554	-0.66157649
0.70000000	1.00989308	-0.16597532
0.80000000	1.00174285	-0.03122781
0.90000000	1.00025623	-0.00550907
1.00000000	1.00000000	-0.00087593

RUN SA-10

0.00000000	1.24683210	-0.00010000
0.10000000	1.24679861	-0.00078207
0.20000000	1.24653831	-0.00625068
0.30000000	1.24423176	-0.05826598
0.40000000	1.22283558	-0.50411170
0.50000000	1.12001624	-1.38764459
0.60000000	1.02171140	-0.46079444
0.70000000	1.00233134	-0.05229624
0.80000000	1.00026314	-0.00559928
0.90000000	1.00002999	-0.00070041
1.00000000	1.00000000	-0.00008956

Table 5.2 (Cont.)

RUN SA-11

0.00000000	1.12645256	-0.00005000
0.10000000	1.12643582	-0.00039104
0.20000000	1.12630567	-0.00312550
0.30000000	1.12515209	-0.02914658
0.40000000	1.11442827	-0.25315490
0.50000000	1.06228550	-0.71089303
0.60000000	1.01139196	-0.24116839
0.70000000	1.00122604	-0.02749467
0.80000000	1.00013842	-0.00294525
0.90000000	1.00001577	-0.00036844
1.00000000	1.00000000	-0.00004711

RUN SA-12

0.00000000	3.04801346	-0.00100000
0.10000000	3.04767864	-0.00782034
0.20000000	3.04507609	-0.06248402
0.30000000	3.02205201	-0.58077902
0.40000000	2.81165147	-4.88898882
0.50000000	1.88493166	-11.51355531
0.60000000	1.14288536	-3.11702293
0.70000000	1.01495766	-0.33657694
0.80000000	1.00168359	-0.03583733
0.90000000	1.00019180	-0.00448005
1.00000000	1.00000000	-0.00057279

Comparing the results of SA-1 with SA-3 and SA-4 with SA-6, we find that the results are insensitive to variation in Υ for the parameters considered. Similar observations were made in the numerical study (Chapter 4) where changing the thermal conductivity of the solid from 0.0 in NR-1 to 2.3 in NR-2 had a negligible effect on the outcome. These cases represent the situations where conductive heat flux in the flow channel is orders of magnitude smaller than the convective heat flux. Therefore, slight variations in thermal conductivity (or Υ) have a negligible effect on the results.

The results of the analytical study were verified by comparing them against the numerical results for identical problems. Figure 5.3 illustrates a typical comparison of the results of the two different methods. Physical parameters from NR-5 used to calculate dimensionless parameters in SA-8 are listed in Table 5.3. Figure 5.3 shows that there is an excellent match between the numerical and the analytical results, thus confirming the analytical solution.

Solutions to Eq. (5.43), i.e., single phase steam flow without phase transformation, are presented in Table 5.4. The six different runs, SSA-1 to SSA-6, are single phase solutions to the problems presented, in the same sequence, in SA-7 to SA-12 (i.e., the parameters used in SSA-1 are identical to those used in SA-7). The results shown in these tables are used in Eq. (5.39) to evaluate En which is listed in Table 5.1.

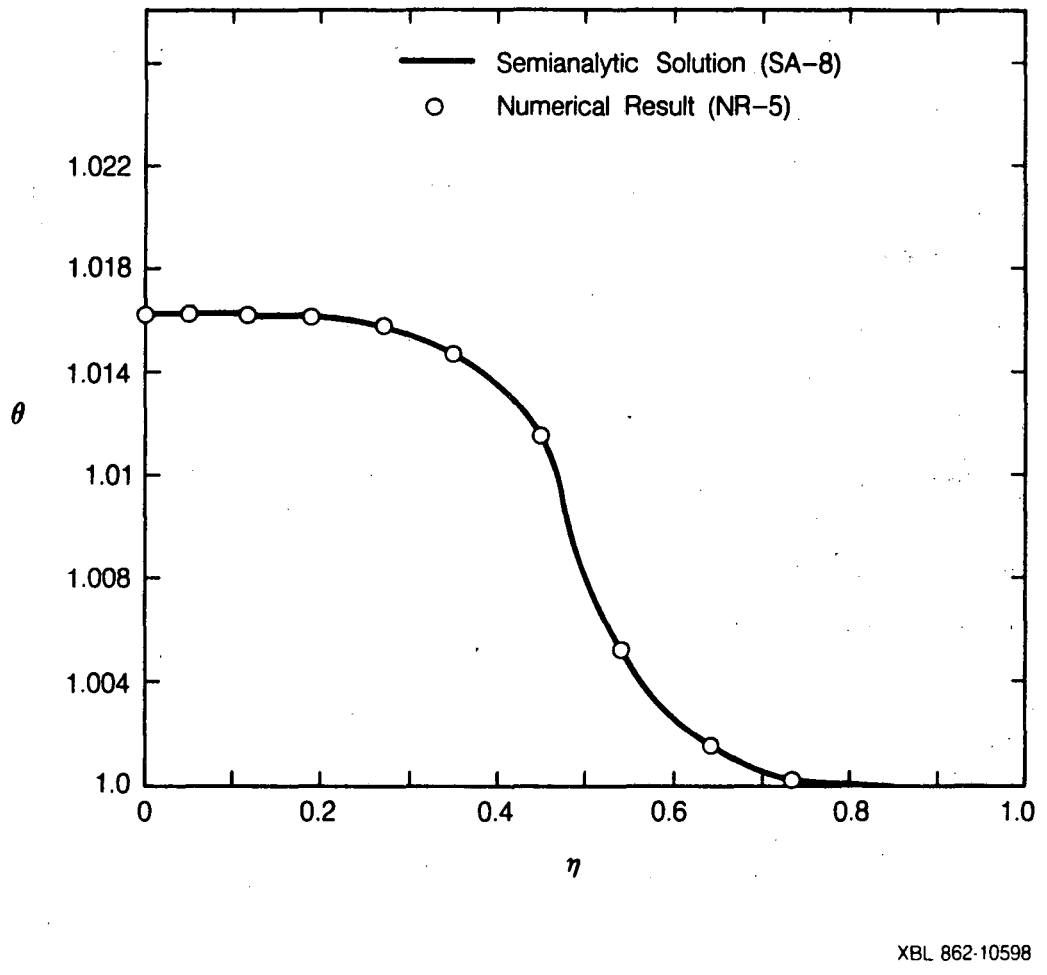

Fig. 5.3. Comparison semianalytic solution (SA-8) with the numerical results for an identical problem (NR-5).

Table 5.4 : Semianalytic Solution to Single Phase Flow

RUN SSA-1

η	θ	θ'
0.00000000	1.03234151	-0.00010000
0.10000000	1.03231225	-0.00062886
0.20000000	1.03214262	-0.00356200
0.30000000	1.03121485	-0.01885543
0.40000000	1.02701111	-0.07380546
0.50000000	1.01617076	-0.12959982
0.60000000	1.00533040	-0.07380550
0.70000000	1.00112666	-0.01885544
0.80000000	1.00019888	-0.00356200
0.90000000	1.00002925	-0.00062886
1.00000000	1.00000000	-0.00010000

RUN SSA-2

0.00000000	1.01617075	-0.00005000
0.10000000	1.01615613	-0.00031443
0.20000000	1.01607131	-0.00178100
0.30000000	1.01560742	-0.00942771
0.40000000	1.01350555	-0.03690273
0.50000000	1.00808538	-0.06479991
0.60000000	1.00266520	-0.03690275
0.70000000	1.00056333	-0.00942772
0.80000000	1.00009944	-0.00178100
0.90000000	1.00001463	-0.00031443
1.00000000	1.00000000	-0.00005000

Table 5.4 (Cont.)

RUN SSA-3

0.00000000	1.32341506	-0.00100000
0.10000000	1.32312256	-0.00628859
0.20000000	1.32142621	-0.03562000
0.30000000	1.31214849	-0.18855427
0.40000000	1.27011110	-0.73805466
0.50000000	1.16170756	-1.29599827
0.60000000	1.05330400	-0.73805501
0.70000000	1.01126658	-0.18855440
0.80000000	1.00198885	-0.03562002
0.90000000	1.00029250	-0.00628860
1.00000000	1.00000000	-0.00100000

RUN SSA-4

0.00000000	1.26043148	-0.00010000
0.10000000	1.26039800	-0.00078208
0.20000000	1.26013767	-0.00625142
0.30000000	1.25782978	-0.05832683
0.40000000	1.23631838	-0.50903394
0.50000000	1.13021577	-1.46409779
0.60000000	1.02411312	-0.50903437
0.70000000	1.00260170	-0.05832689
0.80000000	1.00029381	-0.00625142
0.90000000	1.00003348	-0.00078208
1.00000000	1.00000000	-0.00010000

Table 5.4 (Cont.)

RUN SSA-5

0.00000000	1.13021574	-0.00005000
0.10000000	1.13019899	-0.00039104
0.20000000	1.13006883	-0.00312571
0.30000000	1.12891489	-0.02916342
0.40000000	1.11815919	-0.25451696
0.50000000	1.06510788	-0.73204888
0.60000000	1.01205656	-0.25451718
0.70000000	1.00130085	-0.02916344
0.80000000	1.00014690	-0.00312571
0.90000000	1.00001674	-0.00039104
1.00000000	1.00000000	-0.00005000

RUN SSA-6

0.00000000	3.60431476	-0.00100000
0.10000000	3.60397993	-0.00782076
0.20000000	3.60137669	-0.06251415
0.30000000	3.57829779	-0.58326832
0.40000000	3.36318376	-5.09033938
0.50000000	2.30215771	-14.64097779
0.60000000	1.24113123	-5.09034364
0.70000000	1.02601700	-0.58326892
0.80000000	1.00293808	-0.06251421
0.90000000	1.00033483	-0.00782077
1.00000000	1.00000000	-0.00100000

Table 5.3.
Physical parameters of NR-5.

$m_{v,o} = 1.274 \times 10^{-4}$ kg/sec
$T_{out} = 374.65\,^{\circ}K$
$T_{av} = 377.645\,^{\circ}K$
$\tau_o = 5.09 \times 10^{-14}$ m^4
$\nu_v = 17.6 \times 10^{-6}$ m^2/sec
$v_v = 1.46$ m$^{3/kg}$
$L = 1.732 \times 10^{-3}$ m
$h_{lv} = 2.2446 \times 10^{6}$ J/kg
$R = 10^{-3}$ m
$\lambda = 4.92 \times 10^{-8}$ Wm/$^{\circ}$K
$r_t = 10^{-4}$ m

The effects of phase transformation on effective permeability of the flow channel are reflected in factor En. The results of SA-7, SA-8, and SA-9 indicate that the enhancement effects are very small for small flow velocities and for a moderately constricted flow channel (i.e., $\alpha \geq 0.1$). The factor Υ in all these runs is for materials with typical thermal conductivities of ceramic or geologic materials. The results are expected to be different for more conductive materials such as copper or silver (see the results of NR-3 in Chapter 4).

A comparison of En for SA-7, SA-8, and SA-9 against SA-10, SA-11, and SA-12 shows that the degree of constriction has a significant effect on effective

permeability enhancement. For example, a mere reduction in α by a factor of 0.5 changes En by a factor of 7.46 for SA-8.

5.4. EFFECTS OF PHASE TRANSFORMATION ON IRREDUCIBLE PHASE CONDITIONS

5.4.1. Overview

Phase trapping can occur when one of the phases becomes immobile under the action of capillary pressure in a channel full of the other phase which flows around it. This phenomenon is important in this study for two reasons:

(i) Phase trapping is an important mechanism of permeability reduction; and

(ii) Phase trapping can lead to local changes that are hysteretic in nature as observed by Udell and Burr (1982) in his "Hot Wire" experiment.

For phase trapping to occur in a steady flow of steam and water:

(i) there must exist a balance of mechanical forces at every point of the interface of the trapped phase and the phase surrounding it, and

(ii) all the phases must remain in thermodynamic equilibrium at every point on the interface.

We have used the above mentioned criteria along with the thermodynamic relations proposed in Chapter 3 to obtain the flow conditions where phase trapping can occur. Two separate studies, one for steam trapping and the other for liquid trapping are conducted.

5.4.2. Thermodynamic Control of Steam Trapping

Trapping of steam phase can occur either in a bubble form at a pore throat (Fig. 5.4) or in a cluster form which spans over several pore bodies and throat (Fig. 5.5). The governing equations and the thermodynamic criteria for stability are the same in both these cases. Therefore, the relationships developed below apply to both these cases.

To study the phase trapping mechanism in a two-phase steam/water flow in porous media, the following assumptions are made:

a) Water is the wetting fluid. Steam resides on the concave side of the steam/water interface and both the liquid and the steam phases are superheated (Udell, 1983).

b) Pores are large enough so that the effect of adsorption on phase equilibrium can be neglected.

c) Water, steam and the matrix are locally in thermodynamic equilibrium and any phase transformation is quasistatic.

d) The bubble contains pure steam. This assumption is made only to simplify the problem. Inclusion of non-condensible gas into this analysis is straight forward, at least conceptually.

e) Flow is Darcian, hence the pressure and temperature gradients are small.

Upon invoking these assumptions, the mechanical equilibrium of the bubble (or cluster) is given by the Augmented Young-Laplace equation,

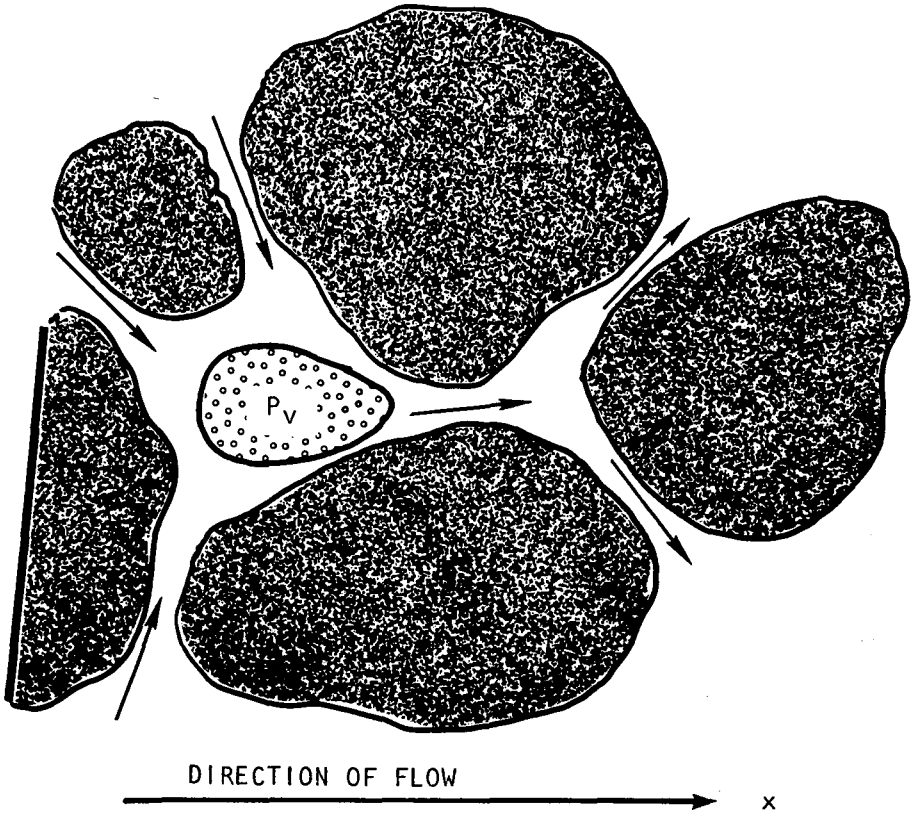

Fig. 5.4. Schematic of a trapped vapor bubble.

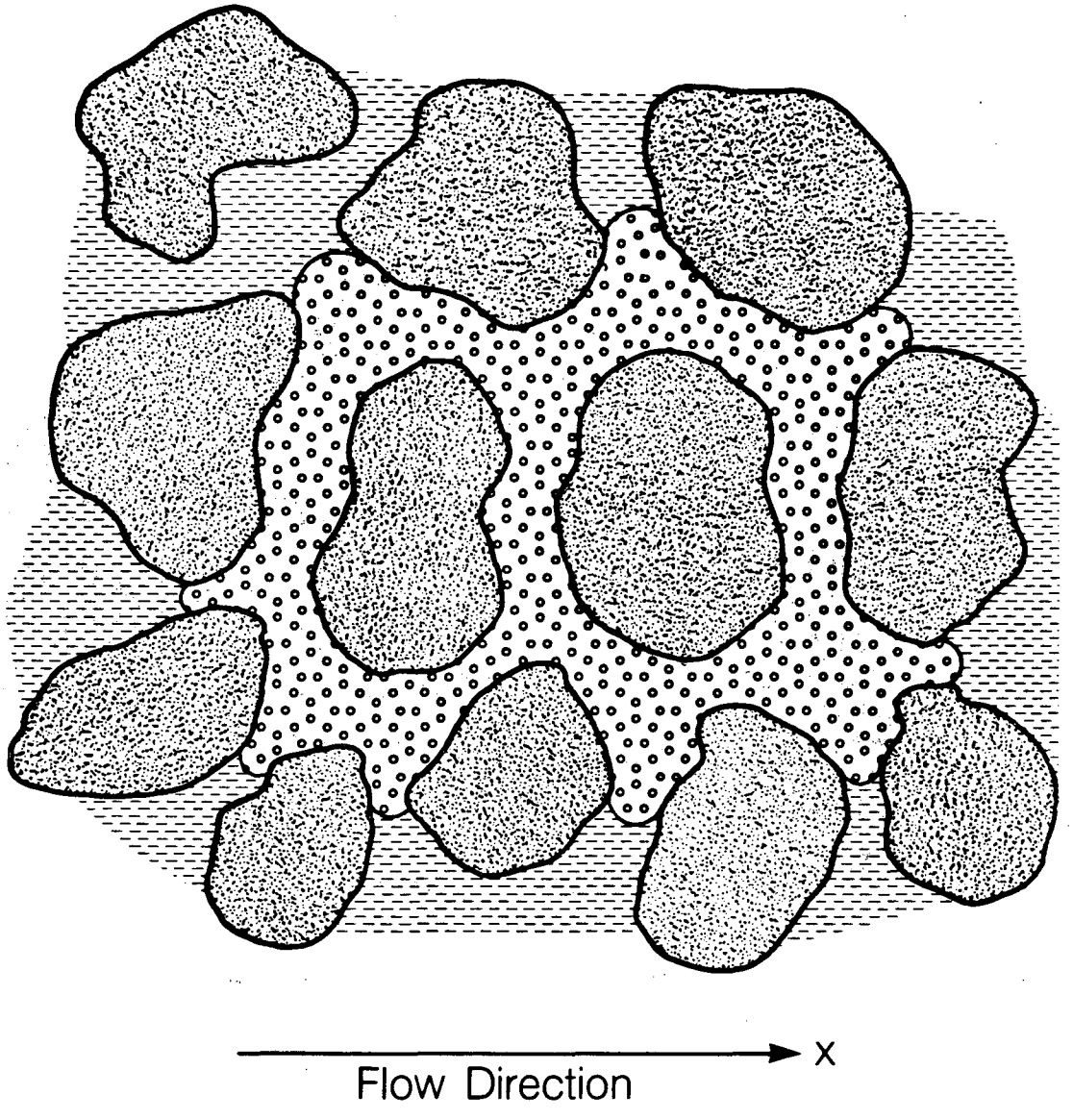

Fig. 5.5. Schematic of a trapped vapor cluster.

$$\Delta P = P_v - P_l = \frac{2\gamma}{r} + \pi \quad , \tag{5.44}$$

and thermodynamic equilibrium is given by modified Kelvin's equation (Eqn. 3.31)

$$\ln \frac{P_v}{P_\infty} = \frac{-\Delta P\ v_l}{RT} \quad . \tag{5.45}$$

Since $\frac{\Delta P\ v_l}{RT}$ is usually $<<1$, Eq. (5.45) can be written as

$$P_v = P_\infty \left(1 - \frac{\Delta P\ v_l}{RT} \right) \quad . \tag{5.46}$$

Neglecting the effect of gravity in the steam phase, we can regard steam pressure within the bubble to be constant. Differentiating Eq. (5.44), with this assumption, with respect to x (scaler distance in the direction of flow), we obtain

$$\frac{\partial \Delta P}{\partial x} = - \frac{\partial P_l}{\partial x} \quad . \tag{5.47}$$

Differentiating Eq. (5.46) for constant P_v, we obtain

$$\left(1 - \frac{\Delta P v_l}{RT} \right) \frac{\partial P_\infty}{\partial x} - \frac{P_\infty v_l}{RT} \left(\frac{\partial \Delta P}{\partial x} - \frac{\Delta P}{T} \frac{\partial T}{\partial x} \right) = 0 \quad . \tag{5.48}$$

Since $\frac{\Delta P v_l}{RT} << 1$ and P_∞ is correlated to temperature according to Clausius-Clapeyron equation

$$d P_\infty = \frac{h_{lv}}{v_v T}\, dT \quad , \tag{5.49}$$

Eq. (5.48) can be simplified and rearranged to obtain

$$\frac{\partial \Delta P}{\partial x} = \left(\frac{R\ h_{lv}}{v_v v_l P_\infty} + \frac{\Delta P}{T} \right) \frac{\partial T}{\partial x} \quad . \tag{5.50}$$

Equating the right hand side of Eqs. (5.47) and (5.50) we obtain a necessary

condition for vapor trapping, i.e.,

$$\frac{\partial P_l}{\partial x} = -\left(\frac{R\, h_{lv}}{v_v v_l P_\infty} + \frac{\Delta P}{T}\right)\frac{\partial T}{\partial x} \tag{5.51}$$

since the coefficient of $\frac{\partial T}{\partial x}$ is always positive, we can simply state that a necessary condition for vapor trapping is given by

$$\frac{\partial P_l}{\partial x}\,\frac{\partial T}{\partial x} < 0 \quad . \tag{5.52}$$

5.4.3. Thermodynamic Control of Liquid Trapping

Liquid can be trapped either as individual cessile drops (Fig. 5.6) or in a cluster form (Fig. 5.7). However, the governing equations for both these cases are the same and, therefore, we shall refer to the trapped clusters as drops.

All the assumptions stated in the previous section are applicable to the present case. However, unlike the previous section, we can not always assume that liquid phase pressure within the drop is the same everywhere. The mechanical and the thermodynamic equilibrium of the drop is given, respectively, by Eqs. (5.44) and (5.46).

Differentiating Eq. (5.44) and rearranging we obtain,

$$\frac{\partial P_v}{\partial x} = \frac{\partial \Delta P}{\partial x} + \frac{\partial P_l}{\partial x} \quad . \tag{5.53}$$

Differentiating Eq. (5.46), substituting Eq. (5.49) and rearranging, we obtain the equation for thermodynamic equilibrium,

$$\left(\frac{h_{lv}}{v_v T} + \frac{P_\infty \Delta P\, v_l}{RT^2}\right)\frac{\partial T}{\partial x} = \left(1 + \frac{P_\infty v_l}{RT}\right)\frac{\partial \Delta P}{\partial x} + \frac{\partial P_l}{\partial x} \quad . \tag{5.54}$$

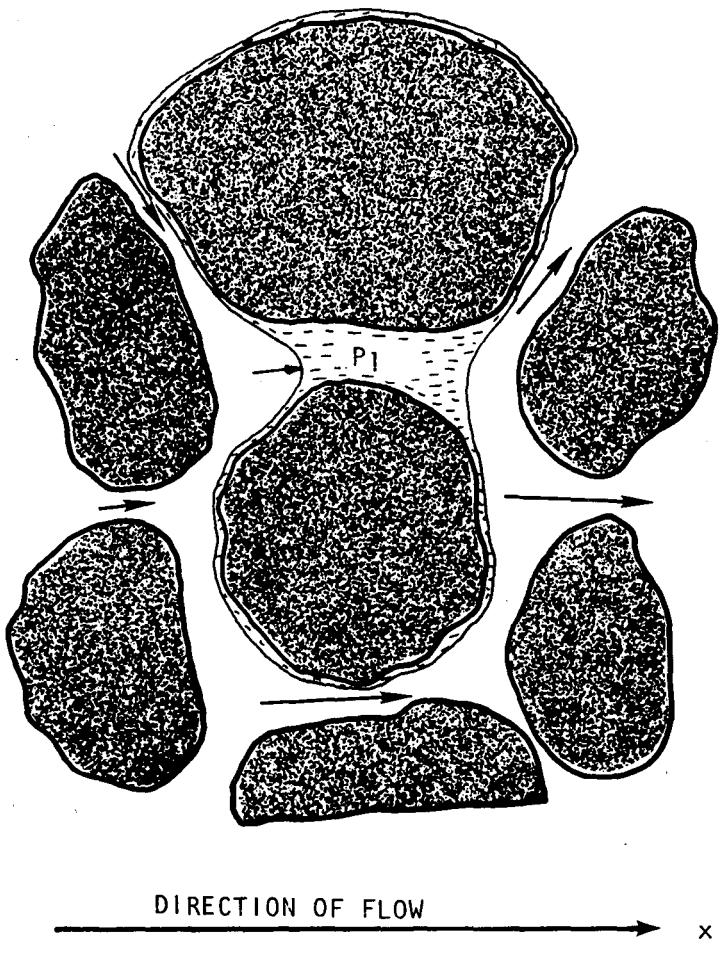

Fig. 5.6. Schematic of a trapped cessile crop of liquid.

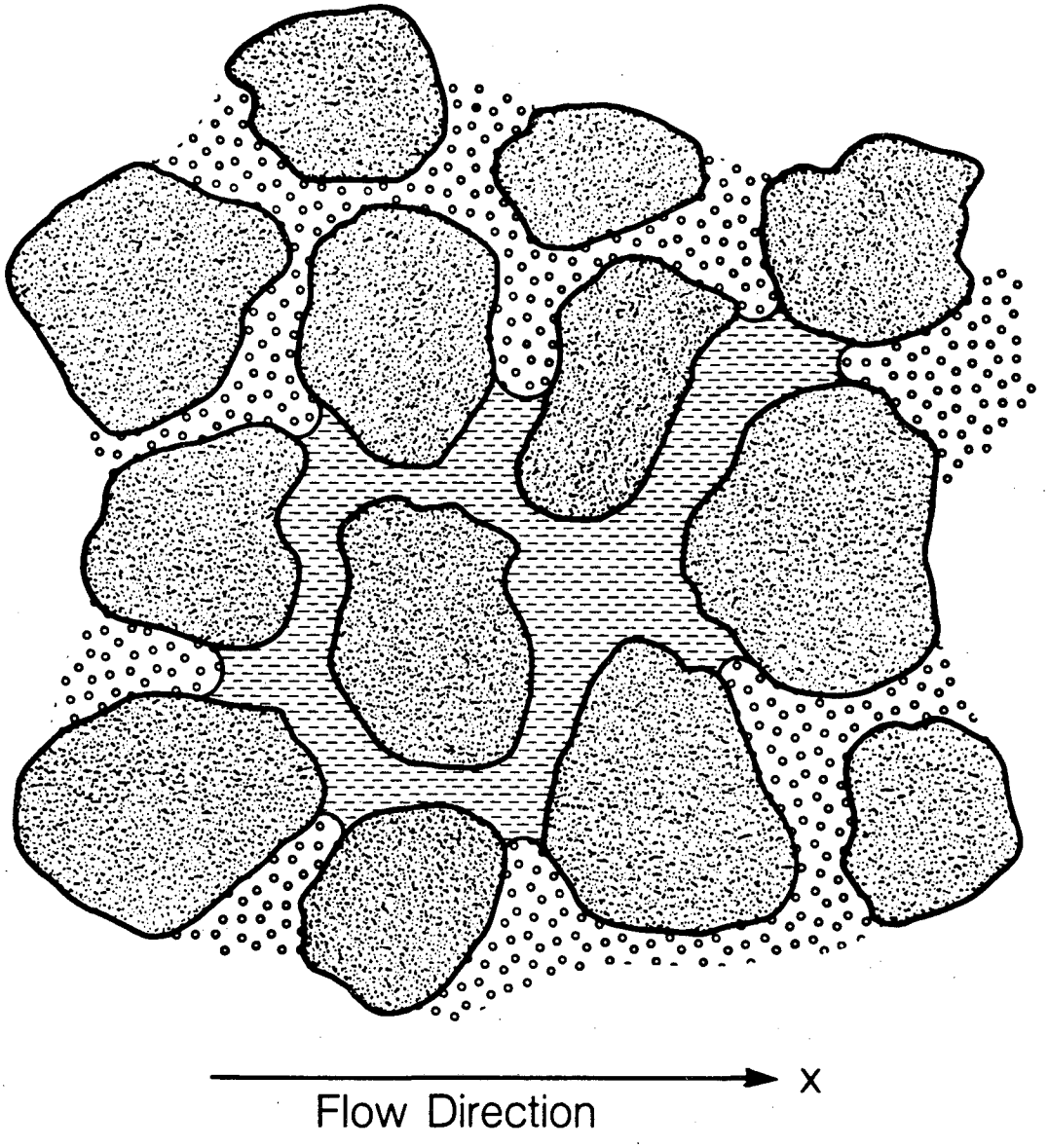

Fig. 5.7. Schematic of a trapped cluster of liquid.

Pressure gradient in a stagnant liquid drop is given by

$$\frac{\partial P_l}{\partial x} = \rho_l \vec{g} \cos\Phi \tag{5.55}$$

where Φ represents the angle that the direction of flow makes with respect to the direction of gravity. It is zero when flow is vertically downwards. Therefore, Eqs. (5.53) and (5.54) can be written as

$$\frac{\partial P_v}{\partial x} = \frac{\partial \Delta P}{\partial x} + \rho_l \vec{g} \cos\Phi \quad , \tag{5.56}$$

and

$$\left(\frac{h_{lv}}{v_v T} + \frac{P_\infty \Delta P v_l}{RT^2} \right) \frac{\partial T}{\partial x} = \left(1 + \frac{P_\infty v_l}{RT} \right) \frac{\partial \Delta P}{\partial x} + \rho_l \vec{g} \cos\Phi \tag{5.57}$$

In order to solve these two equations simultaneously, we have to know $\frac{\partial P_v}{\partial x}$ from the mass flow rate of steam. However, for a simple case where $\Phi = 90°$ (i.e., flow is horizontal, $\frac{\partial P_l}{\partial x} = 0$) Eqs. (5.56) and (5.57) simply reduce to

$$\frac{\partial P_v}{\partial x} = \frac{\partial \Delta P}{\partial x} < 0 \tag{5.58}$$

and

$$\frac{\partial T}{\partial x} = \left(1 + \frac{P_\infty v_l}{RT} \right) \left(\frac{h_{lv}}{v_v T} + \frac{P_\infty \Delta P \, v_l}{RT^2} \right)^{-1} \frac{\partial \Delta P}{\partial x} \quad . \tag{5.59}$$

These equations show that liquid can be trapped when steam flows horizontally toward lower temperature.

APPENDIX 5.A
MODIFIED CLAUSIUS-CLAPEYRON EQUATION

If the effective radius of curvature is "large" and the film thickness is larger than molecular scale than the correlation between vapor pressure and temperature is given by the Clausius-Clapeyron equation (Eq. (3.4)). Since we are interested in variations in thermodynamic properties of the flowing fluids over a small range due to flow across a length scale of a pore, the Clausius-Clapeyron equation can be represented as

$$dP = \frac{h_{lv,av}}{v_{v,av} T_{av}} dT \tag{5.A.1}$$

where the averaged quantities could be derived, based on geometric considerations, from the Clausius-Clapeyron curve (Fig. 5.A.1). For example, integrating the Clausius-Clapeyron equation from (P_1,T_1) to (P_2,T_2), we get

$$\Delta P \equiv (P_2 - P_1) = \int_{T_1}^{T_2} \frac{h_{lv,av}}{v_{v,av}} \frac{dT}{T} \quad . \tag{5.A.2}$$

In terms of the averaged quantities the same equation can be represented as

$$\Delta p = \frac{h_{lv,av}\, \Delta T}{v_{v,av} T_{av}} \tag{5.A.3}$$

where $\Delta T \equiv T_2 - T_1$. Integrating the right hand side of Eq. (5.A.2) and equating it to the right hand side of Eq. (5.A.3), we get

$$T_{av} = \Delta T \left\{ \ln \frac{T_2}{T_1} \right\}^{-1} \quad . \tag{5.A.4}$$

Expressions for other average quantities, $h_{lv,av}$ and $v_{v,av}$, can be obtained in a similar fashion.

APPENDIX 5.B
ENTROPY GENERATION IN TWO-PHASE STREAM-WATER FLOW

Differentiating Eq. (5.18) and making use of Eq. (5.19) we obtain

$$S_{gen} = s_{lv} \frac{dm_v}{dx} + m_v \frac{ds_v}{dx} + m_l \frac{ds_l}{dx} + \frac{1}{T} \frac{dq}{dx} - \frac{q}{T^2} \frac{dT}{dx} \tag{5.B.1}$$

where $s_{lv} = s_v - s_l$. Representing s_{lv} and the gradients of entropy in terms of other thermodynamic properties, and with the aid of Eqs. (5.21) and (5.22) we obtain

$$S_{gen} = \frac{1}{T}\left\{ h_{lv} \frac{dm_v}{dx} + m_v \frac{dh_v}{dx} + m_l \frac{dh_l}{dx} + \frac{dq}{dx} \right\}$$

$$+ \frac{m_v v_v}{T} \frac{dP_v}{dx} + \frac{m_l v_l}{T} \frac{dP_l}{dx} - \frac{q}{T^2} \frac{dT}{dx} \quad . \tag{5.B.2}$$

Differentiating the first two terms of Eq. (5.20) and using Eq. (5.19) we can show that the first term on the right hand side of Eq. (5.B.2) is identically zero. Therefore, Eq. (5.B.2) can be written as

$$S_{gen} = \frac{m_v v_v}{T} \frac{dP_v}{dx} + \frac{m_l v_l}{T} \frac{dP_l}{dx} - \frac{q}{T^2} \frac{dT}{dx} \quad . \tag{5.B.3}$$

Since, $m_v >> m_l$, $v_v >> v_l$ and $\frac{dP_l}{dx} \sim \frac{dP_v}{dx}$, the second term on the right hand side of Eq. (5.B.3) is negligible compared to the first term. We can substitute for m_v from Eq. (5.12), use Eq. (5.10) for pressure gradient, and substitute

$$q = -\lambda \frac{dT}{dx} \tag{5.B.4}$$

into Eq. (4.B.3) to obtain

$$S_{gen} = \left\{ \frac{\lambda}{T^2} - \frac{\tau}{\mu_v T} \left(\frac{h_{lv}}{v_v T} \right)^2 \right\} \left(\frac{dT}{dx} \right)^2 \quad . \qquad \text{(5.B.5)}$$

APPENDIX 5.C
VARIATIONAL PROBLEM IN ENTROPY MINIMIZATION

We have to find the minima of

$$I_0 = \int_0^1 \left(\frac{1}{\theta^2} - \frac{\hat{\tau}}{\theta} \right) \left(\frac{d\theta}{d\eta} \right)^2 d\eta \tag{5.C.1}$$

subject to boundary conditions

$$\left. \frac{d\theta}{d\eta} \right|_{\eta=0} = \theta' (0) \quad , \tag{5.C.2}$$

and

$$\theta(1) = 1 \quad . \tag{5.C.3}$$

Let us consider minimization of

$$I = \int_0^1 \left(\frac{1}{\theta^2} - \frac{\hat{\tau}}{\theta} \right) \left(\frac{d\theta}{d\eta} \right)^2 d\eta - \varsigma\theta^2 \Big|_{\eta=0} \tag{5.C.4}$$

where ς is a constant given by

$$\varsigma = \left(\frac{1}{\theta^3} - \frac{\hat{\tau}}{\theta^2} \right) \frac{d\theta}{d\eta} \Big|_{\eta=0} \quad . \tag{5.C.5}$$

Variation of I is defined as

$$\delta I(\theta) = \frac{d}{d\epsilon} [I(\theta + \epsilon\beta)]_{\epsilon=0} \tag{5.C.6}$$

Therefore,

$$\delta I = \frac{d}{d\epsilon} \int_0^1 \left\{ \frac{1}{(\theta + \epsilon\beta)^2} \text{ mark- } \frac{\hat{\tau}}{\theta + \epsilon\beta} \right\} \left\{ \frac{d(\theta + \epsilon\beta)}{d\eta} \right\}^2 d\eta \Big|_{\epsilon=0}$$

$$- \varsigma \left[\frac{d(\theta + \epsilon\beta)^2}{d\epsilon} \right]_{\epsilon=0} \Bigg|_{\eta=0} \tag{5.C.7}$$

Interchanging integration and differentiation we obtain,

$$\delta I = \int_0^1 \frac{d}{d\epsilon} \left[\left\{ \frac{1}{(\theta + \epsilon\beta)^2} - \frac{\hat{\tau}}{(\theta + \epsilon\beta)} \right\} (\theta' + \epsilon\beta')^2 \right]_{\epsilon=0} d\eta$$

$$- \varsigma\, 2(\theta + \epsilon\beta)\, \beta \Big|_{\epsilon=0} \Big|_{\eta=0} \tag{5.C.8}$$

where primes denote $\frac{d}{d\eta}$. Differentiating with respect to ϵ and setting $\epsilon = 0$, we obtain,

$$\delta I = \int_0^1 \left[\left(\frac{1}{\theta^2} - \frac{\hat{\tau}}{\theta} \right) 2\theta' \beta' + \left(\frac{\hat{\tau}}{\theta} - \frac{2}{\theta^2} \right) \frac{\theta'^2}{\theta} \beta \right] d\eta$$

$$- \varsigma\, 2\theta\beta \Big|_{\eta=0} \quad . \tag{5.C.9}$$

Integrating the first term of the integrand by parts and rearranging we obtain

$$\delta I = \int_0^1 \left[\left(\frac{\hat{\tau}}{\theta} - \frac{2}{\theta^2} \right) \frac{\theta'^2}{\theta} - \frac{d}{d\eta} \left\{ \left(\frac{1}{\theta^2} - \frac{\hat{\tau}}{\theta} \right) 2\theta' \right\} \right] \beta d\eta$$

$$+ \left(\frac{1}{\theta^2} - \frac{\hat{\tau}}{\theta} \right) 2\theta' \beta \Big|_0^1 - \varsigma\, 2\theta\beta \Big|_{\eta=0} \quad . \tag{5.C.10}$$

Using the boundary condition $\theta(1) = 1$, we can set

$$\beta(1) = 0 \quad . \tag{5.C.11}$$

Substituting for ς from Eq. (5.C.5) we obtain

$$2\varsigma\theta\beta \Big|_{\eta=0} - \left(\frac{1}{\theta^2} - \frac{\hat{\tau}}{\theta} \right) 2\theta' \beta \Big|_{\eta=0} = 0 \quad . \tag{5.C.12}$$

Therefore Eq. (5.C.10) reduces to

$$\delta I = \int_0^1 \left[\left(\frac{\hat{\tau}}{\theta} - \frac{2}{\theta^2} \right) \frac{\theta'^{\,2}}{\theta} - \frac{d}{d\eta} \left\{ \left(\frac{1}{\theta^2} - \frac{\hat{\tau}}{\theta} \right) 2\theta' \right\} \right] \beta d\eta \qquad (5.C.13)$$

If θ is the functional form which minimizes I, then θ is the solution to equation

$$\delta I = 0 \quad , \qquad (5.C.14)$$

subject to boundary conditions in Eqs. (5.C.2) and (5.C.3). Substituting for δI from Eq. (5.C.13) we obtain

$$\int_0^1 \left[\left(\frac{\hat{\tau}}{\theta} - \frac{2}{\theta^2} \right) \frac{\theta'^{\,2}}{\theta} - \frac{d}{d\eta} \left\{ \left(\frac{1}{\theta^2} - \frac{\hat{\tau}}{\theta} \right) 2\theta' \right\} \right] \beta d\eta = 0 \quad . \qquad (5.C.15)$$

Since the integral is identically zero for all $\beta(\eta)$, the integrand must identically equal zero. Therefore, upon rearranging, we obtain,

$$\frac{d}{d\eta} \left\{ \left(\frac{1}{\theta^2} - \frac{\hat{\tau}}{\theta} \right) 2\theta' \right\} + \left(\frac{2}{\theta^2} - \frac{\hat{\tau}}{\theta} \right) \frac{\theta'^{\,2}}{\theta} = 0 \quad . \qquad (5.C.16)$$

Differentiating the first term and rearranging we obtain

$$\left(\frac{1}{\theta} - \hat{\tau} \right) \frac{d^2\theta}{d\eta 2} - \frac{d\hat{\tau}}{d\eta} \frac{d\theta}{d\eta} - \left(\frac{1}{\theta^2} - \frac{\hat{\tau}}{2\theta} \right) \left(\frac{d\theta}{d\eta} \right)^2 = 0 \quad . \qquad (5.C.17)$$

Solution of this differential equation (Eqn. 5.C.17) with boundary conditions as in Eqs. (5.C.2) and (5.C.3) give a functional form of θ which minimizes "I", given in Eq. (5.C.4). However, we can recall from Eq. (5.30) that the integrand in Eq. (5.C.4) equals $\hat{S}_{gen}$. Therefore, solution of Eq. (5.C.17) with the given boundary conditions minimizes

$$I = \int_0^1 \hat{S}_{gen}\, d\eta - \left[\left(\frac{1}{\theta} - \hat{\tau} \right) \frac{d\theta}{d\eta} \right]_{\eta=0} \qquad (5.C.18)$$

subject to the same boundary conditions. Since $\left. \frac{d\theta}{d\eta} \right|_{\eta=0}$ is a constant and $\hat{\tau}(0) >> \frac{1}{\theta(0)}$, the second term of Eq. (5.C.17) can be regarded as constant. We

can, therefore, conclude that finding the minima of I is the same as finding the minima of entropy generation in the flow channel.

APPENDIX 5.D
TRANSMISSIVITY OF FLOW CHANNEL

Consider the flow channel in Figure 5.2.

$$L = 2R\cos\Omega \tag{5.D.1}$$

$$x = \frac{L}{2}\left(1 - \frac{\cos\omega}{\cos\Omega}\right) \tag{5.D.2}$$

$$\cos\omega = \cos\Omega(1 - 2\eta) \quad , \tag{5.D.3}$$

where $\eta = x/L$.

$$\sin\omega = \sqrt{1 - \cos^2\omega} = \{1 - \cos^2\Omega(1 - 2\eta)^2\}^{1/2} \quad . \tag{5.D.4}$$

The radius r of the flow channel is given by

$$\begin{aligned} r &= r_t + R(1 - \sin\omega) \\ &= R(1 + \alpha - \sin\omega) \quad , \end{aligned} \tag{5.D.5}$$

where $\alpha = r_t/R$. The transmissivity of the flow channel at any location is given by

$$\tau = \frac{\pi r^4}{8} \quad . \tag{5.D.6}$$

Substituting Eqs. (5.D.4) and (5.D.5) into Eq. (5.D.6) gives

$$\tau = \frac{\pi R^4}{8}\left\{1 - \alpha - \{1 - \cos^2\Omega(1 - 2\eta)^2\}^{1/2}\right\}^4 \quad . \tag{5.D.7}$$

CHAPTER 6
EXPERIMENTAL INVESTIGATION

6.1 INTRODUCTION

The present chapter reports on an experimental study of two-phase steam-water flow through porous media which yielded information on relative permeability functions and the capillary pressure curve. The experiment was conducted on two-phase, one dimensional, steady, and concurrent flow of steam and water through a column (100 cm long, 7.62 cm I.D.) packed with 100 μm diameter glass beads. Temperature, vapor pressure, and liquid pressure were measured at regular intervals along the column. Saturation readings were obtained with the aid of a γ-ray densitometer. From the experimental data we obtained relative permeability and capillary pressure as a function of saturation for the porous medium. These functions were subsequently used in the numerical model to simulate temperature, pressure, and saturation along the entire column. Good agreement with the experimental results was found, thus confirming the relative permeability functions and capillary pressure curves obtained.

6.2 EXPERIMENTAL APPROACH

6.2.1 Experimental Method

The schematic of the experimental setup is presented in Figure 6.1. The test cell consists of a high temperature epoxy tube (7.62 cm I.D. $\times$ 100 cm length) packed with 100 μm pyrex glass beads. The beads are held in place by an inlet-

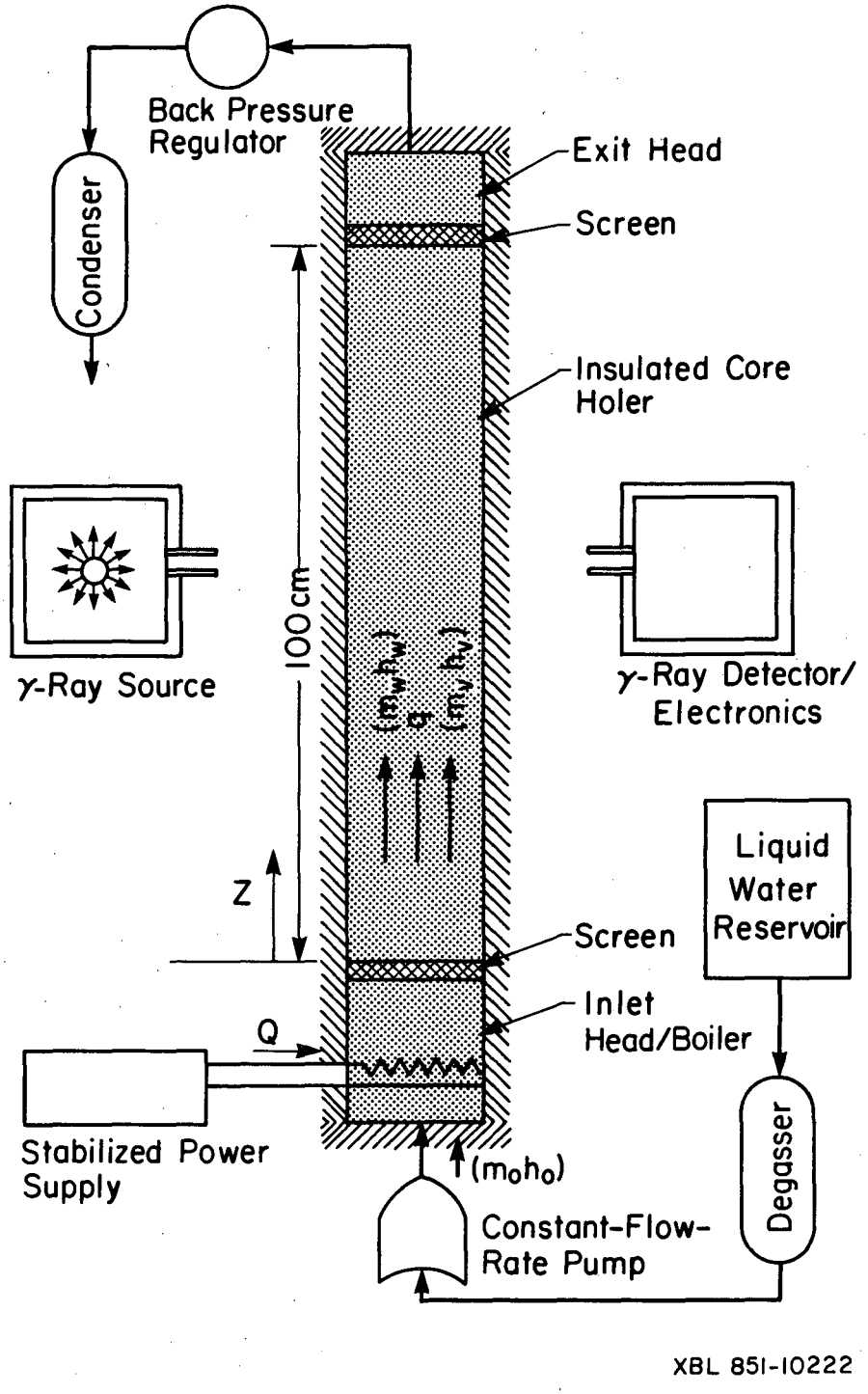

Fig. 6.1. Schematic of the experimental setup used to obtain the relative permeability curves.

head and an exit-head mounted at opposite ends of the tube. The inlet head also serves as a boiling chamber where a controlled fraction of the incoming water was flashed by electric resistance heaters to achieve a desired flow quality in the test section. The outer surface of the test-cell was made adiabatic with the aid of guard heaters wrapped around it at regular intervals.

At regular intervals there are instrument ports for temperature, liquid pressure, and vapor pressure probes. Pressures at the ports and pressure drop between the two neighboring ports are measured with the aid of absolute pressure transducers and differential pressure transducers, respectively. Vapor pressure and liquid pressures at each cross section were measured in separate ports (Fig. 6.2). Internal surfaces of all the tubes connecting the vapor pressure transducers to the ports were coated with Teflon and both the tubes and the pressure transducers were maintained at a temperature of 1–2 °C above the local vapor temperatures with the aid of guard heaters. These precautions were taken to eliminate errors in vapor pressure measurements due to liquid condensation in the tubes and the pressure transducers. (The error in vapor pressure readings due to intentional increase in temperature is expected to be negligible.) On the other hand, all tubes connecting liquid pressure transducers to the test sample were filled with cotton wicks in contact with the porous matrix. The tubes and the transducers were kept cooler than the saturation temperature to prevent evaporation in the liquid pressure measurement unit. The temperature readings were taken with the aid of copper-constantan thermocouples sheathed inside 1/16 in. stainless steel tubes.

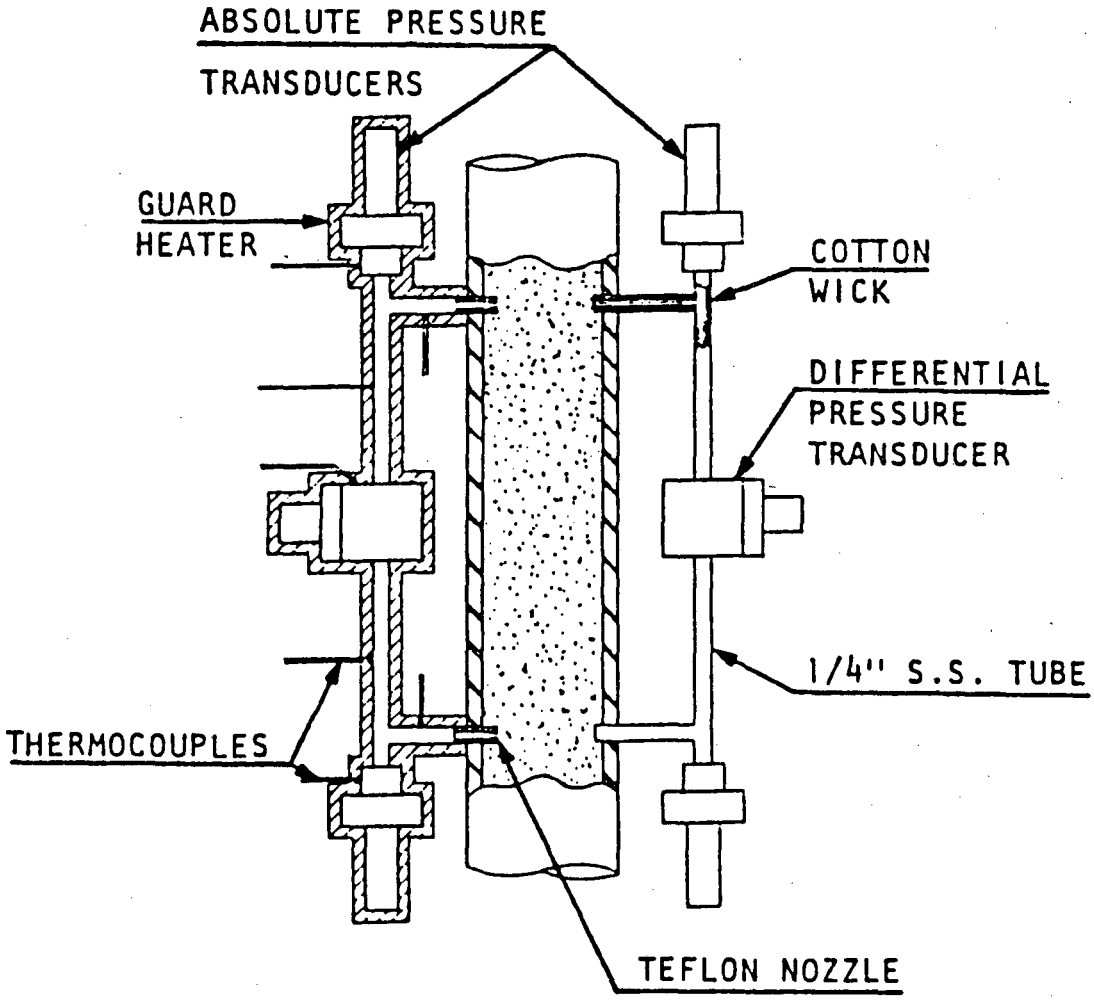

Fig. 6.2. Schematic of the pressure measurement system.

The test cell was mounted vertically, to avoid flow stratification, on an indexing table capable of accurate vertical movement. Double-deionized, degassed water was pumped into the inlet head with the aid of a dual-cylinder, constant flow-rate pump (accurate within $\pm 0.3\%$). Upon entering the chamber, a fraction of the water was flashed into steam by means of electric resistance heaters, causing two-phase concurrent flow in the test column. Temperature, vapor pressure, and liquid pressure were measured at regular intervals along the column. Saturation readings at different cross-sections were taken with the aid of a γ-ray densitometer by moving the indexing table while the γ-ray source and the detector remained fixed to a rigid frame.

Upon leaving the exit head, steam was condensed in a heat exchanger and condensate was discharged through a constant head tank to maintain constant exit pressure.

6.2.2 System Design and Operating Conditions

The optimum design parameters and operating conditions were obtained with the aid of numerical modeling. It was speculated that the effects of capillary pressure, and the end effects resulting from it, could be very significant. To study these effects, various capillary pressure curves were incorporated into a geothermal reservoir simulation code, MULKOM (Pruess, 1983), and test runs were simulated for a 100 cm long column. A typical result of the simulation with the end effects is shown in Figure 6.3, and for the purpose of comparison, a typical result without the end effects is shown in Figure 6.4. From these figures we

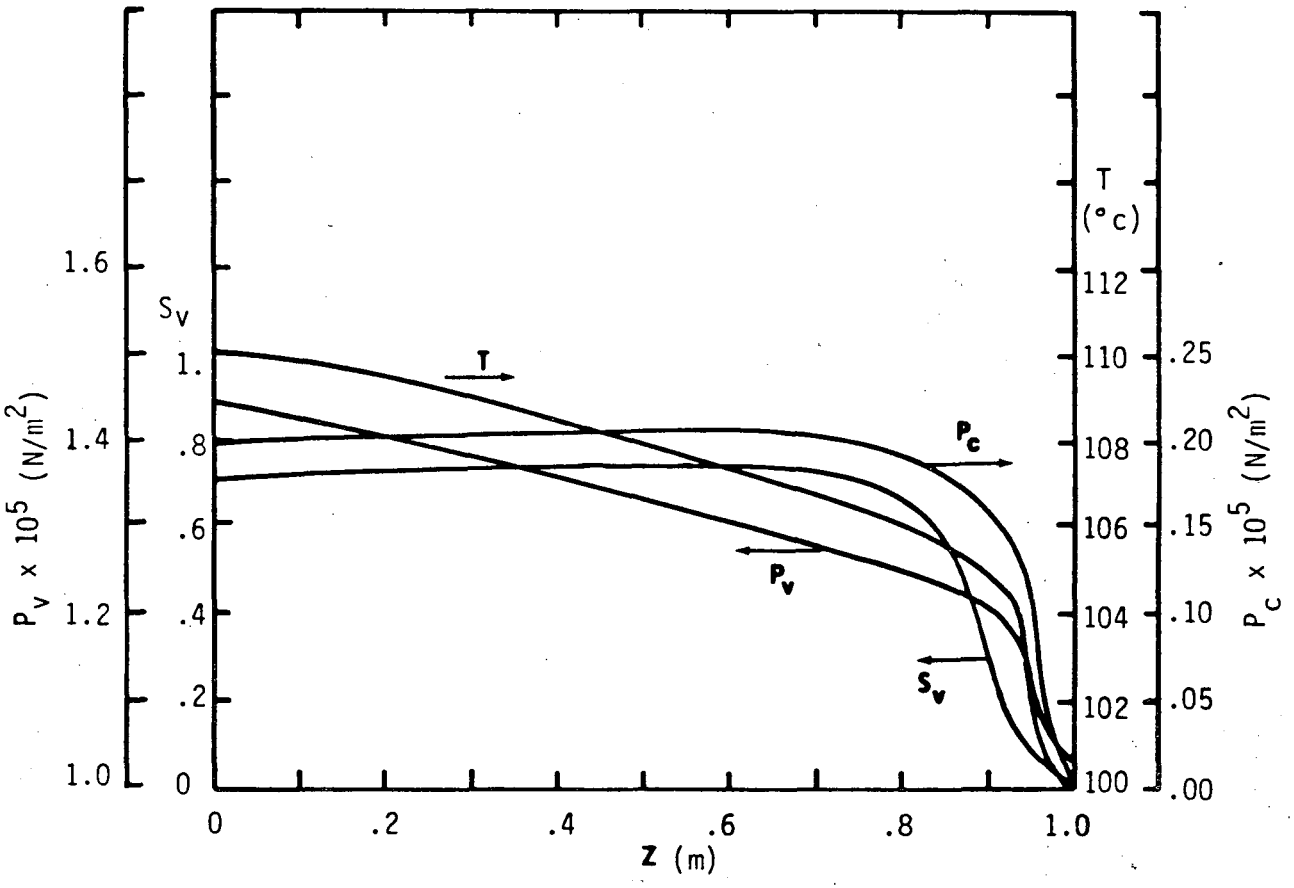

Fig. 6.3. A typical set of results of simulation with the end effect at the exit end.

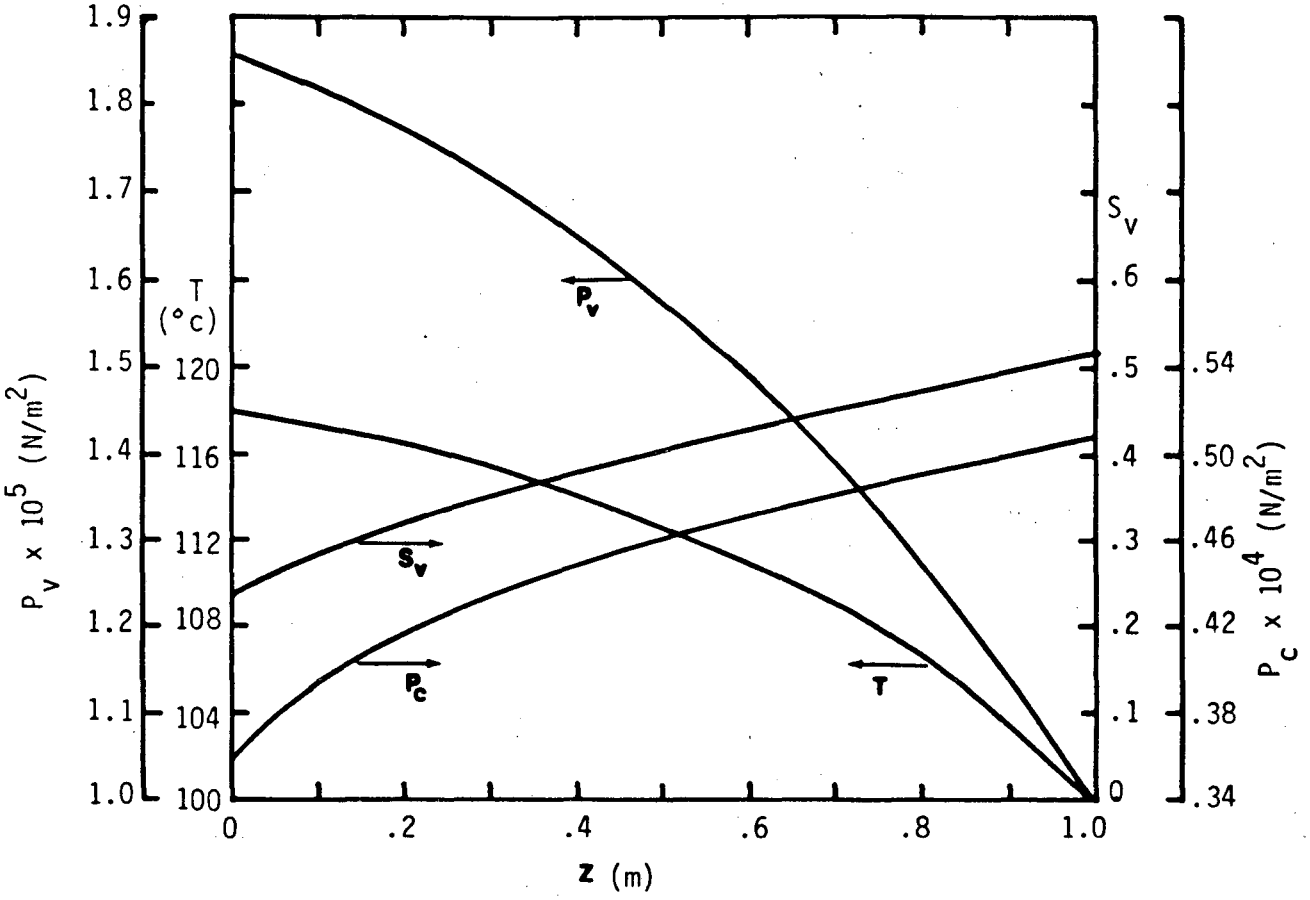

Fig. 6.4. A typical set of results of simulation without the end effects.

can see that, while the four parameters of interest, P_v, P_c, T, and $\dot{S}_v$, vary monotonically with more or less constant gradient in Figure 6.4, the end effects cause a very sharp gradient at the exit end (Fig. 6.3). We found that in a moderately permeable medium ($k = 6.41 \times 10^{-13}$ m^2) the end effects can extend up to 20 cm even at moderate flow rates (0.32×10^{-2} g/cm^2 sec). Readings taken in this region would be difficult to interpret to yield the relative permeabilities.

We also considered the effects of matrix properties and boundary conditions on the experiment. Results of the numerical studies showed that for the test samples under consideration it is possible to obtain a region of almost constant saturation over an extended length in a 100 cm long column. Readings taken in this region can be analyzed directly to yield relative permeabilities.

The inside diameter of the test column was chosen such that the maximum attenuation of the γ-ray beam due to water was approximately 20 percent (i.e., $(I_d - I_s)/I_d \sim 0.2$). For most materials under consideration an I.D. of 7.5 cm (3 in.) was found to be optimum.

The flow rates were chosen such that, while the flow remains Darcian, it produces a measurable pressure drop over a 20 cm segment of the test column. In the present case the flow rate was held constant at 0.2944 g/sec.

6.3 GAMMA-RAY ABSORPTION SYSTEM

A γ-ray absorption system is based on measuring the difference in absorption of γ-rays by steam and water. A monoenergetic collimated beam, when passing through a material of thickness l, is attenuated according to an exponential law

$$I = I_o e^{-\mu l} \tag{6.1}$$

where I_o is the intensity (disintegrations/m^2 s) of the unattenuated beam and μ is the attenuation coefficient of that material. Because the attenuation coefficient is a function of wavelength, the radiation source must be close to monoenergetic. In addition, a collimated beam is necessary so only photons traveling in the same direction, and therefore having traversed the same path, will be detected. A fairly complete discussion of these radiation attenuation techniques to detect two phase flow is given by Schrock (1969). A short discussion of the pertinent points needed for this work is given below.

For a point gamma source of strength S_o (disintegrations/sec), the amount of radiation that arrives at the detector is $(S_o/r_2)A$, where A is the area of the collimated beam and r is the distance from the source to the detector. When the radiation also passes through a test cell, the total number of disintegrations/sec at the detector becomes

$$S = \frac{S_o}{r^2} A \sum_i e^{-\mu_i l_i} \tag{6.2}$$

where the sum is over all the materials through which the beam passes. However, the interest is only in the changes in attenuation of the beam through the water or steam in the pores. Therefore, we can separate out the beam attenuation due to the water and steam and write

$$S = S' \; e^{-\alpha\mu_l\phi L-(1-\alpha)\mu_s\phi L} \tag{6.3}$$

where $S' = (S_o/r^2)A \sum_j e^{-\mu_j l_j}$, the sum now is over all material but the fluids and

ϕ is the porosity, L is the width of the porous medium, α is the liquid saturation, μ_l is the absorption coefficient of the water and μ_s is the absorption coefficient of the steam. The total number of counts measured over a time, t, is

$$N = N' \; e^{-\alpha\mu_l\phi L-(1-\alpha)\mu_s\phi L} \tag{6.4}$$

where $N' = S' \; t$.

The system contrast, I, can now be determined to be

$$I = \frac{N_s}{N_l} = e^{-(\mu_s-\mu_l)\phi L} \tag{6.5}$$

where subscripts s and l refer to the cases when the adsorption media is either all steam or all liquid. The system contrast determines the sensitivity of the system to changes in the water saturation. Schrock (1969) has suggested that this number be between 1.2 and 2.0. If the contrast is too large, differences in the way the steam voids are positioned will affect the data. It is interesting to note that this system contrast is independent of the source strength.

Because the system contrast cannot be very large, small differences must be detected for a measurement of the steam/water saturation. It is important to consider the possible errors. The accuracy of the measurement will always be limited by the counting statistics, i.e., the error in the counts is $\sqrt{N}$, where N is the total number of disintegrations counted. However, the difference in the absorbed radiation when there is all water and when there is all steam is small. Although the error in the number of counts may be small, $\sqrt{N}/N$, the error in the measurement, may still be large.

For a saturation, α, the number of counts detected will be

$$N' \; e^{-(1-\alpha)\mu_s\phi L - \alpha\mu_l\phi L} \tag{6.6}$$

and the error in the counts is

$$\sqrt{N'} \; e^{-(1-\alpha)\mu_s\phi L/2 - \alpha\mu_l\phi L/2} \tag{6.7}$$

For an increase, $d\alpha$, in the water saturation, the change in the number of counts detected is

$$\frac{dN}{d\alpha} = N' \; e^{-(1-\alpha)\mu_s\phi L - \alpha\mu_l\phi L}(\mu_s - \mu_l)\,\phi\, l \tag{6.8}$$

If we want to be able to measure saturations within $\pm 2\%$, then the error in the counts must be less than $|dN/d\alpha|(0.02)$ or

$$\sqrt{N'} \; e^{-(1-\alpha)\mu_s\phi L/2 \,-\, \alpha\mu_l\phi L/2} < N' \; e^{-(1-\alpha)\mu_s\phi L - \alpha\mu_l\phi L} \,|\, \mu_s - \mu_l \,|\, \phi \; l.02 \tag{6.9}$$

or

$$\sqrt{N'} \; > \frac{e^{(1-\alpha)\mu_s\phi L/2 + \alpha\mu_s\phi L/2}}{|\mu_s - \mu_l \,|\, \phi \; l(.02)} \tag{6.10}$$

The quantity $|\mu_s - \mu_l|\phi l$ is just the natural log of the system contrast or $\left|\ln \frac{N_s}{N_l}\right|$.

The additional errors depend on the actual experimental system itself.

6.4 EXPERIMENTAL APPARATUS

This section contains the description of the experimental apparatus (Fig. 6.5 and 6.6). We shall only discuss the non-standard equipments used in the experimental setup for brevity. These equipments are the test cell, pressure measurement system, and gamma-ray densitometer.

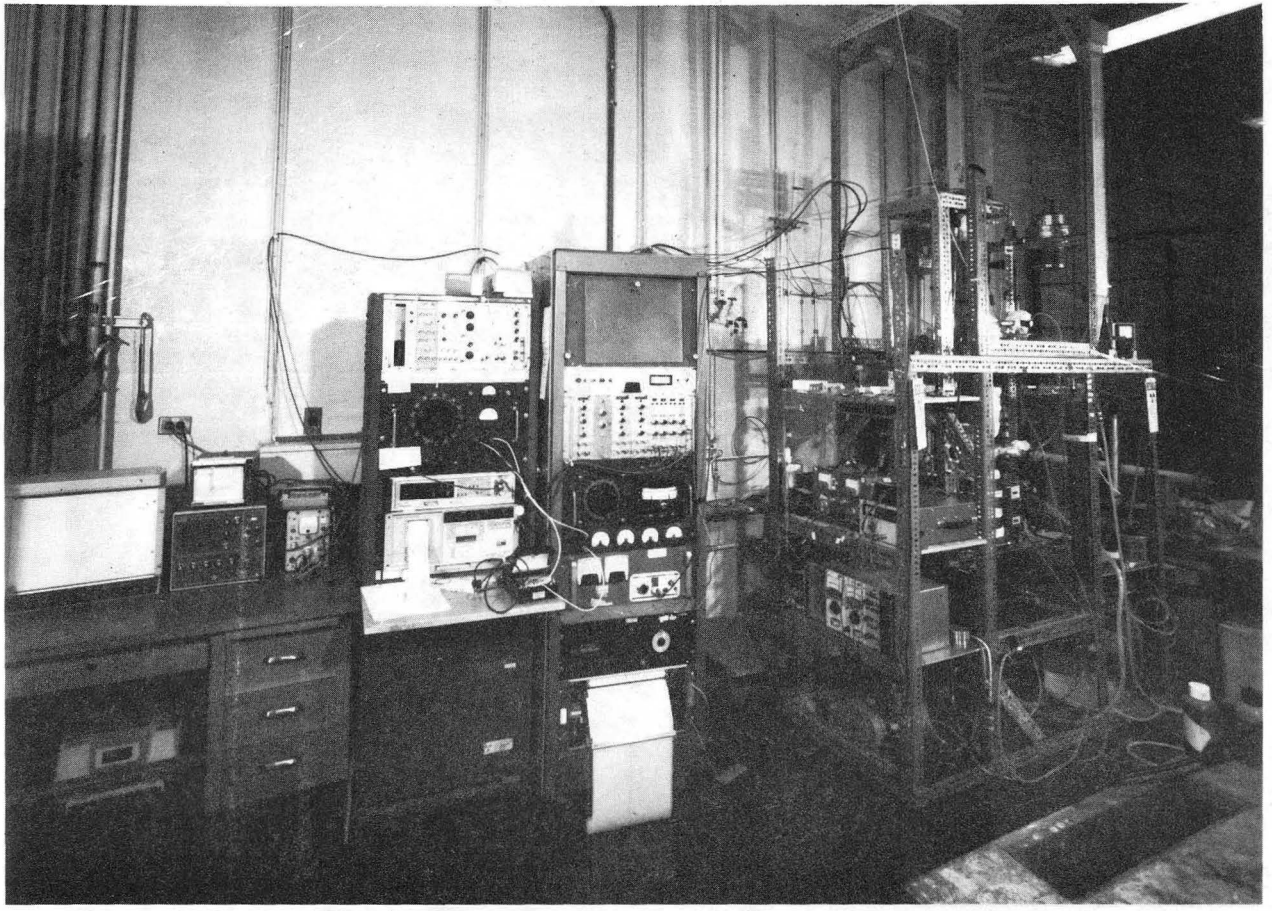

CBB 840-8805

Fig. 6.5. Photograph of the experimental setup.

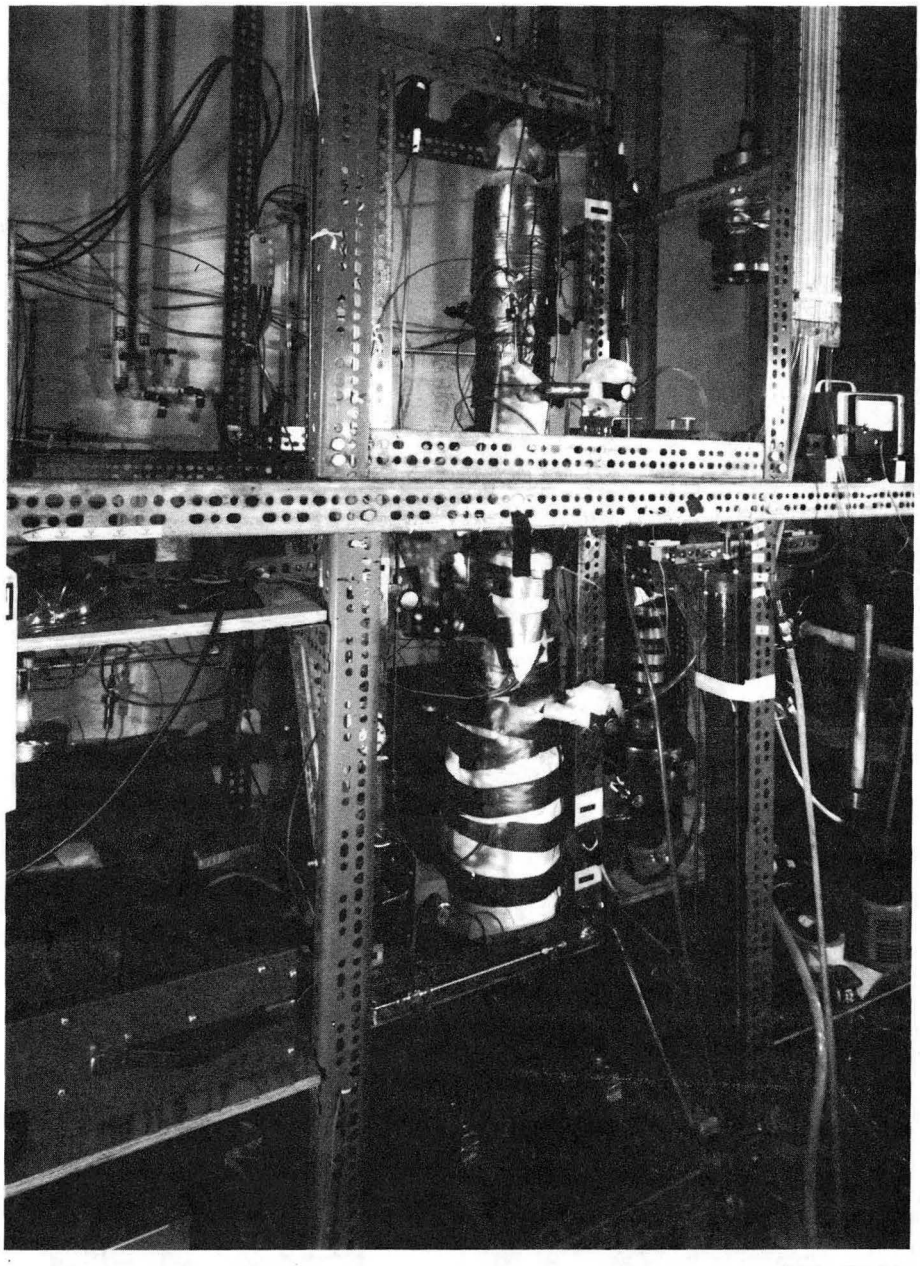

CBB 840-8803

Fig. 6.6. Photograph of the test column.

6.4.1 Test Cell

The test cell (Fig. 6.7) consists of three separate parts namely, an inlet-head, an exit-head, and a tube which contains the test sample. The inlet-head was designed to seal one end of the tube and also to serve as a boiling chamber. This unit consists of a cylindrical boiling chamber, a mounting flange and a cover plate (Fig. 6.8). The cover plate holds four cartridge heaters and two thermocouples sheathed in 1/4'' tubes (Fig. 6.9). One of the thermocouples is used for the monitoring purpose and the other serves as the sensor for an over-temperature protection device. This device was designed to cut off power to the cartridge heaters when temperature in the boiling chamber rises above a preset temperature.

The boiling chamber was filled with 250 μm diameter zirconium oxide beads which completely surround the heaters and the thermocouples. These beads serve as a homogenizing media for heat transfer and help to dampen out instabilities associated with boiling.

The tube serves as a container for the unconsolidated media use in the experiment. It was a 3 inch I.D., fiber glass reinforced, G-11 epoxy tube made by Synthane Taylor, Oaks, PA-19456.

The wall of the tube was drilled and tapped to receive compression fittings for the pressure and temperature probes. It is capable of sustaining high pressure ($\sim$1000 psi) and retains strength at high temperatures, up to 300 $^\circ$F. The thermal conductivity of the tube material is 0.0754 W/m $^\circ$C.

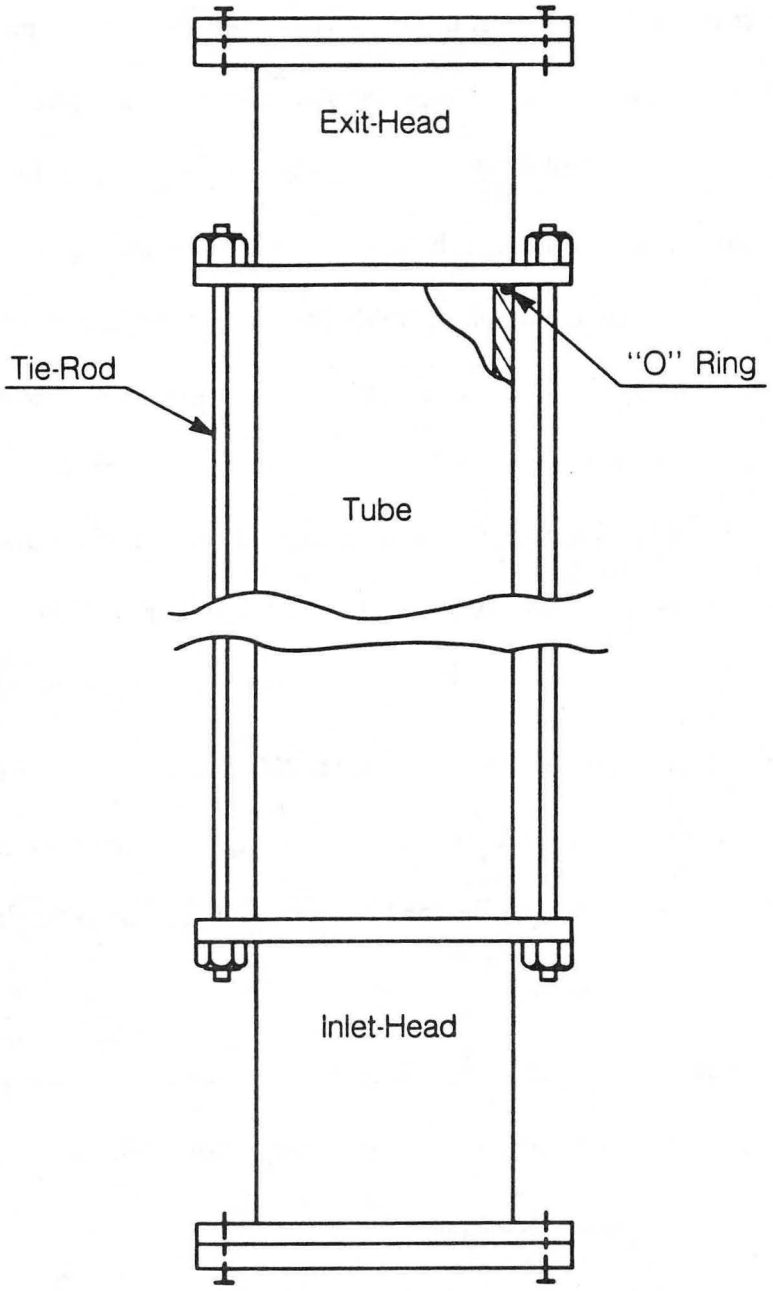

Fig. 6.7. Schematic of the test cell.

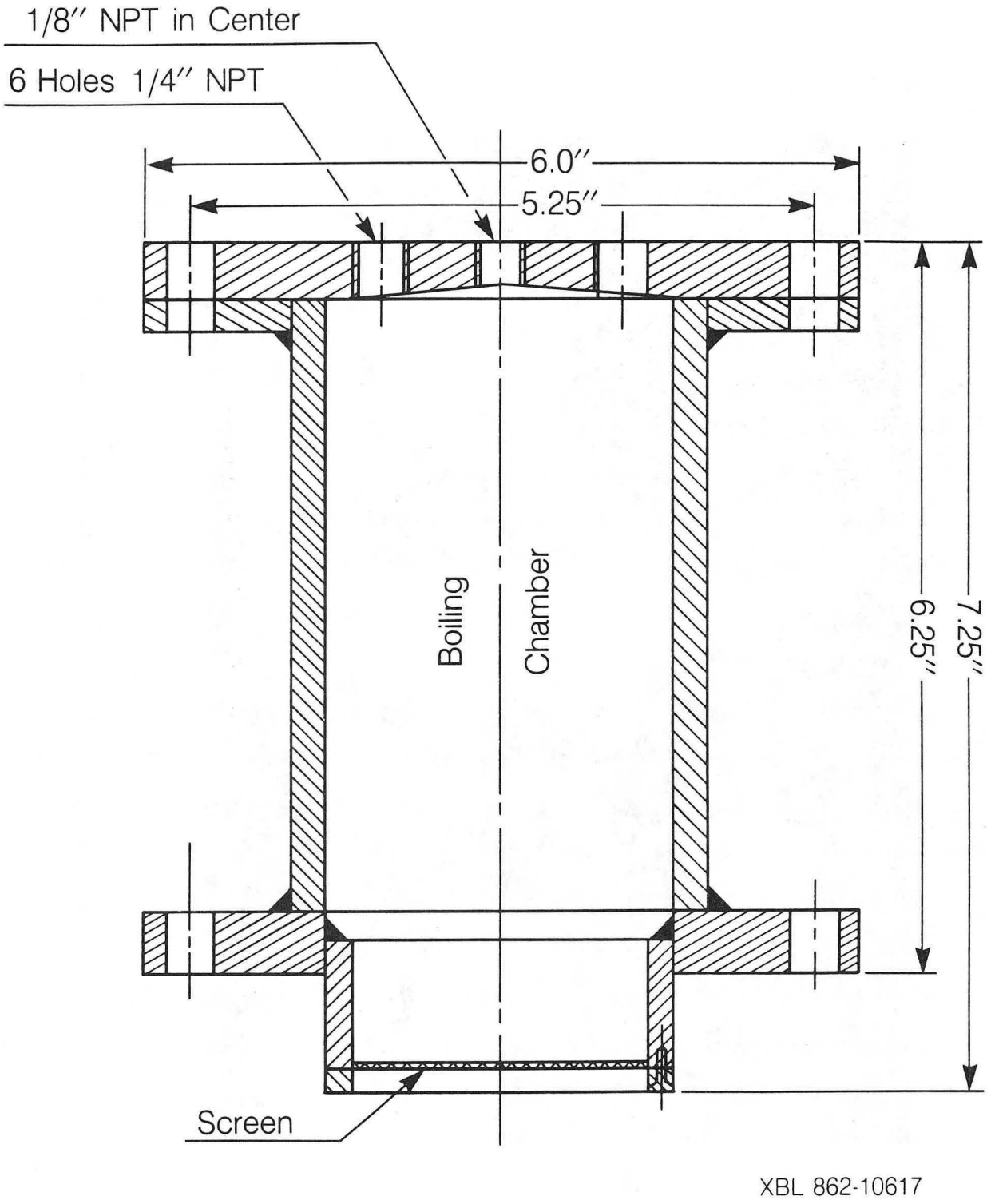

Fig. 6.8. Schematic of the inlet-heat chamber.

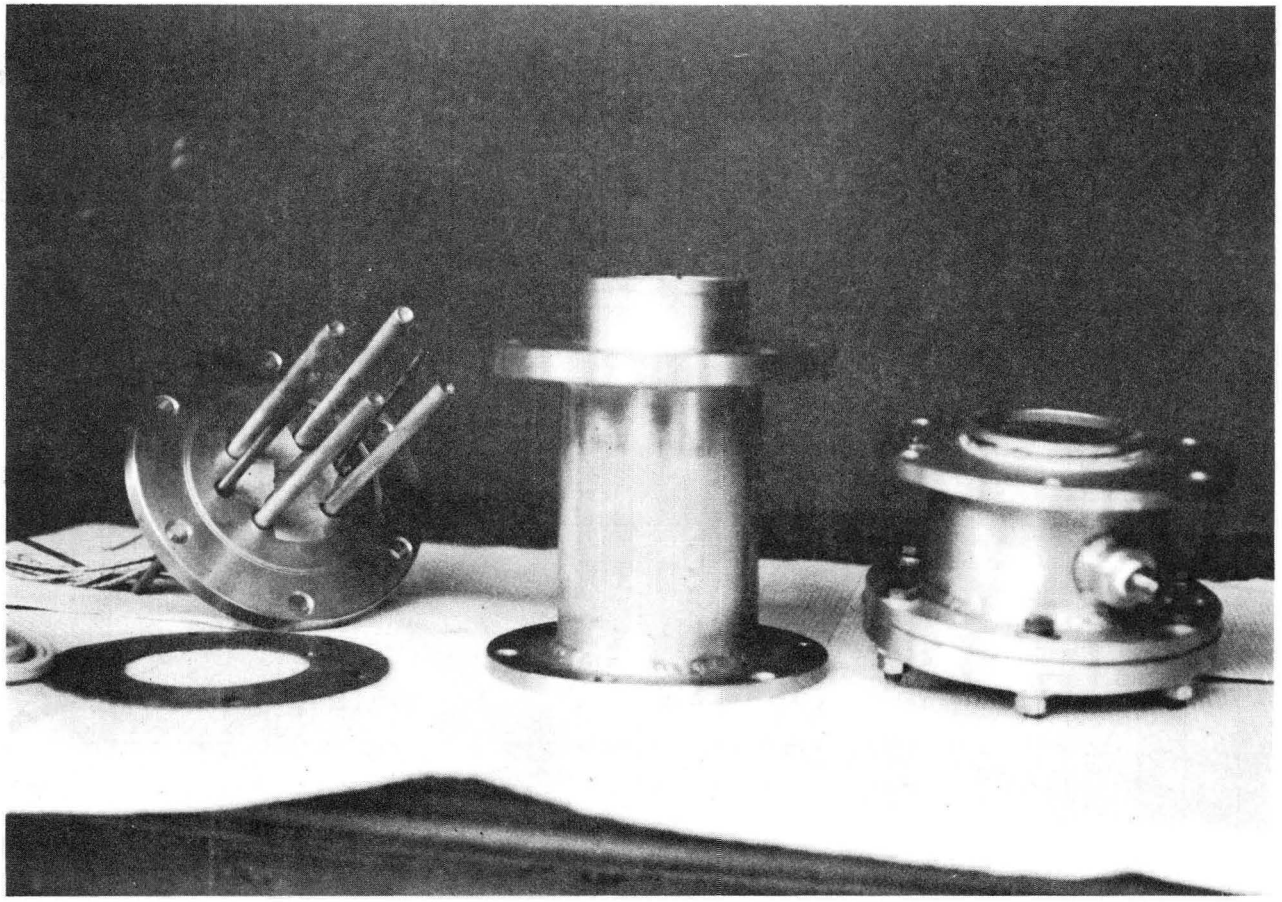

CBB 862-1063

Fig. 6.9. Photograph of the inlet and exit heat chambers.

The exit-head (Fig. 6.10) was designed such that the orientation of the test cell with respect to gravitational direction will have no effect on the exit-face boundary conditions. This requirement is fulfilled by allowing the outcoming liquid to flow in the radial direction only. Therefore, any liquid coming out of the chamber will not accumulate on the surface and provide a barrier through which steam will have to bubble out when flow is vertically upwards.

6.4.2 Pressure Measurement Unit

The pressure measurement unit used in the test section was designed to measure steam and water pressures separately (Udell, 1984). The unit (Fig. 6.2) consists of two separate units — a liquid pressure unit and a steam pressure unit. These subunits are identical in layout and instrumentation. Each subunit consists of two absolute pressure transducers (Precise Sensor, 0–100 psid) and a differential pressure transducer (Celesco, 0–5 psia). These pressure transducers were connected in the arrangement shown in Figure 6.2 and mounted on the tube using 1/4" s.s. tubing and Swagelok compression fittings.

Tubing in the liquid-pressure subunit were filled with cotton wicks which extended into the porous medium so that the pressure transducers sensed only the local liquid phase pressure. The pressure transducers and the tubing in this subunit were insulated to reduce heat loss. It was postulated that only liquid could reside in the tubes of this subunit because of high capillarity in the cotton wicks, which results in high superheat requirements for phase transformation (see Chapter 3).

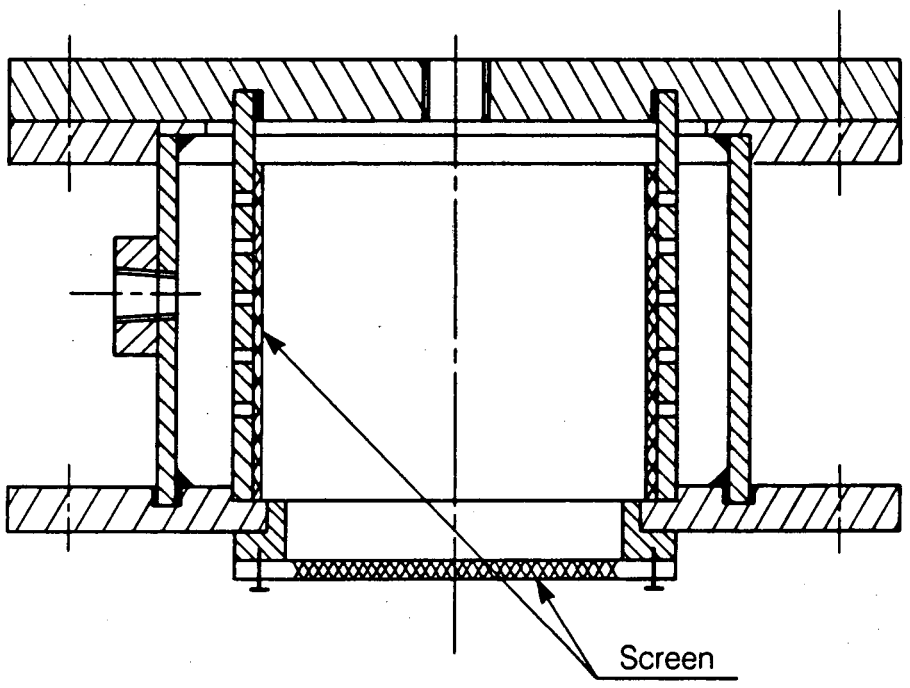

XBL 862-10618

Fig. 6.10. Schematic of the exit head.

The internal surface of the steam-pressure subunit, shown on the left in Figure 6.2, was coated with Teflon and the sensing nozzles were made from Teflon rod. Since Teflon is a hydrophobic material, no liquid will be sucked into the Teflon nozzle due to capillarity and steam will find a continuous path from the test section into the tubing. However, it is possible to have condensation in the tubing where condensates may reside in the form of liquid droplets on the hydrophobic surfaces of the tubing and pressure transducers.

In order to prevent condensation in the steam-pressure subunit, the whole unit was wrapped with guard heaters and heated to about 2 ° C above the local test-section temperature. We experimented with different subunit temperatures and found that the measured pressures are unstable when the subunit temperature was raised more than 6 ° C above the test-section temperature. This phenomenon could be attributed to a heat pipe mechanism where heat transfer between the subunit and the test section takes place by counter flow of steam and water (Udell, 1983). However, there was no instability when the temperature difference was maintained between 2 and 4 ° C.

6.4.3 Gamma-ray Densitometer

The γ-ray system, shown schematically in Figure 6.11, consists of a γ-ray source, a scintillation crystal, a photomultiplier tube, and a counter. The system components are listed in Table 6.1. Each component will be considered separately.

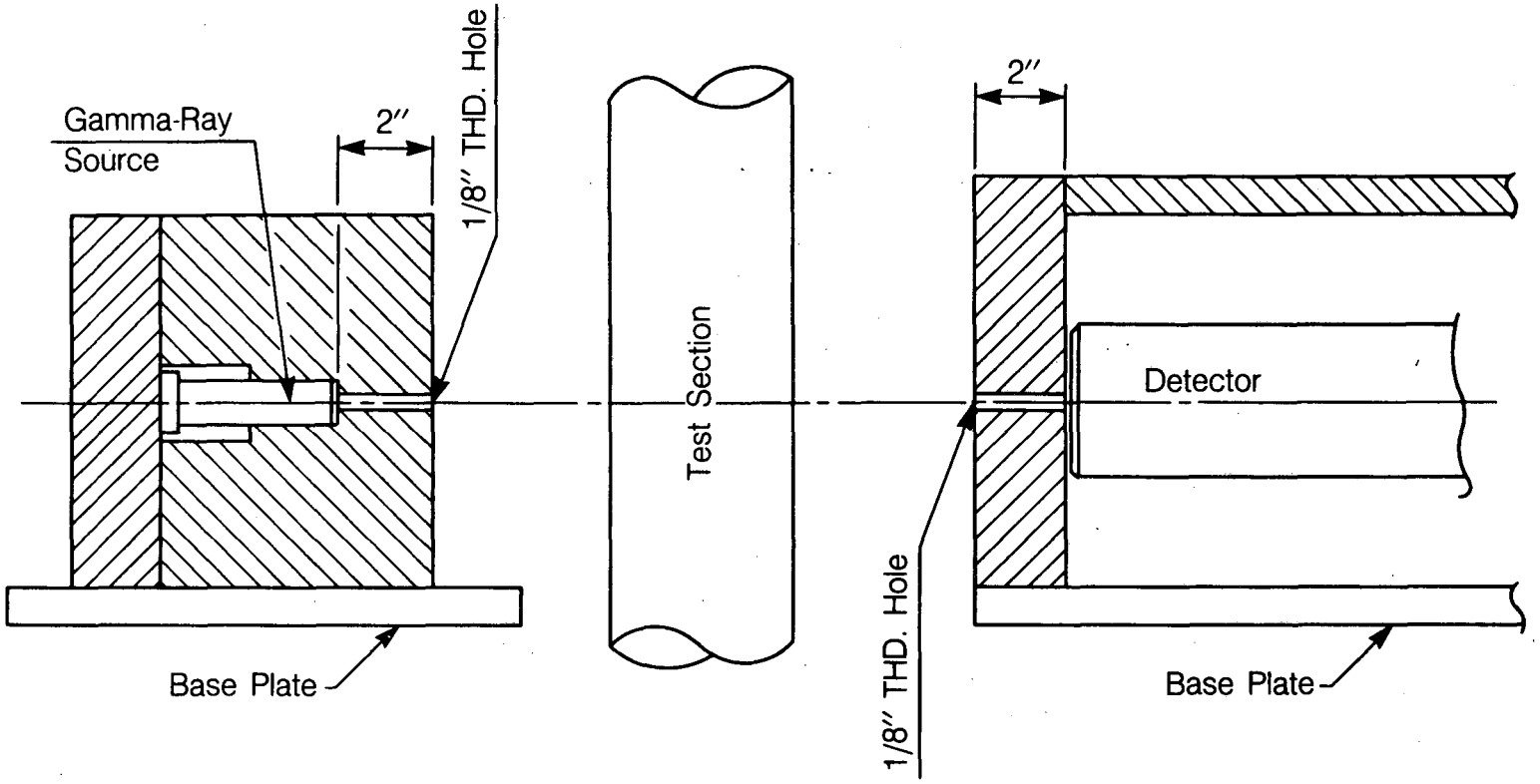

XBL 862-10616

Fig. 6.11. Schematic of gamma-ray densitometer.

Table 6.1. Components of gamma-ray densitometer.

COMPONENT	MANUFACTURER	MODEL	FUNCTION
Cesium 137 Source	IPL	50 mCuries	Supply Gamma Radiation
NaI II Scintillation Crystal	Harshaw Chemical Company	8S8	Detector
Photomultiplier	Harshaw Chemical Company	8S8	Produces pulses
Scintillation Preamplifier	Harshaw Nuclear Electronics	NB-15X	Amplifies pulses
High Voltage Power Supply	Hewlett Packard	6516A	Power source
Multichannel Analyzer	Norland Electronics	IT5300	Displays spectrum; integrates about chosen region of interest and displays count
Linear Amplifier and Shaper	Lawrence Berkeley	198	Amplifies and shapes waveform
Magnetic Cassett Deck	Norland Electronics	IT610	Stores spectrum for subsequent analysis

A Cesium 137 source was chosen because of its stable life, availability, and still reasonable absorption. A 157 μCi source was used for the testing of the system on known materials. Readings were taken over 10 minutes. However, a 50 mCi source is available for the experiment when readings are to be taken over shorter times, say 4 min. The source strength needed was determined by considering the expected conditions of the actual experiment.

A NaI scintillation crystal was used because of its high efficiency ($\sim$15%) in converting γ-rays to light. The NaI crystal does have a dead time of approximately 10^{-6} s. The dead time is the minimum time that can separate two

consecutive recorded photons. The observed counting rate, R, must be corrected for this resolving time, τ, so

$$R' = \frac{R}{1 - \tau R}$$

where R' is the true counting rate. For high counting rates, say 10^6 cts/s, the crystal saturates and cannot be used. For a count rate of 10^6 cts/min, the error in the number of counts is only 1.6%. As only about 10^5 cts/min are needed, the NaI crystal is sufficient. A faster response can be obtained with plastic scintillators which have dead times of 10^{-9} s. However, plastic scintillators have very low efficiencies (about 2% of a NaI crystal) so a much stronger γ-source is needed. Also, the plastic scintillators do not preserve the energy spectrum of the γ-source. Slight drifts in the output from the photomultiplier are easier to correct if the original energy spectrum is maintained.

The photomultiplier is model 8S8 from the Harshaw Chemical Company. It was bought in conjunction with the NaI crystal.

The resulting signal from the photomultiplier was analyzed with a Norland Electronics Multichannel Analyzer. A multichannel analyzer has a dead time also so the counting rate is limited by this instrument too. Nevertheless, it was chosen instead of a single channel analyzer which is faster, because the Cs spectrum can be observed with the multichannel analyzer. Because of this capability, it is possible to count only pulses centered around the Cs peak at 0.66 MeV, and to discriminate against most of the Compton scattering and spurious radiation. If the peak shifts during the experiment, adjustments can be made. The ability

to monitor the energy spectrum of the absorbed radiation was found to be one of the most important points in the design of this γ-ray absorption system. Since very small differences in absorption are being measured, a very slight drift in the output from the photomultiplier can completely obliterate the signal differences that are being measured.

Collimators were used both at the source and at the photomultiplier. The diameter of the collimated beam is 3 mm, and the length of the collimator is 5 cm. Also, the photomultiplier was shielded with lead to prevent detection of any spurious radiation. A block diagram of the γ-ray system is given in Figure 6.12 and shows all the components discussed.

6.5 INSTRUMENT CALIBRATION AND PERFORMANCE

All the measuring instruments were calibrated prior to and again immediately after the experiment to ensure the reliability of the readings obtained. The thermocouples were calibrated against a master platinum resistance thermometer and all the readings were within $\pm 0.3\,^{\circ}$C in the range of $80\,^{\circ}$ to $120\,^{\circ}$C. All the probes worked satisfactorily and no failure was detected during the experiment.

The absolute pressure transducers and the differential pressure transducers were calibrated over the entire range of working temperatures ($80\,^{\circ}$C–$120\,^{\circ}$C). They were checked for drift, hysteresis, repeatability and linearity. Since the differential pressure transducers showed some fluctuations during the experiment, all the pressure readings were taken with the aid of the absolute pressure transducers. These transducers were found to be accurate within ± 0.003 bars in the

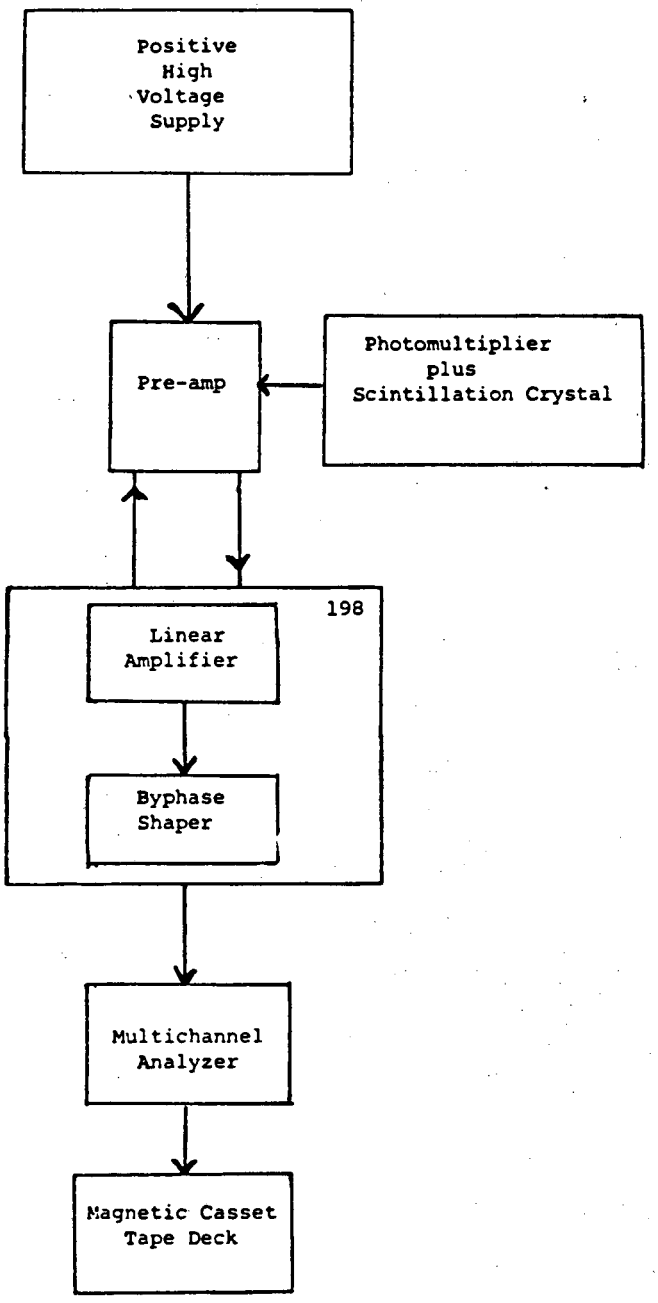

Fig. 6.12. Block diagram of gamma-ray densitometer.

entire range of interest (1–3 bars absolute). Therefore, both the pressure drop and the capillary pressure readings are believed to be accurate within ±0.006 bars.

The γ-ray densitometer was tested by measuring the absorption of the γ-rays through known materials of known thickness. Figure 6.13 is a plot of the γ-ray absorption through brass, copper, aluminum, and lucite. The slope of each line gives the absorption coefficient, μ, of each material. The calculated absorption coefficients are listed below. For copper and aluminum, the calculated μ's are compared to those reported elsewhere (Handbook of Chemistry and Physics, 1967). The literature value for the absorption coefficient of brass is extrapolated from mass absorption coefficients of zinc and copper and is only an estimate. The results for the brass and aluminum are good while those for the copper do not agree. However, in all cases the measured absorption coefficients consistently are less than the reported absorption coefficient at 0.66 MeV (peak energy of Cs^{137}). The absorption coefficient decreases with higher energy (shorter wavelengths). Because the Cs^{137} spectrum has been preferentially discriminated against at the lower energy levels, the average energy of the γ-rays is most likely to be at a greater energy than 0.66 MeV explaining the lower absorption coefficients.

A second test was conducted to determine if it is possible to accurately measure 10% water saturation changes within ±2%. A set of 1/16" lucite plates

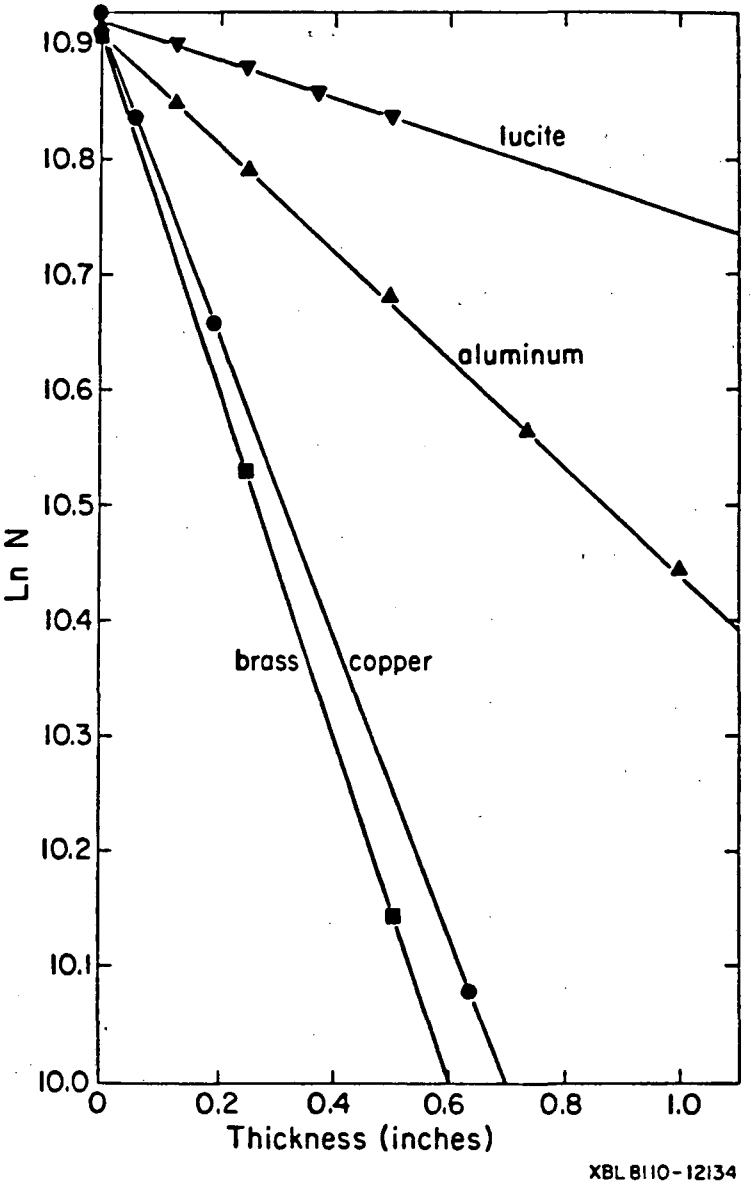

Fig. 6.13. Plot of gamma-ray attenuation through different materials.

Material	μ measured	μ literature (0.66 MeV)	Error
Brass (70% Cu, 30% Zn)	0.625/cm	0.645/cm	3%
Copper	0.516/cm	0.626/cm	17%
Aluminum	0.183/cm	0.191/cm	4%
Lucite	0.066/cm	—	—

were used to simulate the water. Nine plates were used in all so a removal of one plate would simulate 89% saturation, two plates removed would simulate 78% saturation, etc. The test was also conducted to determine if the arrangement of the lucite plates would make a measurable difference, i.e., if the first plate was removed near the source or near the detector.

Figure 6.14 is a plot of the $\log_e N$ versus the number of lucite plates between the source and detector. The error of each measurement $1/\sqrt{N}$, is included on the graph. We see it is possible to measure these small changes accurately. The second run where the lucite plates were removed in the opposite order, i.e., nearest the detector first instead of nearest the source, have not been plotted as they fell within the error bars of the plotted measurements.

The tests run indicated that accurate and small changes can be detected and that it will be possible to make water/steam saturation measurements in a porous medium. In the case of the present experiment the errors at the lower saturation ($S_w = 0.4$) are within $\pm 3\%$ and those for the higher saturation readings ($S_w = 0.8$) are within $\pm 5\%$.

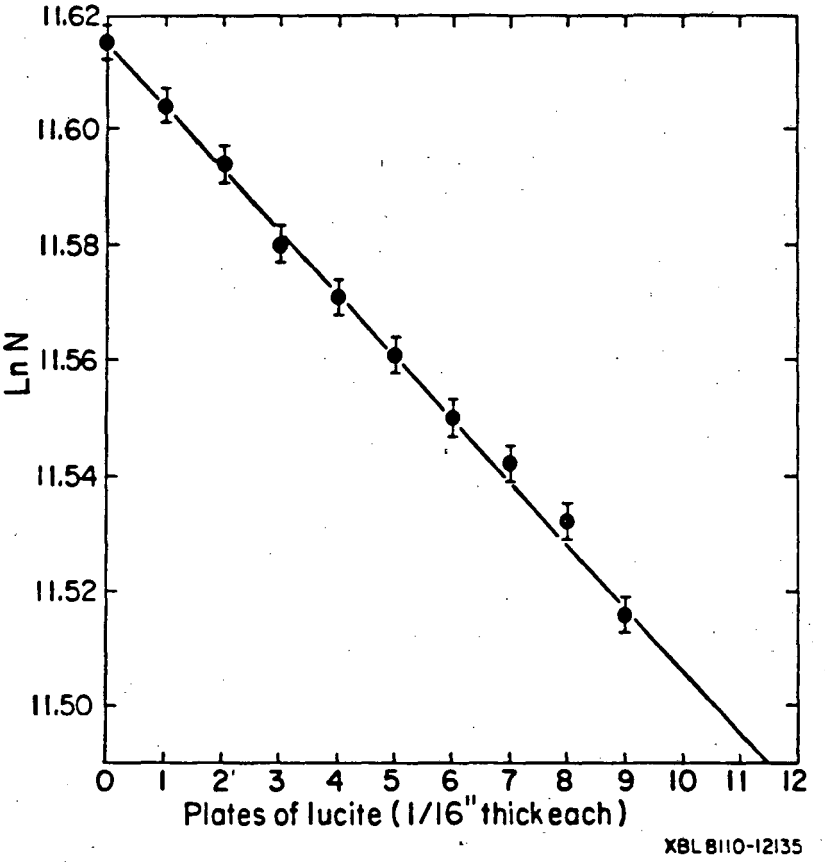

Fig. 6.14. Plot of gamma-ray attenuation for nine lucite plates.

6.6 EXPERIMENTAL PROCEDURE

The experimental procedure followed in our study is presented, step by step, below.

(1) The pressure transducers, tubing and the thermocouples were mounted onto the tube and valves Ml, M2, M3, VP1, and VP2 were closed (Fig. 6.15).

(2) The tube was placed vertically on top of the inlet-head with the "O" ring and the tie rods in place and the tube was filled with glass beads. The exit-head was placed on top and the two heads were secured with the aid of the tie rods.

(3) The test cell was mounted on the indexing table, all the pressure transducers and manometers were connected, and a pressure test with pressurized N_2 (at 100 psi) was conducted to ensure that there was no leak.

(4) The axis of the test cell was aligned with the axis of the γ-ray densitometer with the aid of a LASER beam (Fig. 6.16).

(5) Guard heaters were wrapped around the test cell and the whole unit was insulated (Fig. 6.6). All electrical and hydraulic connections were made.

(6) Pressure and temperature readings were taken to ensure that all the thermocouples and the pressure transducers were functioning. At this stage all the temperature and pressure readings should agree within the measurement error.

(7) Gamma-ray intensity readings were taken at three different locations, at the same elevations as Ml, M2, and M3. These γ-ray beam intensities

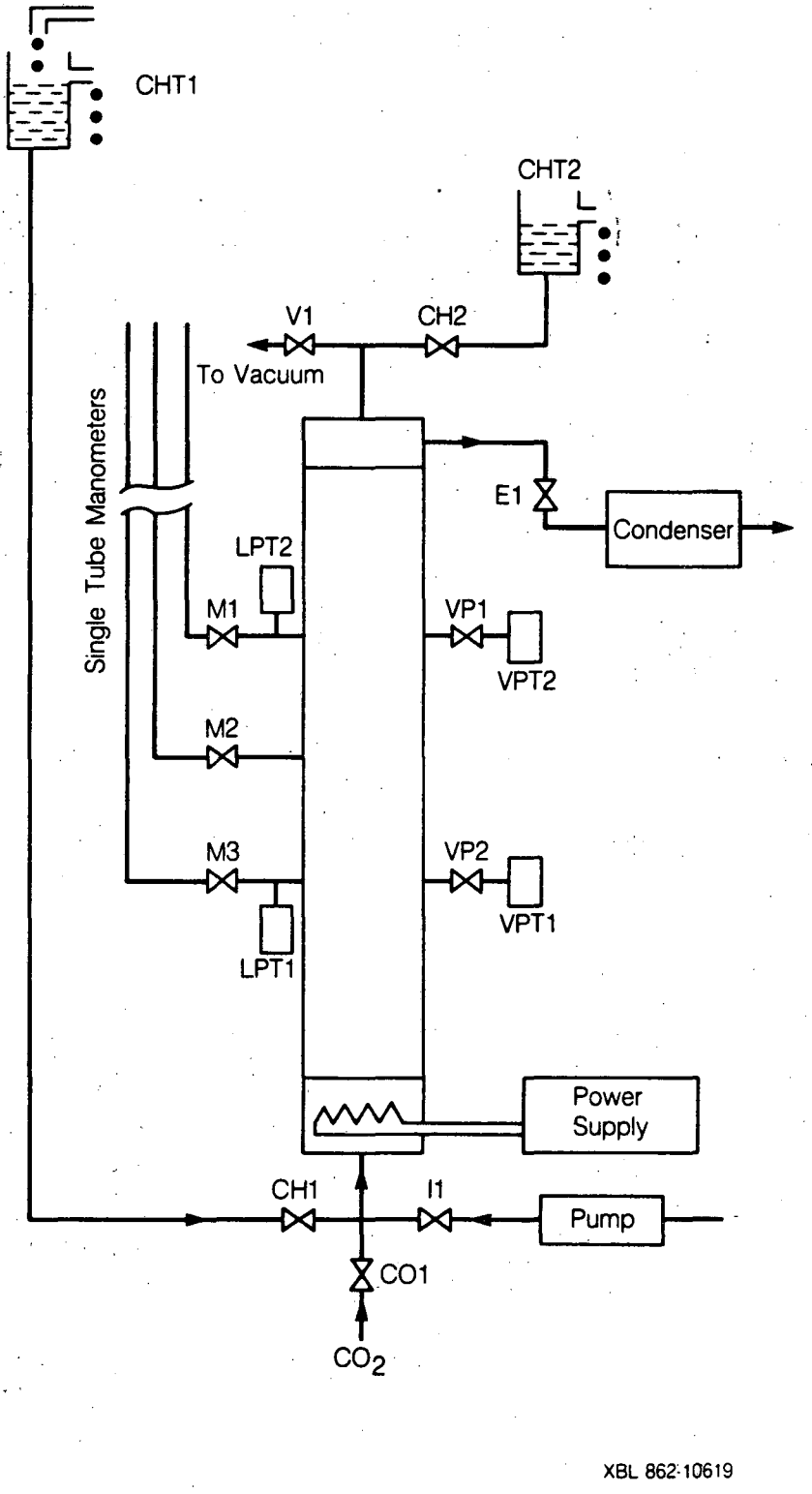

Fig. 6.15. Circuit diagram of the relative permeability experiment.

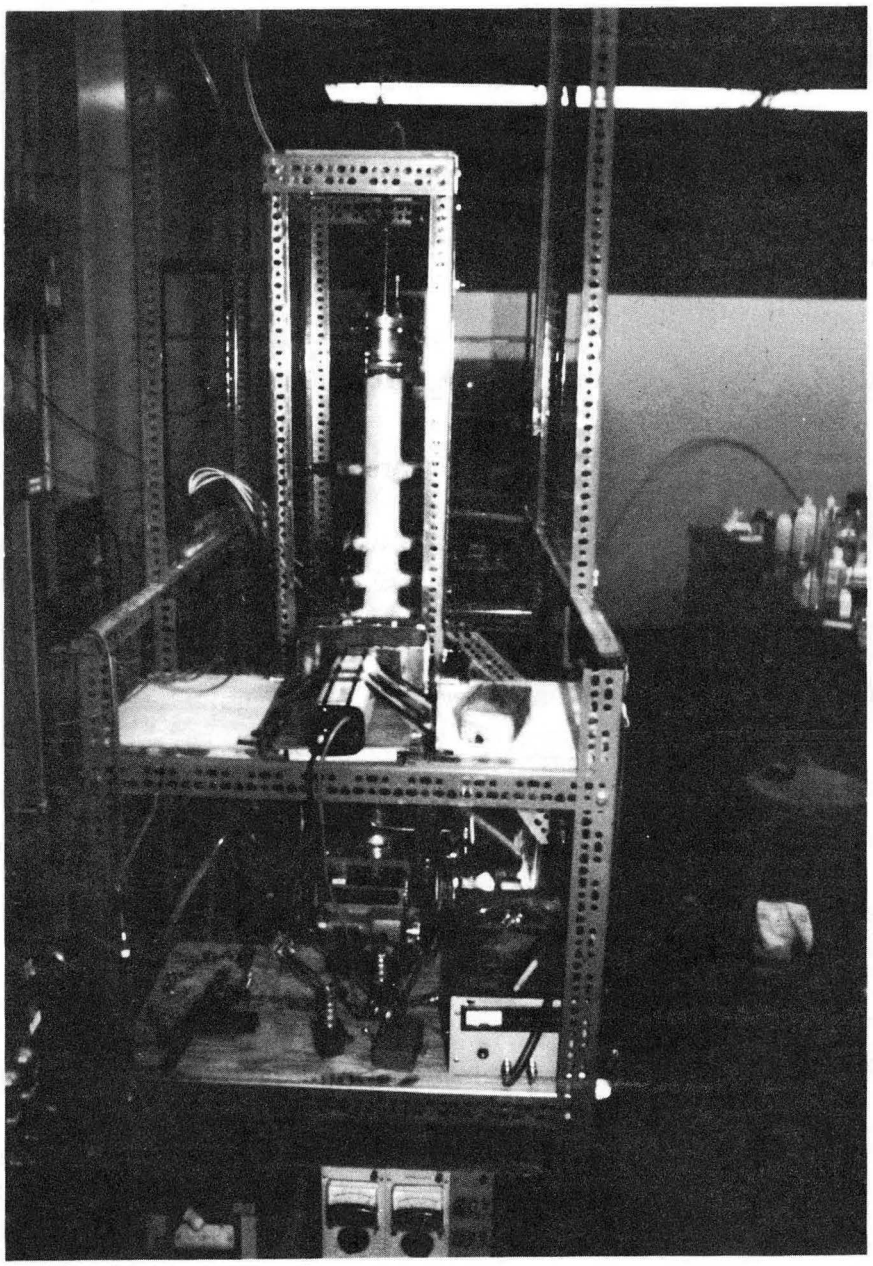

CBB 862-1061

Fig. 6.16. Alignment of the test column using a laser beam.

correspond to attenuation by the test cell and fully dry sample.

(8) All the valves except V1 (Fig. 6.15) were closed and the vacuum pump was started to draw all the air out of the test cell.

(9) Valve V1 was closed and valve CO1 was opened to charge the test cell with CO_2 at 1 atm. Valves V1 and CO1 were closed.

(10) Valves CH1 and CH2 were opened and the test cell was allowed to saturate with double-deionized, degassed water. The test section was flushed overnight to dissolve and remove CO_2 gas bubbles from the test section.

(11) Step 7 was repeated to obtain γ-ray beam intensity for fully saturated medium at the exact three locations as in Step 7.

(12) Valves M1, M2, and M3 were opened and water was allowed to rise in the nanometer. When the water levels in the nanometers stabilized, the piezometric head readings were taken. The volumetric flow rate was measured by tapping the discharge from CHT2. These data were analyzed to obtain the intrinsic permeability between M1 and M2, and between M2 and M3. Valves M1, M2 and M3 were closed.

(13) Valves CH1 and CH2 were closed. Valve I1 was opened and a constant-flow-rate pump was started to pump double-deionized, degassed water into the test sample. An immediate rise in signal output of liquid pressure transducers, LPT1 and LPT2, indicated that there was no noticeable volume of trapped gas in the test cell. Exit valve, E1, was opened.

(14) Power to the cartridge heaters in the inlet-head boiling chamber and the guard heaters were turned on. Power supply to the boiling chamber was adjusted to achieve a desired flow quality and power to the guard heaters was adjusted to maintain adiabatic conditions at the outer surface of the test cell.

(15) The boiling chamber pressure and temperature were monitored to check for steady flow conditions. A double check was made by also monitoring pressure and temperature at the exit end. It took about 6 hrs to obtain first steady state.

(16) Valves VP1 and VP2 were opened slowly and steam was allowed to flow into the vapor pressure transducers VPT1 and VPT2, which were already heated to about 2 °C above the local test section temperature. From this time onwards valves VP1 and VP2 were left open.

(17) Liquid pressure, vapor pressure and saturation readings, at the same spots as in Step 7, were taken.

(18) Power to the boiling chamber was increased and Steps 14 to 17 were repeated.

Six different runs for six different flow qualities were made. The experimental observations for these runs are listed in Table 6.3 below. The mass flow rate into the inlet chamber was maintained at 0.2944 g/sec.

The locations of the measurement probes indicated in Table 6.3 correspond to Figure 6.15. Probes LPT-1 and VPT-1 are at the same elevation and LPT-2

Table 6.3. Readings of experimental runs.

Parameters and location	ER-1	ER-2	ER-3	ER-4	ER-5	ER-6
P_l (Psia) LPT-1	16.775	17.00	17.35	18.54	22.62	27.1
P_l (Psia) LPT-2	16.151	16.3	16.46	17.38	20.12	23.2
P_v (Psia) VPT-1	17.58	17.82	18.17	19.37	23.49	27.97
P_v (Psia) VPT-2	16.95	17.14	17.3	18.21	21.01	24.1
P_c (Psia) Average	0.7985	0.83	0.83	0.835	0.88	0.885
S_w M1-M2	0.82	0.751	0.661	0.563	0.38	0.376
S_w M2-M3	0.781	0.72	0.648	0.551	0.362	0.371
S_w Average	0.8005	0.735	0.654	0.557	0.371	0.373
Q (watts)	110.5	116.0	129.0	151.0	327.0	500.00
f Average	0.0096	0.0169	0.035	0.0664	0.323	0.581

and VPT-2 are at an elevation 30 cm above them. Location of saturation measurements are indicated by two surrounding ports, e.g., M1-M2 indicates the location to be between port M1 and M2. Location depicted by "Average" indicates an averaged value between M1 and M3.

6.7 DATA ANALYSIS

The theoretical considerations involved in analyzing the experimental data have been presented by Reda and Eaton (1981), so that they need not be discussed in detail here. The only major departure from their method is that while they neglect the capillary pressure and associate the measured pressure with both the liquid and the vapor phases, we measure the pressures in the two phases separately and obtain capillary pressures at different cross-sections.

We consider a steady-state, one dimensional, vertical forced convection of steam and water through an insulated cylindrical test sample (Fig. 6.1). Conservation of mass and energy is considered in order to interpret the experimental data for the steam/water relative permeabilities of the porous medium. The equation for flowing steam quality, f, and water and vapor relative permeabilities k_{rl} and k_{rv} are, respectively, (see Appendix 6.A)

$$f = \frac{m_o(h_o - h_l + Q - q}{m_o(h_v - h_l)} \tag{6.11}$$

$$k_{rl} = \frac{(f-1)m_o\mu_l v_l}{k\,A\,\frac{d}{dz}(P_l + \rho_l\, gz)} \tag{6.12}$$

$$k_{rv} = -\frac{fm_o\mu_v v_v}{kA\,\frac{dP_v}{dz}} \tag{6.13}$$

and

$$P_c = P_v - P_l \tag{6.14}$$

Here q represents the conductive heat flow along the flow direction given by

$$q = -\frac{dT}{dz}\{\lambda_t A_t + (1-\phi)\lambda_m A + \phi[S_l\lambda_l + (1-S_l)\lambda_v]A\}$$

where λ_t, λ_m, λ_l and λ_v represent the thermal conductivities of the core holder, the matrix, water, and steam respectively. A_t is the cross-sectional area of the core-holder wall. Other notations have their usual meaning.

The right hand side of Equations 6.11–6.14 consist of quantities which are either known or can be measured from the experiment. Hence, Equations 6.12–6.14 can be used to obtain the relative permeabilities and the capillary pressure.

6.8 RESULTS

The experiment resulted in a set of relative permeability and capillary pressure curves shown in Figures 6.17a and b. The readings presented cover only a limited range of saturation ($0.38 < S_l < 0.8$) because (i) the readings taken at saturations above 0.8 are not accurate because of the difficulties involved in evaluating the flow quality; and (ii) the lower limit ($S_l = 0.38$) represents very nearly the irreducible water saturation. An attempt to reduce this saturation further was abandoned because the system temperature rose beyond the operating temperature of the differential pressure transducers.

Figure 6.17a shows that the measured values of the relative permeabilities can be represented by:

$$k_{rl} = S_e^3 \quad , \tag{6.16}$$

and

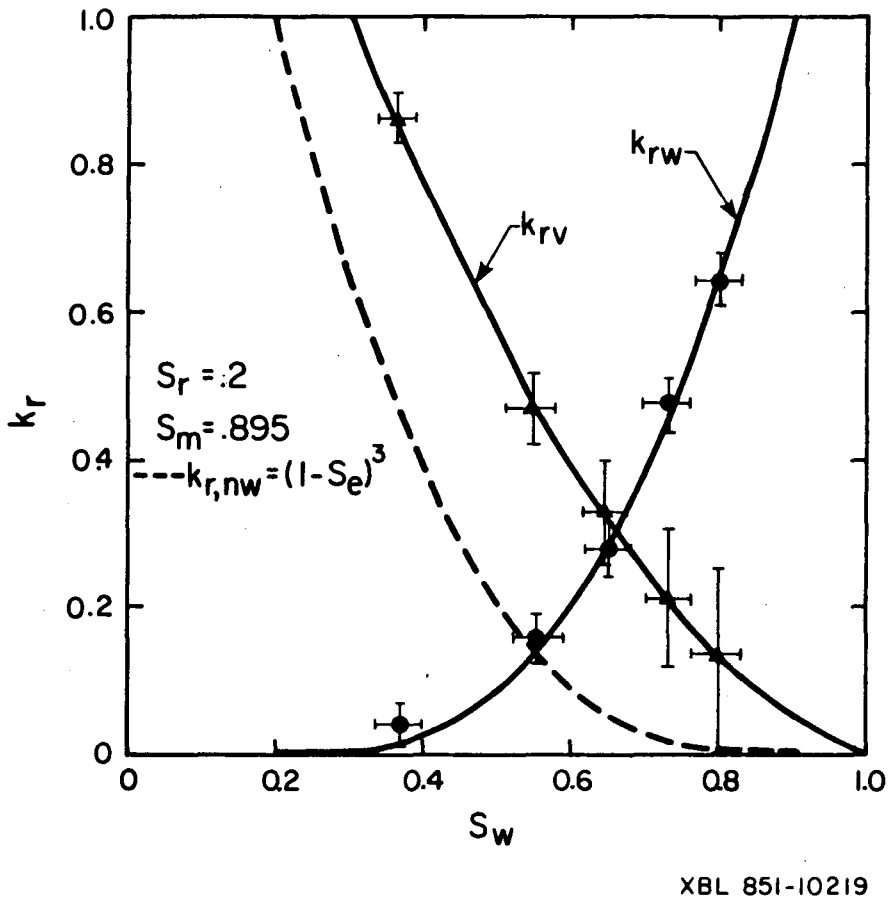

Fig. 6.17a. Relative permeability curves obtained experimentally.

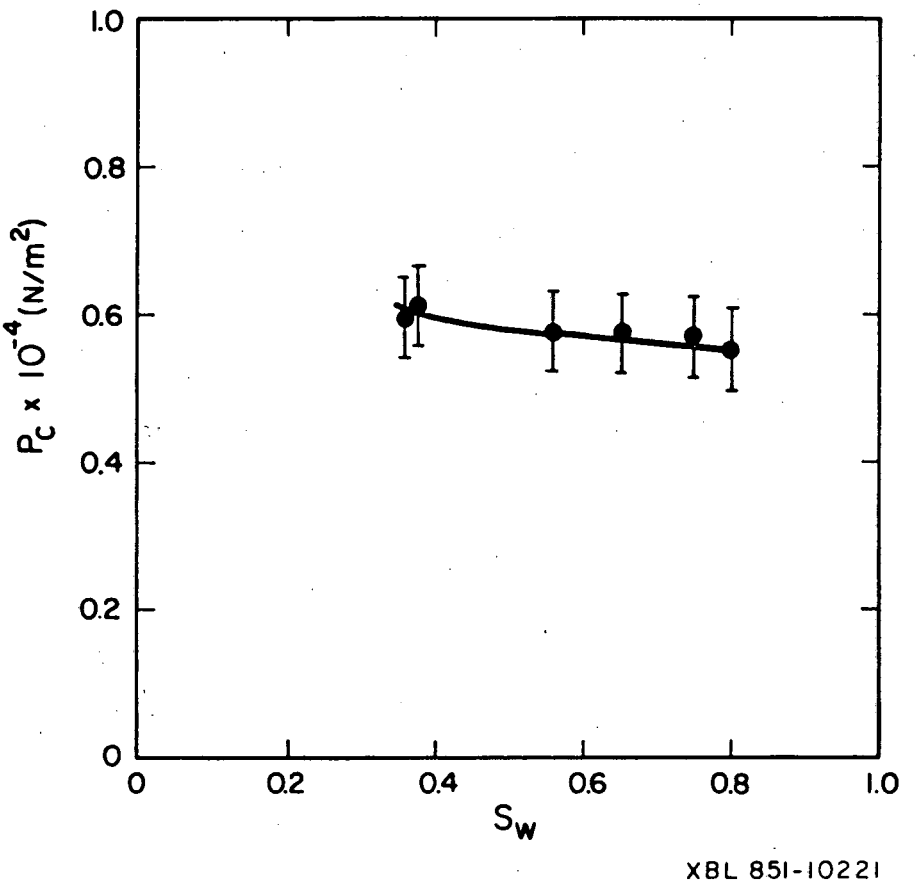

Fig. 6.17b. Plot of capillary pressure against saturation obtained experimentally.

$$k_{rv} = 1.2984 - 1.9832\, S_e + 0.7432\, S_e^2 \qquad (6.17)$$

where

$$S_e = \frac{S_l - S_r}{S_m - S_r} \quad . \qquad (6.18)$$

Since the limits S_r and S_m of the mobile saturation range for the liquid phase are not measured in the present experiment, but obtained by curve fitting ($S_r = 0.2$, $S_m = 0.895$), they should be considered approximate. Since the irreducible steam saturation could not be measured accurately it was assumed that there is no irreducible steam saturation for the present experimental configuration where the liquid water flows towards lower thermodynamic pressure and temperature (see Chapter 5). This assumption was invoked in curve fitting to obtain Eq. (6.17)).

These measured curves were implemented in our numerical simulator and the flow along the entire column was simulated. A typical set of simulated results along the entire column using the experimental relative permeability and capillary pressure curves is presented in Figure 6.18. These are compared against the experimental data and a good agreement is found, thus confirming our analysis of experimental data. The flow quality along the flow path for this test-run is presented in Figure 6.19. It indicates that the flow quality in the region of interest is very nearly constant.

It is interesting to note that Equation 6.18 for wetting phase relative permeability has been suggested independently by many investigators, including: (i) Irmay (1954), semi-empirical study of flow in unsaturated soils; (ii) Hauzenberg and Zaslavsky (1963), experimental study on well sorted sand; (iii) Brooks and

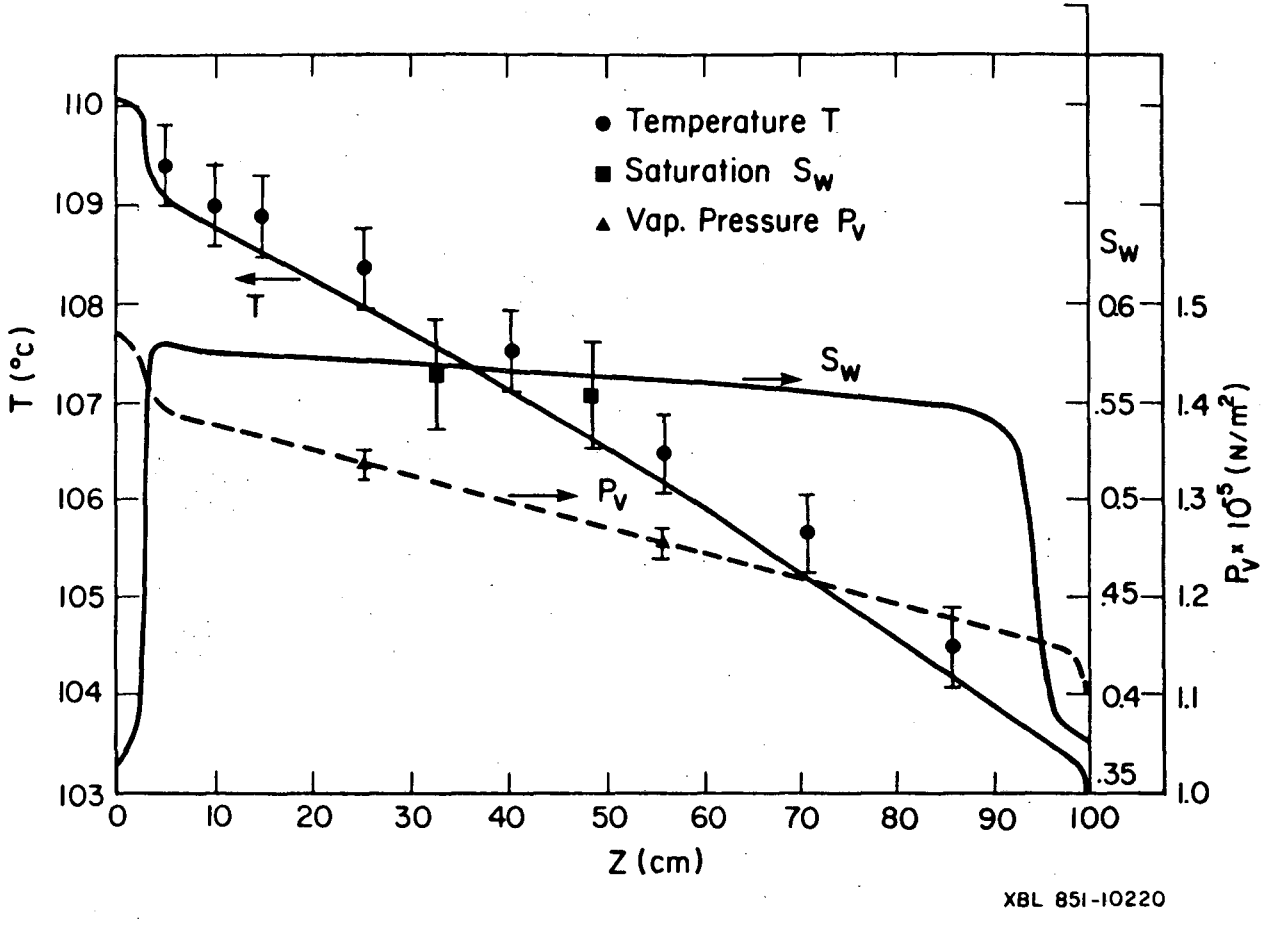

Fig. 6.18. Comparison of experimental data with numerical results.

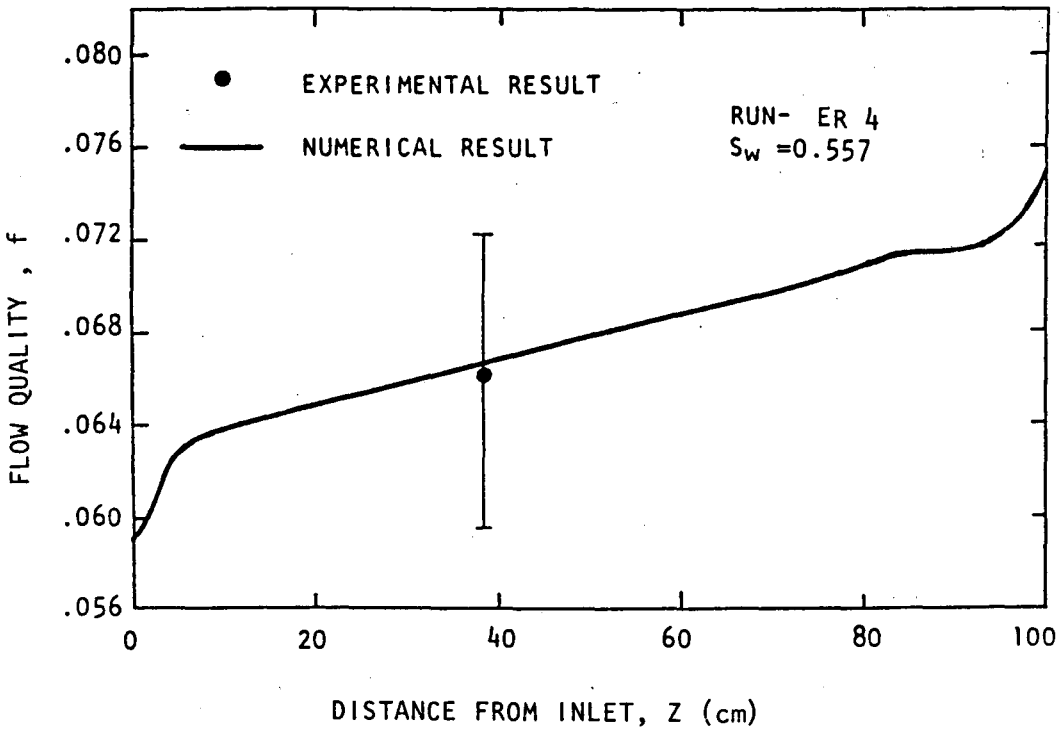

Fig. 6.19. Plot of flow quality along the test section.

Corey (1964), semi-empirical study.

Brooks and Corey (1964) also suggested that for a well sorted sand, the relative permeability to the non-wetting phase could be represented by

$$k_{r,nw} = (1 - S_e)^3 \tag{6.19}$$

However, upon comparing the experimental vapor phase relative permeability to Eq. (6.19) (Fig. 6.17a), we find that the measured values are much larger than the ones given by Eq. (6.19). Similar differences are found upon comparing the present results to those of other investigators (e.g. Osoba et al., 1951; and Johnson et al., 1959). These comparisons are plotted in Figure 6.20. Johnson et al. conducted their studies on flow of oil and water through a packed column (permeability = 11.5 Darcies) of glass beads, and Osoba et al.'s studies were conducted on oil and gas through consolidated rock core of permeability = 4.18 Darcies. Figure 6.20 also indicates that over the entire two-phase zone ($0 < S_l < 1$), the sum of the relative permeabilities ($k_{rw} + k_{r,nw}$) are larger in the case of steam and water flow, suggesting a more efficient advection of the two phases.

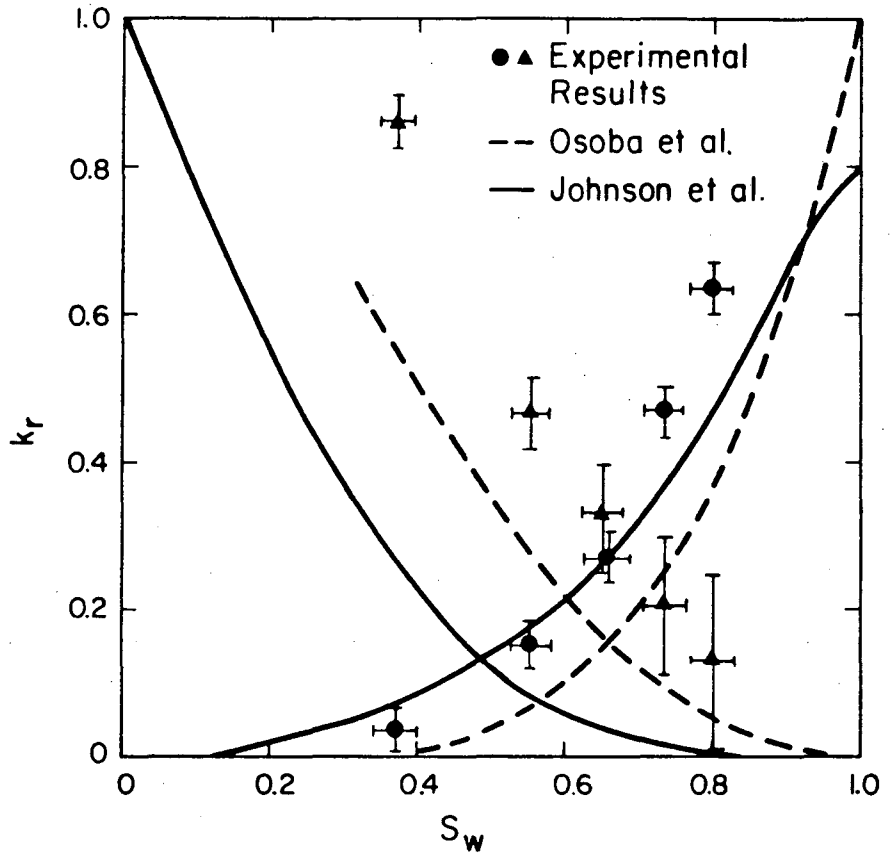

Fig. 6.20. Comparison of our experimental results with these of Johnson et al. (1959) and Osoba et al. (1951). The circles denote the liquid phase and triangles denote the steam phase.

APPENDIX 6.A
ANALYSIS OF THE RELATIVE PERMEABILITY EXPERIMENT

We consider a one-dimensional, steady-state, adiabatic flow of steam and water in a porous medium (Fig. 6.1). The conservation of mass is expressed by,

$$m_o = m_v + m_l \tag{6.A.1}$$

where m_o is the known input mass flow rate, and m_v and m_l are the mass flow rates of steam and liquid water, respectively.

The potential energy and kinetic energy effects are negligible for the conditions of the experiment, so that the energy equation is

$$m_o h_o + Q = m_v h_v + m_l h_l + q \tag{6.A.2}$$

where Q is the energy input to the boiling chamber and q is the conductive heat flux at any cross section (cf Eq. 6.15). Other notations have their usual meaning.

Assuming Darcy's Law, the momentum equations for the liquid and the vapor phases are given by

$$m_l = - \frac{k\, k_{rl}\, A\rho_l}{\mu_l} \frac{d}{dz} (P_l + \rho_l g z) \tag{6.A.3}$$

and

$$m_v = - \frac{k\, k_{rv}\, A\rho_v}{\mu_v} \frac{dP_v}{dz} \quad . \tag{6.A.4}$$

The flowing steam quality is defined as

$$f \equiv \frac{m_v}{m_v + m_l} \quad . \tag{6.A.5}$$

Combining Equations 6.A.1 and 6.A.5 yields

$$1 - f = \frac{m_l}{m_o} \quad . \tag{6.A.6}$$

Substituting Equations 6.A.5 and 6.A.6 into the Energy Equation 6.A.2, and solving for f yields

$$f = \frac{m_o(h_o - h_l) + Q - q}{m_o(h_v - h_l)} \quad . \tag{6.A.7}$$

Equations for k_{rl} and k_{rv} are obtained by substituting for m_v from Equation 6.A.5 into Equation 6.A.4 and for $\dot{m}_l$ from Equation 6.A.6 into Equation 6.A.3. Solving for k_{rl} and k_{rv} we obtain (Reda and Eaton, 1981)

$$k_{rl} = \frac{(f - 1)\, m_o \mu_l v_l}{kA \frac{d}{dz} (P_l + \rho_l gz)} \tag{6.A.8}$$

and

$$k_{rv} = \frac{-f\, m_o\, \mu_v v_v}{kA \frac{d}{dz} P_v} \quad . \tag{6.A.9}$$

CHAPTER 7
DISCUSSION

The results of the experimental study indicate that steam relative permeabilities in steam-water flow are larger than the relative permeabilities of the non-wetting phases in two-phase two-component flow, suggesting a more efficient advection of steam. It is postulated that this enhancement is caused by a combination of three mechanisms, namely (i) channeling, (ii) diffusion, and (iii) phase transformation. A detailed discussion of the effects of each of these mechanisms on the experimental results is presented below.

Effect of Channeling

Channeling is a process by which a flowing phase forms a preferential flow path, thereby causing a reduction in pressure gradient compared to homogeneous two-phase flow for a given flux. These channels could be formed either along the contact surfaces between the glass beads and the confining tube and/or within the porous medium itself (Udell, 1985).

The possibility of preferential channeling within the porous medium in our experiment is very small, however, because our saturation readings at three different locations along the flow direction change consistently with changing flow quality. In the presence of preferential channeling this could happen only if all the channels formed within the porous medium were intersected by the γ-ray beam. Since the γ-ray beam covers only about 5% of the cross-sectional area of the porous medium, the probability of the beam encountering the same

channel(s) at three different locations, where saturation readings are taken, is very low.

However, we cannot be certain about the absence of preferential channels, based on these arguments alone. Their presence could be discovered by scanning a cross section of the test sample for saturation. Any saturation anamoly detected by such a scan would indicate the presence of preferential channels. Since the experiment was not setup to make a cross-sectional scan, we cannot be absolutely sure about the absence of preferential channels within the porous medium.

It is well known that a thin region of high permeability forms near the wall in a column packed with unconsolidated porous medium. This region is usually confined within a few grain diameters from the wall and serves as a possible preferential path for one of the phases. The permeability of this region is usually 2 to 5 times that of the bulk permeability of the packed column. If we assume its thickness to equal two grain diameters (i.e., 200 μm), The region of enhanced permeability in our experiment covers approximately 1% of the cross-sectional area of the test section, Therefore, its effect on overall steam transport at high steam saturation ($>$10%) will not be significant. Since the experiment indicates large enhancement of steam phase relative permeability over the entire range of steam saturations (Fig. 6.17a and 6.20), we can conclude that the enhancement could not have been caused by flow in this region alone.

Effect of Vapor Diffusion

We have assumed in the present study that advection is the only mode of mass transport (Eq. (2.2)). Therefore, flux of a given liquid in single phase flow is adequately defined by the applied potential gradient and the intrinsic permeability (k) of the porous medium. Intrinsic permeability is usually measured experimentally under isothermal conditions. The transport process in these studies is advective (macroscopic flow) and often referred to as "Darcian." But, in non-isothermal, two-phase flow of steam and water, the mass flux may arise in four different ways: (i) the flux due to mechanical potential gradient — Darcian flow; (ii) the flux due to the gradient in concentration, as considered in simple kinetic theory; (iii) flux due to external forces, such as occurs in the diffusion of electrically charged particles in an ionized gas under the influence of an electric field; and (iv) flux due to a temperature gradient, giving rise to thermal diffusion (Hirschfelder et al., 1954). The exact description of the mechanisms (ii), (iii), and (iv) for the current experiment is very (and needlessly) complex because of the uncertainties involved in evaluating the pertinent parameters. We therefore adopt a simpler approach suggested by Ertekin et al. (1983). We assume that vapor is flowing under the simultaneous influence of two fields; a pressure field and a concentration field, and their influences on flux are additive. We can further simplify the analysis by assuming that the diffusive flux due to concentration gradient is adequately defined by the mechanism of self diffusion, as described in Chapter 8 of Hirschfelder et al. (1954).

The effect of diffusion on overall flux of vapor due to the combined mechanical potential and concentration gradient can be expressed in terms of a modified Peclet number

$$P_e \equiv m_v/m_{v,d} \tag{7.1}$$

Where m_v is the total flux of vapor and $m_{v,d}$ is the flux due to the concentration gradient alone. An expression for P_e, for concurrent two-phase flow of steam and water has been developed in Appendix 7.A.

The modified Peclet numbers for all the experimental runs in this study are very large ($P_e > 10^3$) indicating that the diffusive flux of the steam was very small compared to the advective flux. Hence, the enhancement of steam relative permeability could not be attributed to this phenomenon.

Effects of Phase Transformation

The mechanism of phase transformation in two-phase flow of a single component, such as water, gives an additional degree of freedom to these flows compared to two-phase flow of two-component, immiscible fluids such as gas-oil, oil-water, or gas-water. There are two separate mechanisms by which phase transformation affects the relative permeability curves of steam and water: (1) Phase transformation in converging-diverging flow channels with hydrophilic walls that can cause an enhancement of the steam phase relative permeability; and (2) phase transformation along the interface of a stagnant phase and the other phase flowing around it controls the irreducible saturation of the stagnant phase. We shall discuss these mechanisms one by one.

The former mechanism could be attributed primarily to the non-uniformity in the cross sectional area of the flow channels found in most naturally occurring porous materials. Although a porous material is considered to be homogeneous on a *Representative Elementary Volume* (REV) scale for the purpose of macroscopic flow analysis, the individual flow channels are highly non-uniform on the pore level. The flow channels can be considered to be an assemblage of pore bodies connected by pore throats (see Chapter 3). The pore throats can be orders of magnitude less transmissive to fluids compared to the larger openings in the system. In two-phase flow of steam and water, each phase flows in distinctly separate flow channels at the microscopic level (see Chapter 3). However, a thin film of liquid water resides on the walls of the channels occupied primarily by steam. The two phases are in thermodynamic equilibrium when the flow is Darcian and it is defined completely by any two independent thermodynamic properties such as temperature and capillary pressure, temperature and vapor pressure etc.

When steam flows in a channel, the temperature and pressure gradients along the flow path vary considerably from point to point. There are large temperature and pressure gradients across the pore throats and very small gradients across the pore bodies. The combined effect of this variation in the gradients of temperature and the nature of conductive flow paths is such that when steam encounters the throat of a highly constricted flow channel (i.e., $\frac{r_t}{r_b} \ll 1$), a fraction of the flowing steam condenses upstream from the constriction, releasing its

latent heat of condensation. This heat is conducted through the solid grains around the pore throat, and evaporation takes place downstream. Therefore, for a given bulk flow quality, a smaller fraction of steam actually flows through the throat segments. Since steam has a much higher kinematic viscosity than liquid water, and since the throat segments are the primary contributors to the overall flow resistance in the flow channels, the phase transformation effects reduce the overall resistance to steam flow along channels with varying cross sections. This pore-level effect manifests itself as relative permeability enhancement on a macroscopic level. However, our studies indicate that for typical pores found in sandstone this effect is negligible (see Chapters 4 and 5).

The second effect refers to the phenomenon of an irreducible phase saturation. When a cluster of a phase is rendered immobile under the combined action of viscous and capillary forces, it occupies a fraction of the void volume available to the fluids without contributing to flow. The fraction of void volume occupied by such clusters is known as the irreducible phase saturation. In case of immiscible, two-component flow, the necessary and sufficient condition for phase trapping is given by the mechanical force balance. However, in case of single-component, two-phase flow it is only a necessary condition but not sufficient. In order to have an irreducible phase saturation in a steady, single-component, two-phase flow system, a cluster of phase should not only be rendered immobile by capillary forces but the cluster should also be thermodynamically stable within its environment.

The criteria for thermodynamic stability obtained in Chapter 5 indicate that (1) irreducible saturation for the steam phase will be negligible when the liquid phase is flowing in a direction where both the thermodynamic pressure and temperature are decreasing; and (2) irreducible saturation for the liquid phase will generally be negligible when steam is flowing horizontally in the direction of decreasing thermodynamic pressure and increasing temperature.

These results indicate that the relative permeabilities for steam and water will depend, among other factors (see Chapter 2), on the boundary conditions of the flow channels.

Since the current experiment was set such that water was flowing in the direction of decreasing thermodynamic pressure and temperature, the irreducible saturation of steam phase was very small. Therefore, the relative permeability curve for steam was shifted towards the right compared to the non-wetting phase curves for two-component fluids (Figs. 6.17a and 6.20). We believe that the observed enhancement of steam phase relative permeability could be attributed primarily to this mechanism of phase transformation.

APPENDIX 7.A
SELF-DIFFUSION OF VAPOR IN FLOW CHANNELS

The diffusive mass flux in flow channels is given by (Walker et al., 1981)

$$m_{v,d} = -\phi S_v D\alpha\nu\nabla\rho_v \tag{7.A.1}$$

where D is the molecular diffusivity of the vapor phase, α is the empirical tortuosity factor allowing for extra path length, ν is the liquid island enhancement factor (Walker et al., 1981); ϕ denotes porosity and other notations have the usual meanings defined previously. Assuming (i) local thermodynamic equilibrium, (ii) vapor behaves as perfect gas, (iii) effect of capillary pressure on vapor pressure reduction in negligible, (iv) P_v and T are correlated according to Clausius-Clapeyron equation

$$\frac{dP_v}{dT} = \frac{h_{lv}}{T(v_v - v_l)} \tag{7.A.2}$$

(v) $v_v >> v_l$, and, (vi) one dimensional flow, the vapor density gradient can be expressed as

$$\frac{d\rho_v}{dx} = \frac{P_v}{RT^2}\left\{\frac{h_{lv}}{RT} - 1\right\}\frac{dT}{dx} \tag{7.A.3}$$

From Eqs. (7.A.1) and (7.A.3) we have for diffusive mass flux

$$m_{v,d} = -\phi S_v D\nu\alpha \frac{P_v}{RT^2}\left\{\frac{h_{lv}}{RT} - 1\right\}\frac{dT}{dx} \tag{7.A.4}$$

The advective component of vapor flux is given by

$$m_v = \frac{-kk_{rv}\rho_v}{\mu_v}\frac{dP_v}{dx} \tag{7.A.5}$$

From Eqs. (7.A.5) and (7.A.2)

$$m_v = \frac{-kk_{rv}}{\mu_v} \frac{\rho_v h_{lv} P_v}{RT^2} \frac{dT}{dx} \tag{7.A.6}$$

Defining a modified Peclet number $Pe \equiv \frac{m_v}{m_{v,d}}$

$$Pe = \frac{kk_{rv} P_v h_{lv}}{\phi S_v \alpha \nu D \mu_v (h_{lv} - RT)} \tag{7.A.7}$$

For the present calculations we take both ν and $\alpha = 1$ because our test sample is well-sorted and the value of ν is unknown.

CHAPTER 8
RECOMMENDATIONS

The purpose of this research was to investigate how the phenomenon of phase transformation affects the relative permeabilities of steam and water. Since this was a pioneering work in this direction, a lot of time and effort was spent in understanding the pore level mechanisms that can have a bearing on relative permeability functions. As a result of this, it was not possible to conduct extensive experimental studies to examine the effects of other factors such as thermodynamic conditions, capillary number, and boundary conditions on relative permeabilities. However, this work provides a solid foundation for any such research in future. Moreover, there are some lingering doubts about the effects of some of the factors, discussed in Chapter 7, on the results. Further studies should be conducted to put these doubts to rest.

It is highly recommended that an experiment on a consolidated core be conducted to seek answers to some of the questions raised in Chapter 7. The consolidated core should be cast inside a tube with high temperature epoxy to prevent formation of the troublesome high permeability zone along the walls. Moreover, horizontal scans of saturation should be made to check for existence of preferential channels. It is not necessary to do cross-sectional scans at all elevations because if these channels exist they will have to be continuous for them to have any significant effect on the overall pressure gradient. The effects of thermodynamic conditions on the relative permeability functions could easily be studied

by changing the back pressure at the exit end. Since flow is produced by a constant flow-rate pump, an increase in back pressure will not affect the capability to maintain a desired flow rate. However, since pressure and temperature are correlated, care should be taken so as not to exceed the operating temperature range of the present instrumentation.

The effects of capillary number could easily be verified by conducting the experiment at different flow rates. The existing pump is capable of delivering a wide range of flow rates from 49 cc/hr to 947 cc/hr.

The effects of boundary conditions could easily be examined by doing a heat pipe experiment. This experiment involves heating one end of the test column above the saturation temperature while the other end is maintained below it. This imposed boundary condition causes a countercurrent flow of steam and water in which liquid water flows towards the high temperature boundary, flashes into steam, and steam flows towards the low temperature boundary, where it condenses. It is expected that in this configuration, the irreducible water saturation will be lower than that obtained in the present experiment on concurrent flow but the irreducible saturation of steam will be higher.

REFERENCES

Almon, W. R., 1977. Sandstone Diagenesis is Stimulation Design Factor, Oil and Gas J., Vol. 75, pp. 56–59.

Amaefule, J. O., and Hardy, L. L., 1981. The Effect of Interfacial Tensions of Relative Oil-Water Permeabilities of Consolidated Porous Media, Paper SPE/DOE 9783 presented at Second Joint Symp. on Enhanced Oil Recovery, April 5–8, Tulsa, OK.

Amott, E., 1959. Observations Relating to the Wettability of Porous Rock, Trans. AIME, Vol. 216, pp. 156–162.

Arihara, N., Ramey, H. J., Jr., and Brigham, W. E., 1976. Nonisothermal Single- and Two-phase Flow Though Consolidated Sand-Stone, Soc. Pet. Eng. J., pp. 137–146.

Arriola, A., Willhite, G. P. and Green, D. W., 1980. Trapping of Oil Drops in a Non-Circular Pore Throat, paper SPE 9404 presented at the 55th Annual Fall Technical Confer. of the SPE-AIME, Dallas, Sept. 21–24.

Bangham, D.H. and Fakhoury, N., 1931. The Translational Motion of Molecules in the Adsorbed Phase on Solids, J. Chem. Soc., pp. 1324–1333.

Bankoff, S. G., 1957. Eubllition from Solid Surfaces in Absence of Pre-Existing Gaseous Phase, Trans. ASME, Vol. 79, p. 735.

Bejan, A., 1982. *Entropy Generation Through Heat and Fluid Flow*, John Wiley & Sons, New York.

Bobek, J. E., Mattax, C. C., and Denekas, M. O., 1958. Reservoir Rock Wettability — Its Significance and Evaluation, Trans. AIME., Vol. 213, pp. 155–160.

Bodvarsson, G. S., O'Sullivan, J. J. and Tsang, C. F., 1980. The Sensitivity of Geothermal Reservoir Behavior to Relative Permeability Parameters, Proc. 6th Workshop Geothermal Res. Eng., Stanford.

Bordon, C., and Longeron, D. G., 1980. Influence of Very Low Interfacial Tensions on Relative Permeability, Soc. Pet. Eng. J., Oct., pp. 391–401.

Bretherton, F.P., 1962. The Motion of Long Bubbles in Tubes. J. Fluid Mech., Vol. 10, pp. 166–188.

Brooks, R.H., and Corey, A.T., 1964. Hydraulic Properties of Porous Media, Colorado State University, Hydro. paper No. 3, March.

Brown, J. S., and Fatt, I., 1956. Measurement of Fractional Wettability of Oil Field Rocks by a Nuclear Magnetic Relaxation Method, Trans. AIME, Vol. 207, pp. 262–264.

Brown, R. A., Orr, F. M. and Scriven, L. E., 1980. Pore Character and Meniscus Movement in Diagenetically Altered Reservoir Rock, Canad. J. Pet. Tech.

Buscall, R. and Ottewill, R.H., 1975. Thin Films, Specialist Periodical Report, Colloid Sci., Vol. 2, Ed. D.H. Everett.

Chen, H. K., Counsil, J. R., and Ramey, H. J., 1978. Experimental Steam-Water Permeability Curves, Trans. Geothermal Resources Council, Vol. 2, pp. 102–104.

Coley, F. H., Marsden, S. S., and Calhoun, J. C., 1956. A Study of the Effect of Wettability on the Behavior of Fluids in Synthetic Porous Media, Producers Monthly, June, pp. 29–45.

Corey, A. T., 1954. The Interrelation Between Gas and Oil Relative Permeabilities, Prod. Mon., Vol. 19, pp. 38–41.

Counsil, J. R., and Ramey, H. J., 1979. Drainage Relative Permeabilities Obtained from Steam-Water Boiling — Flow and External Gas Drive Experiments, Transactions Geothermal Resources Council, Vol. 3, pp. 141–143.

Davidson, L. B., 1969. The Effect of Temperature on Relative Permeability Ratio of Different Fluid Pairs in Two-Phase Systems, J. Pet. Tech., Aug., p. 1037.

Davis, H.T. and Scriven, L.E., 1981. Gradient Theory of Fluid Microstructure. J. Stat. Phys., Vol. 24, pp. 243–268.

Defay, R. and Prigogine, I., *Surface Tension and Adsorption*, Longmans, Green &

Co., Ltd., London, U. K., 1966.

Denekas, M. O., Mattax, C. C., and Davis, G. T., 1959. Effects of Oil Components on Rock Wettability, Trans. AIME, Vol. 216, pp. 330–333.

Deryaguin, B.V., 1937. Theory of Particle Action in the Pressure of Electric Double Layers and Aggregational Stability of Lyobhobic Colloids and Disperse Systems. Izv. AN SSSR ser khim., Vol. 6, pp. 1153–1164.

Deryaguin, B.V., 1957. Correct Form of the Equation of Capillary Condensation in Porous Bodies. Proc. 2nd Int. Congr. Surface Activity, Vol. 2, pp. 153–159.

Deryaguin, B.V., Martynov, G.A. and Gutap, Yu. V., 1965. Thermodynamics and Stability of Free Films, Kolloidnyi Zhurnal, Vol. 27, pp. 357–364.

Deryaguin, B.V., Rabinovich, Y.I., and Churaev, N.V., 1978. Nature, Vol. 272, p. 313.

Deryaguin, B.V. and Churaev, N.V., 1974. Structural Component of Disjoining Pressure, J. Colloid Interface Sci., Vol. 49, pp. 249–255.

Deryaguin, B.V. and Gutop, Yu. V., 1968. Thermodynamic Discussion of Equilibrium and Stability of a Free Film Containing two Nonvolatile Components. Kolloidnyi Zhurnal, vol. 30, pp. 13–21.

Deryaguin, B.V. and Shcherbakov, L.M., 1961. Effect of Surface Forces on Phase

Equilibrium of Polymolecular Layers and on Contact Angle. Kolloidnyi Zhurnal, Vol. 23, pp. 40–52.

Deryaguin, B.V., and Zorin, Z.M., 1957. Optical Study of Adsorption and Surface Condensation of Vapor in Vicinity of Saturation on a smooth Surface. Proc. 2nd Int. Congr. Surface Activity, Vol. 2, pp. 145–152.

Donaldson, E. C., Lorenz, D. B., and Thomas, R. D., 1966. The Effects of Viscosity and Wettability on Oil and Water Relative Permeabilities, paper SPE 1562.

Downie, J., and Crane, F. E., 1961. Effects of Viscosity on Relative Permeability, Soc. Pet. Eng. J., June, pp. 59–60.

Duff, I.S., 1977. MA28 — A Set of FORTRAN Subroutines for Sparse Unsymmetric Linear Equations, Report No. AERE-R-8730, Computer Sciences and Systems Division, AERE Harwell, Oxfordshire, U.K., July.

Dzyaloshinkii, I.E., Lifshitz, E.M., and Pitaevskii, L.P., 1960. VanderWaals Forces in Liquid Films, Soviet Physics JETP, Vol. 37, pp. 161–170.

Edmondson, T. A., 1965. Effect of Temperature on Waterflooding, J. Can. Pet. Tech., Oct.–Dec., p. 236.

Edwards, A.L., 1972. TRUMP: A Computer Program for Transient and Steady State Temperature Distributions in Multidimensional Systems, National

Technical Information Service, National Bureau of Standards, Springfield, VA.

Ertekin, T., King, G.R., and Schwerer, S., 1983. Dynamic Gas Slippage: A Unique Dual-Mechanism Approach to the Flow of Gas in Tight Formation, paper No. SPE 12045, presented at the 58th Annual Tech. Conf. and Exhibition, San Francisco, CA, Oct. 5–8.

Fatt, I., 1956. The Network Model of Porous Media, Trans. AIME, Vol. 207, pp. 144–181.

Fulcher, R. A., Jr., Ertekin, T., and Stahl, C. D., 1983. The Effects of the Capillary Number and its Constituents on Two-Phase Permeability Curves, Paper SPE 12170.

Gaffen, T. M., Owens, W. W., Parrish, D. R., and Morse, R. A., 1951. Experimental Investigation of Factors Affecting Laboratory Relative Permeability Measurements, Pet. Trans. AIME, vol. 192, pp. 99–110.

Grant, M. A., 1977. Permeabilities Reduction Factors at Wairaki, Paper presented at AIChE-ASME Heat Transfer Conference, AIChE, Salt Lake City, Utah, Aug., pp. 15–17.

Gundmundsson, J. S., Menzies, A. J., and Horne, R. N., 1983. Streamtube Relative Permeability Functions for Flashing Steam-Water Flow in Fractures, SPE Paper No. 11686 presented at the California Regional Meeting of the

SPE, Ventura.

Handbook of Chemistry and Physics, Sixth Edition, Chemical Rubber Co., 1967, Ohio, p. E121.

Hardy, W.B., 1919. Phil. Mag., Vol. 38, p. 49.

Hauzenberg, I., and Zaslavsky, D., 1963. The Effect of Size of Water Stable Aggregates on Field Capacity, Department of Civil Engineering, Technion, Haifa, P.H. Vol. 35, as quoted by Bear (1972).

Heiba, A. A., Davis, H. T., and Scriven, L. E., 1983. Effect of Wettability on Two-Phase Relative Permeabilities and Capillary Pressures, paper SPE 12172 presented at the 58th Annual Technical Conference and Exhibition, San Francisco, CA, Oct. 5–8.

Hiemenz, P. C., *Principles of Calloid and Surface Chemistry*, Marcel Dekker, Inc., New York, 1977.

Hirschfelder, J.O., Curtiss, C.F. and Bird, R.B., 1954. *Molecular Theory of Gases and Liquids*, John Wiley & Sons, New York.

Hirschfelder, J.O., Curtiss, C.F. and Bird, R.B., 1954. *Molecular Theory of Gases and liquids*, John wiley & Sons, New York.

Hjelmeland, O. S., and Larrondo, L. E., 1983. Experimental Investigation of the Effects of Temperature, Pressure, and Crude Oil Composition on Interfacial

Properties, paper SPE 12124 presented at SPE 58th Annual Technical Conference, San Francisco, CA, Oct. 5–8.

Holbrook, O. C., and Bernard, G. G., 1958. Determination of Wettability by Dye Adsorption, Trans. AIME, Vol. 213, pp. 261–264.

Horne, R. N., and Ramey, H. J., 1978. Steam/Water Relative Permeability from Production Data, Transactions, Geothermal Research Council, Vol. 2, pp. 291–293.

Huh, C., 1969. Capillary Hydrodynamics: Interfacial Instability and the Solid/Liquid/Fluid Contact Line. Ph.D. Thesis, University of Minnesota.

International Formulation Committee, 1967. A Formulation of the Thermodynamic Properties of Ordinary Water Substance, IFC Secretariat, Duesseldorf, Germany.

International Formulation Committee, 1967. A formulation of the Thermodynamic Properties of Ordinary Water Substance, IFC Secretariat, Dunesseldorf, Germany.

Irmay, S., 1954. On the Hydraulic Conductivity of Unsaturated Soils, Trans. Amer. Geophys. Union, Vol. 35.

Johnson, E.F., Bossler, D.-P., and Naumann, V.O., 1959. Calculation of Relative Permeability from Displacement Experiments, Trans. AIME, 216, 370–376.

Kast, W., 1964. Bedentung der Keimbildung und der Instationanen Varmeubertragung fur den Warmeubergang bei Blasenverdamp-fung und Topfenkondensation, Chemie Ing. Teckn., 36 Jahrg., 1964/N9. pp. 933–940.

Keller, H.F., 1968. *Numerical Methods for Two-Point Boundary Value Problems*, Ginn-Blaisdell, Waltham, Massachusetts.

Kesghi, H.S. and Scriven, L.E., 1979. Rising Film Flow: First Order Approximation Solved. Bull. Amer. Phys. Soc., Vol. 24, p. 1131.

Koplik, J. and Lassetor, T. J., 1982. Two-Phase Flow in Random Network Models of Porous Media, Paper SPE 11014, presented at 57th Ann. Fall Tech. Confr. and Exhibition of the Society of Petroleum Engineers of AIME, New Orleans, LA., Sept. 26–29.

Kremesec, V. J., and Treiber, L. E., 1978. Effect of System Wettability on Oil Displacement by Miceller Flooding, J. Pet. Tech., Jan., pp. 52–60.

Kyte, J. R., and Rapoport, L. A., 1958. Linear Waterflood Behavior and End Effects in Water-Wet Porous Media, Trans. AIME, Vol. 213, pp. 423–426.

Lafebvre du Prey, E. J., 1973. Factors Affecting Liquid-Liquid Relative Permeabilities of a Consolidated Porous Medium, Soc. Pet. Eng. J., Feb., pp. 39–47.

Lee, J. F. and Sears, F. W., *Thermodynamics*, Addison-Wesley Publishing Co.,

Inc., Cambridge, MA, 1955.

Leppest, G. and Pitts, C.C., 1964. Boiling, Adv. Heat Transfer, Vol. 1.

Leverett, M. C., 1939. Flow of Oil-Water Mixtures Through Unconsolidated Sands, Pet. Trans. AIME, Vol. 132, p. 149.

Lienhard, J.H., 1977. Correlation of the Limiting Liquid Superheat, Chem. Eng. SC., Vol. 31, pp. 847–849.

Lifshitz, E.M., 1956. The Theory of Molecular Attractive Forces Between Solids, Soviet Physics JETP. Vol. 2, pp. 73–83.

Lo, H. Y., 1976. The Effect of Interfacial Tension on Oil-Water Relative Permeabilities, Research Report RR-32, Petroleum Recovery Institute, Nov.

Lo, H. Y., and Mungan, N., 1973. Effect of Temperature on Water-Oil Relative Permeabilities in Oil-Wet and Water-Wet Systems, paper SPE 4505 presented at the SPE 48th Annual Meeting, Las Vegas, Sept. 30 – Oct. 3.

Lorentz, J. J., Mikic, B. B., and Rohsenow, W. M., 1974. The Effect of Surface Conditions on Boiling Characteristics, Heat Transfer, Vol. 4, Proc. of 5th Int. heat Transfer Conference, Tokyo, Japan. Mohanty, K.K., 1981. Fluids in Porous Media: Two-Phase Distribution and Flow. Ph.D. thesis, University of Minnesota.

McCaffery, F. G., and Bennion, D. W., 1974. The Effect of Wettability on Two-

Phase Relative Permeabilities, J. Can. Pet. Tech., Oct. - Dec., pp. 42–53.

Melrose, J. C. and Brander, C. F., 1974. Role of Capillary Forces in Determining Microscopic Displacement Efficiency for Oil Recovery by Waterflooding, J. Canad. Pet. Tech., October, Vol. 13, pp. 54–62.

Menzies, A. J., 1982. Flow Characteristics and Relative Permeability Functions for Two-Phase Geothermal Reservoirs from a One-Dimensional Thermodynamic Model, M. S. Thesis , Stanford University.

Millar, M. A., and Ramey, H. J., Jr., 1983. Effect of Temperature on Oil/Water Relative Permeabilities of Unconsolidated and Consolidated Sands, paper SPE 12116 presented at 58th Annual Technical Conference, San Francisco, CA, Oct. 5–8.

Mohanty, K. K., and Saltor, S. J., 1982. Multiphase Flow in Porous Media: II. Pore-Level Modeling, paper SPE 11018 presented at the 57th Annual Fall Technical Conference, New Orleans, LA, Sept. 26–29.

Naar, J., Wygal, G. R., and Henderson, J. H., 1962, Imbibation Relative Permeability in Unconsolidated Porous Media, SPEJ, Vol. 2, pp. 13–17. Kanpp, R. T., 1958. Cavitation and Nuclei, Trans. ASME, Vol. 80, p. 1321.

Narasimhan, N.T. and Witherspoon, P.A., 1976. An Integrated Finite Difference Method for Analyzing Fluid Flow in Porous Media, Water Resources Research, Vol. 12, No. 1, pp. 57-64.

Odeh, A. S., 1959. Effects of Viscosity Ratio on relative Permeabilities, Pet. Trans. AIME, Vol. 216, pp. 346–353.

Osoba, J. S., Richardson, J. G., Kerner, J. K., Hafford, J. A., and Blair, P. M., 1951. Laboratory Measurements of Relative Permeability, Pet. Trans. AIME, pp. 47–55.

Owens, W. W., and Archer, D. L., 1971. The Effect of rock Wettability on Oil-Water Relative Permeability Relationships, J. Pet. Tech., July, pp. 873–878.

Pathak, P., 1981. Doctoral Dissertation, Univ. of Minnesota, Minneapolis, Dec.

Peaceman, D.W., 1977. *Fundamentals of Numerical Reservoir Simulation*, Elsevier, Amsterdam.

Perkins, F. M., Jr., 1957. Investigation of the Role of Capillary Forces in Laboratory Waterfloods, Trans. AIME, Vol. 210, pp. 409–411.

Poston, S. W., Ysrael, S., Hossain, A. K. M. S., Montgomery, E. F., III, and Ramey, H. J., Jr., 1970. The Effect of Temperature on Irreducible Water Saturation and relative Permeability of Unconsolidated Sands, Soc. Pet. Eng. J., June, p. 171.

Pruess, K., 1983. Development of the General Purpose Simulator MULKOM, Annual Report, 1982, Earth Sc. Div., Lawrence Berkeley Laboratory, Berkeley, CA.

Pruess, K., 1985. TOUGH User's Guide, Lawrence Berkeley Laboratory Report No. LBL-20700, November.

Rapoport, L. A., and Leas, W. A., 1953. Properties of Linear Water Floods, Trans. AIME, Vol. 198, pp. 139–148.

Reda, D. C., and Eaton, R. R., 1980. Influence of Steam/Water Relative Permeability Models on Predicted Geothermal Reservoir Performance: A Sensitivity Study, 6th Annual Workshop on Geothermal Reservoir Engineering, Stanford, Dec. 15–18.

Reda, D. C., and Eaton, R. R., 1981. Definition of a Facility for Experimental Studies of Two-Phase Flows and Heat Transfer in Porous Material, AIAA 16th Thermophysics Conference, Paper No. AIAA-81-1190.

Richardson, J. G., 1957. The Calculation of Water-Flood Recovery from Steady-State Relative Permeability Data, Pet. Trans. AIME, pp. 373–375.

Richardson, J. G., and Perkins, F. M., 1957. A Laboratory Investigation of Effect of Rate on Recovery of Oil by Waterflooding, Trans. AIME, Vol. 210, pp. 114–121.

Roof, J. G., 1970. Snap-off of Droplets in Water Wet Cores, Soc. Pet. Eng. J., Vol. 10, pp. 85–90.

Rose, W., 1979. Measuring Relative Permeabilities for Estimating Reserves,

Proc., Congreso Panamericano de Ingeniesia del Petroleo, Mexico City, March 19–23.

Rose, W. and Witherspoon, P. A., 1956. Studies of Waterflood Performance: II. Trapping Oil in a Pore Doublet, Div. Ill. State Geol. Survey Circular No. 224.

Ruschak, K.J., 1978. Flow of a Falling Film Into a Pool. AIChE J., Vol. 24, pp. 705–709.

Sandberg, C. R., Gournay, L. S., and Sipple, R. F., 1958. The Effect of Fluid-Flow Rate and Viscosity on Laboratory Determinations of Oil-Water Relative Permeabilities, Pet. Trans. AIME, Vol. 213, pp. 36–43.

Schneider, F. N., and Owens, W. W., 1980. Steady-State Measurements of Relative Permeability for Polymer-Oil Systems, paper SPE 9408 presented at the 55th Annual Fall Technical Conference, Dallas, TX, Sept. 21–24.

Schrock, V.E., 1969. Radiation Attenuation Techniques in Two Phase Flow Measurements, Proceedings Two Phase Flow Instrumentation, Heat Transfer Conference, ASME.

Schuh, M.T. and Udell, K.S., 1985. A Study of the Thermodynamics of Evaporation and Condensation in a Porous Media. Heat Transfer in Porous Media and Particulate Flows, Proc. 23rd ASME/AIChE National Heat Transfer Conf., Denver, Colorado, Aug. 4–7, HTD-Vol. 46, pp. 159–165.

Shinohara, K., 1978. Calculations and Use of Steam/Water Relative Permeabilities in Geothermal Reservoirs, M. S. Thesis, Stanford University.

Singhal, A. K., and Somerton, W. H., 1977. Quantitative Modeling of Immiscible Displacement in Porous Media: A Network Approach, Rev. Int. Franc. Petrol., Nov.–Dec., Vol. 32, pp. 897–920.

Slobod, R. L., and Blum, H. A., 1952. Method for Determining Wettability of Reservoir Rock, Trans. AIME, Vol. 195, pp. 1–10.

Somerton, W.H., El-Shaarani, A.H. and Mobarak, S.M., 1974. High Temperature Behavior of Rocks Associated with Geothermal Type Reservoirs, paper SPE-4897, presented at 44th Annual California Regional Meeting of the Society of Petroleum engineers, San Francisco, CA.

Somerton, W.H., Keese, J.A. and Chu, S.L., 1973. Thermal Behavior of Unconsolidated Oil Sands, paper SPE-4506, presented at 48th Annual Fall Meeting of the Society of Petroleum Engineers, Las Vegas, NV.

Sufi, A. S., Ramey, H. J., Jr., and Brigham, W. E., 1982. Temperature Effects on Relative Permeabilities of Oil Water Systems, paper SPE 11071 presented at the SPE 57th Annual Technical Conference and Exhibition, New Orleans, Sept. 26–29.

Sun, H., and Ershaghi, I., 1979. The Influence of Steam-Water Relative Permeability Curves on the Numerical Results of Liquid Dominated Geothermal

Reservoirs, Transaction, Geothermal Resources Council, Vol. 3, pp. 697–700.

Udell, K. and Burr, M.W., 1982. Heat Transfer in Porous Media Heated from Above with Evaporation, Condensation and Capillary Effects, Proc. ASME Conf., HTD-Vol. 22, Phoenix, AZ, Nov. 14–19.

Udell, K., 1984, Personal communication.

Udell, K.S., 1985. Heat Transfer in Porous Media Considering Phase Changes and Capillarity — The Heat Pipe Effect. Int. J. of Heat and Mass Transfer, Vol. 28, No. 2, pp. 485–495.

Van Brakel, J., 1975. Pore Space Models for Transport Phenomena in Porous Media — Review and Evaluation with Special Emphasis on Capillary Liquid Transport, Powder Technology, Vol. 11, pp. 205–236.

Vargaftik, N.B., 1975. *Tables on the Thermophysical Properties of Liquids and Gases*, Second Edition, John Wiley and Sons, New York.

Wagner, O. R., and Leach, R. O., 1959. Improving Oil Displacement Efficiency by Wettability Adjustment, Trans. AIME, Vol. 216, pp. 65–72.

Walker, W.R., Sabey, J.D. and Hampton, D.R., 1981. Studies of Heat Transfer and Water Migration in Soils, Final Report, Department of Agricultural and Chemical Engineering, Colorado State University, Fort Collins, CO, April.

Walker, W.R., Sabey, J.D. and Hampton, D.R., 1981. Studies of Heat Transfer

and Water Migration in Soils, Final Report, Department of Argicultural and Chemical Engineering, Colorado State University, Fort collins, CO, April.

Wardlaw, N. C. and Cassan, J. P. 1978. Estimation of Recovery Efficiency by Visual Observation of Pore Systems in Reservoir Rocks, Bull. Canad. Pet. Geol., Vol. 26, pp. 572–585.

Weinbrandt, R. M., Ramey, H. J., Jr., and Casse, F. J., 1975. The Effect of Temperature on Relative and Absolute Permeability of Sand-Stones, Soc. Pet. Eng. J., Oct., p. 376.

Wilson, M. D. and Pittman, E. D., 1977. Anthigenic Clays in Sandstones: Recognition and Influences on Reservoir Properties and Paleoenvoironmental Analysis, J. Sedimentary Petrology, Vol. 47, pp. 3–31.

Yuster, S. T., 1951. Theoretical Considerations of Multiphase Flow in Idealized Capillary Systems, Proc. 3rd World Petroleum Congress.

LAWRENCE BERKELEY LABORATORY
TECHNICAL INFORMATION DEPARTMENT
UNIVERSITY OF CALIFORNIA
BERKELEY, CALIFORNIA 94720